

1 **Anthropogenic activities significantly increase annual**  
2 **greenhouse gas (GHG) fluxes from temperate headwater**  
3 **streams in Germany**

4 **Authors:** Ricky Mwangada Mwanake<sup>1</sup>; Gretchen Maria Gettel<sup>2,7</sup>, Elizabeth Gachibu  
5 Wangari<sup>1</sup>, Clarissa Glaser<sup>5</sup>, Tobias Houska<sup>4</sup>, Lutz Breuer<sup>4,6</sup>, Klaus Butterbach-Bahl<sup>1,3</sup>, Ralf  
6 Kiese<sup>1</sup>

7

8 <sup>1</sup>Karlsruhe Institute of Technology, Institute for Meteorology and Climate Research, Atmospheric  
9 Environmental Research (IMK-IFU), Kreuzeckbahnstrasse 19, Garmisch-Partenkirchen 82467, Germany

10 <sup>2</sup>IHE-Delft Institute for Water Education, Westvest 7 2611 AX Delft the Netherlands

11 <sup>3</sup>Pioneer Center Land-CRAFT, Department of Agroecology, University of Aarhus, Denmark

12 <sup>4</sup>Institute for Landscape Ecology and Resources Management (ILR), Research Centre for BioSystems, land use /  
13 land cover and Nutrition (iFZ), Justus Liebig University Giessen, Giessen, 35392, Germany

14 <sup>5</sup>Center for Applied Geoscience, University of Tübingen, Tübingen, Germany

15 <sup>6</sup>Centre for International Development and Environmental Research (ZEU), Justus Liebig University Giessen,  
16 Senckenbergstrasse 3, 35390 Giessen, Germany

17 <sup>7</sup>Department of Ecoscience, Lake Ecology, Aarhus University, Denmark

18

19 *Correspondence to* Ralf Kiese (ralf.kiese@kit.edu)

## 20 Abstract

21 Anthropogenic activities increase the contributions of inland-waters to global greenhouse gas (GHG;  
 22 CO<sub>2</sub>, CH<sub>4</sub>, and N<sub>2</sub>O) budgets, yet the mechanisms driving these increases are still not well constrained. In this  
 23 study, we quantified year-long GHG concentrations ~~and fluxes, as well as, fluxes, and~~ water physico-chemical  
 24 variables from ~~23 streams, 3 ditches, and 2 wastewater inflow~~ 8 sites contrasted by land use across five  
 25 headwater catchments in Germany ~~contrasted by land use~~. Based on linear mixed effects models, Using mixed-  
 26 effects models, we determined the overall impact of land use and seasonality on the intra-annual variabilities of  
 27 these parameters. We found showed that land use was more significant than seasonality in controlling the intra-  
 28 annual variability of the GHG concentrations and fluxes. Streams in a Agricultural-land usedominated  
 29 catchments and or with wastewater inflows in settlement areas resulted in had up to 10 times higher daily riverine  
 30 CO<sub>2</sub>, CH<sub>4</sub>, and N<sub>2</sub>O emissions, and were also more temporally variable (CV > 55%) than forested areas streams,  
 31 as substrate inputs by these sources appeared to favor in situ GHG production processes. Dissolved GHG inputs  
 32 directly from agricultural runoff and waste water inputs also contributed substantially to the annual emissions  
 33 from these sites Our findings also suggested that nutrient, labile-carbon, and dissolved GHG inputs from the  
 34 agricultural and settlement areas may have supported these hotspots and hot-moments of fluvial GHG emissions.  
 35 Drainage ditches were hotspots for CO<sub>2</sub> and CH<sub>4</sub> fluxes due to high dissolved organic matter concentrations,  
 36 which appeared to favor in situ production via respiration and methanogenesis. Overall, the annual emission from  
 37 anthropogenic-influenced streams in CO<sub>2</sub>-equivalents was up to 20 times higher (~71 kg CO<sub>2</sub> m<sup>-2</sup> yr<sup>-1</sup>) than from  
 38 natural streams (~3 kg CO<sub>2</sub> m<sup>-2</sup> yr<sup>-1</sup>), with CO<sub>2</sub> accounting for up to 81 % of these annual emissions, while N<sub>2</sub>O  
 39 and CH<sub>4</sub> accounted for up to 18 and 7 %, respectively. The positive influence of anthropogenic activities on  
 40 fluvial GHG emissions also resulted in a breakdown of the expected declining trends of fluvial GHG emissions  
 41 with stream size. Therefore, future studies should focus on anthropogenically perturbed streams, as their GHG  
 42 emissions are much more variable in space and time and can potentially introduce the largest uncertainties to  
 43 fluvial GHG estimates Overall, the annual emission from anthropogenic influenced streams in CO<sub>2</sub>-equivalents  
 44 was up to 20 times higher (~71 kg CO<sub>2</sub> m<sup>-2</sup> yr<sup>-1</sup>) than from natural streams (~3 kg CO<sub>2</sub> m<sup>-2</sup> yr<sup>-1</sup>). Future studies  
 45 aiming to estimate the contribution of lotic ecosystems to GHG emissions should therefore focus on  
 46 anthropogenically perturbed streams, as their GHG emission are much more variable in space and time.

47

## 48 1 Introduction

49 Streams and rivers cover only a small fraction of the ~~earth's~~ earth's land surface (0.4%; Allen et al.,  
 50 2018), yet they are significant contributors to global greenhouse ~~gases~~ (CO<sub>2</sub>, CH<sub>4</sub>, and N<sub>2</sub>O) budgets, emitting  
 51 approximately 7.6 (6.1–9.1) Pg-CO<sub>2</sub> equivalent into the atmosphere per year (Li et al., 2021). Headwater  
 52 streams are hotspots for GHG emissions within fluvial ecosystems due to their large surface area to volume ratio  
 53 compared to larger rivers, allowing for close connectivity with GHG sources (Hotchkiss et al., 2015; Turner et  
 54 al., 2016). Several biogeochemical processes are responsible for GHG production and consumption within  
 55 fluvial-headwater ecosystems. Biogenic CO<sub>2</sub> production is mainly attributed to the respiration of organic matter  
 56 (Battin et al., 2008). Production of CH<sub>4</sub> occurs through methanogenesis, with carbon dioxide and acetic acid as  
 57 substrates under anaerobic conditions (Stanley et al., 2016). Consumption of methane Methane consumption is

58 also possible through methanotrophy in ~~oxygen-oxygen~~-rich stream waters, producing CO<sub>2</sub> ~~in the process~~  
 59 (Shelley et al., 2014). N<sub>2</sub>O is mainly a byproduct in nitrification (under aerobic conditions) or an intermediate  
 60 product in denitrification (under anaerobic conditions), but it can also be reduced to N<sub>2</sub> in organic-rich and  
 61 nitrate-poor ecosystems (Quick et al., 2019). Apart from instream biogeochemical production, GHG  
 62 concentrations in headwater streams may also come from external sources such as groundwater and terrestrial  
 63 soils (e.g., Borges et al., 2015; Hotchkiss et al., 2015). These external sources are generally dominant during  
 64 periods of heavy precipitation when the hydrological connectivity between the streams and their surrounding  
 65 terrestrial landscape and groundwater is activated. Yet, partitioning the sources of these GHGs between in-situ  
 66 production and external sources remains a challenge to aquatic scientists, as their contributions are mainly  
 67 compounded and also vary widely depending on discharge conditions and the surrounding land use (e.g., Aho &  
 68 Raymond, 2019; Borges et al., 2019; Mwanake et al., 2022).

69 Within headwaters, aAnthropogenic practices such as fertilizer application and construction of drainage  
 70 ditches to allow agricultural use of former wetlands alter the rates of instream GHG production and their external  
 71 sources, thereby influencing their spatial-temporal dynamics~~these processes, thereby influencing in-stream GHG~~  
 72 dynamics (Peacock et al., 2021; Wallin et al., 2020; Mwanake et al., 2019). Elevated hydrological inputs of  
 73 dissolved GHGs, inorganic nitrogen nutrients, and labile carbon in-to streams ~~within-from~~ fertilized croplands ~~has~~  
 74 ~~have~~ been shown to ~~favor in situ increase their~~ N<sub>2</sub>O (e.g., Beaulieu et al., 2009), CO<sub>2</sub> ~~production~~ (e.g., Bodmer et  
 75 al., 2016; Borges et al., 2018), and CH<sub>4</sub> ~~production fluxes~~ (e.g., Mwanake et al., 2022), by favoring instream  
 76 GHG production processes and also ensuring steady supplies in periods of low in-situ biogeochemical  
 77 production. While such trends in agricultural streams show similarities across different catchment locations,  
 78 GHG emissions from streams in predominantly forested catchments with minor influences from croplands and  
 79 wetlands show more diverse patterns. Some studies indicated that forest streams are hotspots for GHG fluxes  
 80 (e.g., Wallin et al., 2018; Audet et al., 2019; Herreid et al., 2021), while others found the opposite with much  
 81 lower fluxes in forests as compared ~~d~~ to other land uses (e.g., Bodmer et al., 2016; Mwanake et al., 2022).  
 82 ~~Drainage ditches, Besides draining CH<sub>4</sub> and CO<sub>2</sub>-rich terrestrial soils, drainage ditches which~~ are characterized  
 83 by short water residence times, high organic loads, and highly variable O<sub>2</sub> levels, ~~-, which~~ can simultaneously  
 84 support ~~both aerobic and anaerobic organic carbon mineralization, driving~~ vigorous CH<sub>4</sub> and CO<sub>2</sub> production  
 85 and, subsequently, higher fluxes and subsequent fluxes. ~~I. For example, in~~ a recent meta-analysis, ditches, and  
 86 canals accounted for up to 3% of the global anthropogenic CH<sub>4</sub> emissions (Peacock et al., 2021). Yet, studies on  
 87 them are scarce, and thus the main factors making them hotspots of carbon fluxes are still not well-constrained.

88 In fluvial ecosystems ~~located in within~~ settlement areas, point-source inflows of wastewater effluents  
 89 have also been reported to alter natural GHG trends along the river continuum (Park et al., 2018). also act as  
 90 important drivers of GHG fluxes. ~~The wastewater effluent is either -by indirectly influencing insitu substrate~~  
 91 ~~availability of nutrient rich and labile carbon substrate-rich, -to the streams that favoring~~ insitu ~~for~~ GHG  
 92 production, and through GHG-rich, resulting in high riverine GHG emissions downstream of the inflow point  
 93 direct inflows of dissolved GHGs (e.g., Marescaux et al., 2018; Begum et al., 2021; Zhang et al., 2021; Wang et  
 94 al., 2022). For example, in a study of urban-impacted rivers in the Seine basin in France, Marescaux et al. (2018)  
 95 found elevated CO<sub>2</sub>, CH<sub>4</sub>, and N<sub>2</sub>O concentrations and fluxes downstream of wastewater inflows, which  
 96 ~~dispropotenately~~ disproportionately contributed higher up to 52 % of the basin-wide annual GHG fluxes. Similar  
 97 findings were also found in urban-impacted rivers in China, ~~where~~ their GHG emissions were up to 14 times

98 higher than ~~those from~~ other land uses (Zhang et al., 2021). Yet, studies on GHG emissions from urban-  
 99 impacted fluvial ecosystems are still scarce, and therefore their contributions to riverine annual GHG budgets are  
 100 not well constrained. ~~Moreover, little is known about the cumulative effects of diffuse and point pollution~~  
 101 ~~sources on the magnitude of riverine GHG fluxes and whether the diffuse pollution sources exert longer-lasting~~  
 102 ~~controls on their fluxes than the point sources.~~

103 ~~Moreover, little is known about the interactive effects of land use and wastewater effluent inflows on~~  
 104 ~~riverine GHG fluxes, and whether land use is the overarching controlling factor.~~

105 ~~Under temperate climatic conditions, pronounced seasonality regulates the availability of nutrients and,~~  
 106 ~~to some extent, the O<sub>2</sub> in lotic ecosystems, which are both key factors driving *instream* GHG production and gas~~  
 107 ~~exchange rates (Borges et al., 2018; Rocher-Ros et al., 2019; Herreid et al., 2021; Aho et al., 2022). Cold winter~~  
 108 ~~periods are generally characterized by low *instream* carbon and nitrogen processing, which results in nutrient~~  
 109 ~~accumulation (e.g., Herreid et al., 2021). In contrast, while high *instream* C and N processing are characteristic~~  
 110 ~~of warm summer periods (e.g., Borges et al., 2018; Aho et al., 2021, 2022). Seasonality in precipitation regulates~~  
 111 ~~discharge, whereby heavy precipitation events or snowmelt during spring result in high discharge events. At the~~  
 112 ~~same time, dry summers and winter periods are often characterized by lower discharge (e.g., Aho et al., 2022).~~  
 113 ~~Discharge in turn determines the water residence times in streams, which controls the rates of *instream* C and N~~  
 114 ~~processing. P. thereby influencing rates of carbon and nitrogen processing previous studies have shown that low~~  
 115 ~~discharge periods with longer water residence times favor *instream* GHG production processes (e.g., Borges et~~  
 116 ~~al., 2018; Mwanake et al., 2022). In comparison, high discharge periods with shorter water residence times are~~  
 117 ~~unfavorable to *instream* C and N cycling, resulting in the dominance of externally sourced GHGs (e.g., Borges~~  
 118 ~~et al., 2018; Mwanake et al., 2022). High discharge events may also increase dissolved GHG supply from~~  
 119 ~~upstream terrestrial sources and *instream* GHG production depending on the surrounding land use. For example,~~  
 120 ~~studies have found that during high discharge periods, streams draining wetlands show peak CO<sub>2</sub> and CH<sub>4</sub>~~  
 121 ~~concentrations (e.g., Aho et al., 2019; Borges et al., 2019), and pronounced N<sub>2</sub>O concentrations are found in~~  
 122 ~~streams of cropland-dominated catchments (e.g., Mwanake et al., 2022).~~

123 ~~The dynamic aforementioned interactions between seasonality and land use indicate that temporally~~  
 124 ~~sporadic measurements of GHG concentrations and fluxes are limited in revealing intra annual variations, which~~  
 125 ~~are necessary for better estimating annual emissions interactions between seasonality and land use discussed~~  
 126 ~~above indicate that less frequent measurements of riverine GHG concentrations and fluxes may fail to capture~~  
 127 ~~periods of elevated fluvial emissions at spatially hotspot areas, resulting in an underestimation of the annual~~  
 128 ~~emissions. Yet, only a handful of studies in temperate streams have assessed the seasonal dynamics of GHG~~  
 129 ~~fluxes at sampling points with contrasting land uses (e.g., Marescaux et al., 2018; Borges et al., 2018; Herreid et~~  
 130 ~~al., 2021; Galantini et al., 2021), resulting in uncertainties in the mechanisms that drive either hot periods or~~  
 131 ~~hotspots of fluvial GHG fluxes. As climate change causes more extreme discharge conditions and as agricultural~~  
 132 ~~intensification and settlement areas continue to increase (Winkler et al., 2021), more studies that cover a wide~~  
 133 ~~array of land uses, discharge, and temperature conditions are needed to allow developing better mechanistic~~  
 134 ~~understanding of their effects on fluvial GHG dynamics by unraveling synergistic or antagonistic relationships~~  
 135 ~~amongst them. These increased process understanding will form the basis of future mechanistic modeling~~  
 136 ~~approaches, which are essential to predict better how fluvial GHG emissions will respond to future climate and~~

137 ~~land use changes (Battin et al., 2023). As climate change drives more extreme discharge conditions, and as~~  
138 ~~agricultural intensification and settlement areas continue to increase (Winkler et al., 2021), studies that cover a~~  
139 ~~wide array of land uses, discharge, and temperature conditions are needed to constrain better the effects of land~~  
140 ~~use in controlling intra-annual GHG flux variabilities and to unravel synergistic or antagonistic relationships~~  
141 ~~amongst them.~~

142 The main objective of this study was to assess the seasonality-land use relationships of water physico-  
143 chemical variables and GHG concentration and fluxes by comparing temperate lotic ecosystems of forests and  
144 wetlands with those from more human-influenced agricultural and settlement catchments. To do so, we  
145 conducted at least tri-weekly measurements covering a full year of observations and mainly focused on  
146 headwater streams (stream orders 1–6), which ~~are known hotspots despite being hotspots~~ of fluvial emissions, ~~but~~  
147 remain currently underrepresented in global GHG datasets (Drake et al., 2018; Li et al., 2021). We hypothesize  
148 that catchment land use is the most ~~important-critical~~ control for stream GHG concentration and fluxes, with  
149 higher seasonal variability in human-influenced ecosystems than in natural ones. Moreover, we hypothesized  
150 that drainage ditches and headwater streams with wastewater inflow within agricultural and settlement areas are  
151 hotspots for GHG emissions, driven by direct dissolved GHG inputs or substrate inputs that favor *in situ* GHG  
152 production.

## 153 2 Materials and methods

### 154 2.1 Study areas and sampling design

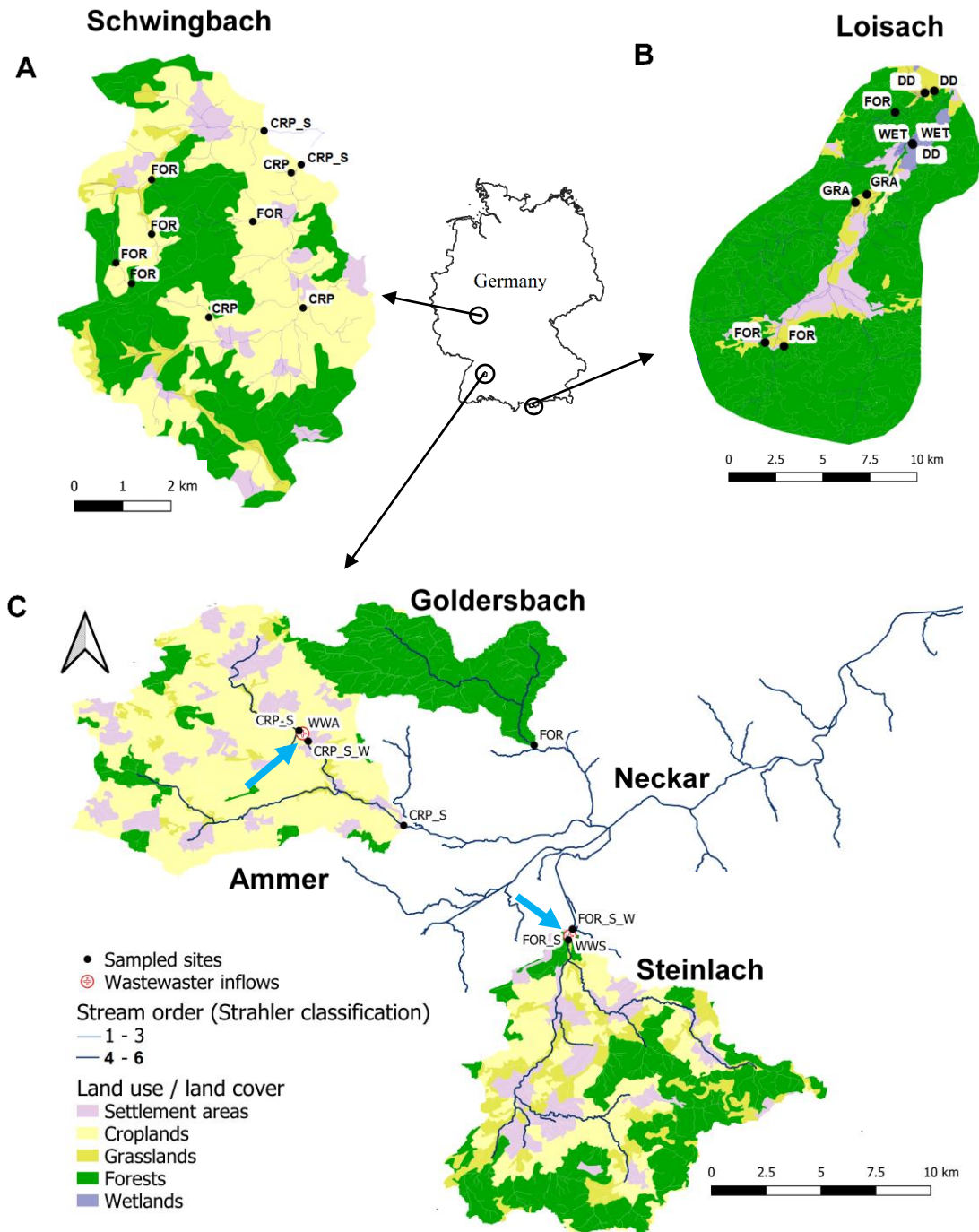
155 Five headwater catchments in central (Schwingbach), southeast (Loisach), and southwest (Ammer,  
156 Goldersbach, and Steinlach) Germany were investigated in this study. The catchments covered a wide range of  
157 fluvial ecosystems with different stream orders and land use characteristics (Table 1; Fig. 1). The catchment  
158 boundaries for each site were determined based on the most downstream sampling location within each  
159 catchment (Fig. 1). Elevation of the Schwingbach catchment (54 km<sup>2</sup>), located in the central-German state of  
160 Hessen, ranges from 176–480 m above sea level (a.s.l.). The catchment has a mixed land use of ~41 % mixed  
161 forests, 46% croplands, 8 % settlement areas, and 5 % pasturelands (Wangari et al., 2022) (Fig. 1A). The climate  
162 is warm and temperate (Cfb, Köppen climate classification), with an annual rainfall of 742 mm (monthly mean  
163 min: 51 mm, monthly mean max: 72 mm) (1999–2019) and a mean annual temperature of 9.8 °C (monthly mean  
164 min: 1.3 °C, monthly mean max: 18.8 °C) (1991–2021) (Climate-data.org, [https://en.climate-](https://en.climate-data.org/europe/germany/hesse/giessen-151/)  
165 [data.org/europe/germany/hesse/giessen-151/](https://en.climate-data.org/europe/germany/hesse/giessen-151/)).

166 The Upper Loisach catchment (467 km<sup>2</sup>, outlet Eschenlohe town) is located in the mountainous region  
167 of the Bavarian Alps, Germany. The catchment is characterized by a pronounced relief and steep slopes, with  
168 elevations ranging from 616–2,963 m a.s.l. Land use in the catchment comprises coniferous and deciduous  
169 forests interspersed with natural grasslands and rocky surfaces on the mountain slopes (78%). At the valley  
170 bottom, the land use is mainly settlement areas (9%), managed grasslands (8%), and wetlands (5%) (Fig. 1B).  
171 The climate is cold and temperate (Dfb, Köppen climate classification), with annual precipitation of 1,693 mm  
172 (monthly mean min: 87 mm, monthly mean max: 207 mm) (1999–2019) and mean annual temperature of 3.8 °C

173 (monthly mean min: -6.6 °C, monthly mean max: 13.1 °C) (1991–2021) (Climate-data.org, [https://en.climate-  
data.org/europe/germany/free-state-of-bavaria/garmisch-partenkirchen-8762/](https://en.climate-<br/>174 data.org/europe/germany/free-state-of-bavaria/garmisch-partenkirchen-8762/)).

175 The other three catchments are sub-catchments of the Neckar river (Fig. 1C). The Goldersbach (116  
176 km<sup>2</sup>), a tributary of the main Ammer stream, is a forested catchment (95%), with elevations ranging from 366–  
177 583 m a.s.l. The Steinlach catchment (513 km<sup>2</sup>) is also dominated by forests (74%), with agricultural lands  
178 (croplands and grasslands) and settlement areas occupying 21% and 5% of the landscape, respectively. The  
179 elevation range of the hilly area is 321–878 m a.s.l (Fig. 1C). The Ammer catchment (304 km<sup>2</sup>, outlet  
180 Pfäffingen) is dominated by agricultural lands (80%), with 11% forests and 9% settlement areas (Fig. 1C). It has  
181 moderate slopes with an elevation ranging from 319–610 m a.s.l. The Ammer stream is a gaining stream fed by  
182 an extensive groundwater karst system and has significant discharge levels even during the driest periods of the  
183 year (Glaser et al., 2020). The climate is warm and temperate (Cfb, Köppen climate classification), with a mean  
184 annual rainfall of 923 mm (monthly mean min: 63 mm, monthly mean max: 98 mm) (1999–2019) and a mean  
185 annual temperature of 9.3 °C (monthly mean min: 0.2 °C, monthly mean max: 18.6 °C) (1991–2021) (Climate-  
186 data.org, <https://en.climate-data.org/europe/germany/baden-wuerttemberg/tuebingen-22712/>).

187 Across the five catchments, a total of 28 sites at headwater streams (N=23, orders 1–6, defined after  
188 Strahler, 1952), drainage ditches (N=3), and waste-water outflows (N=2, Text A1) were sampled every 2–3 weeks  
189 for an entire year (Table 1, Fig. 1). The Schwingbach and Loisach catchments were sampled from June 2020 to  
190 June 2021 while the Goldersbach, Ammer, and Steinlach catchments, were sampled from April 2021 to April  
191 2022.



192

193

194 Fig. 1: Land cover maps of the (A) Schwingbach, (B) Loisach, and (C) Neckar sub-catchments (Goldersbach,  
 195 Ammer, and Steinlach) derived from the Corine Land Cover 2018 inventory with a 25 ha spatial resolution  
 196 (<https://land.copernicus.eu/pan-european/corine-land-cover/clc2018?tab=mapview>). Black dots with labels  
 197 (abbreviations explained in Table 1) represent sampled headwater streams and drainage ditch sampling points.  
 198 Wastewater inflows sampled are indicated by blue arrows on the maps. Drainage ditches in the Loisach  
 199 catchment were dug in the 1930s to 1960s to lower water levels to improve grassland productivity in areas  
 200 formerly occupied by wetlands.

## 201 2.2 Sub-catchment delineation and land use classification

202 Sub-catchments for each sampling point in the Loisach, Goldersbach, Steinlach, Ammer, and  
203 Schwingbach catchments were delineated in QGIS from a Digital Elevation Model (DEM) (EU-DEM v1.1) with  
204 a 25 m resolution (European Copernicus mission, retrieved August 1, 2021, [https://land.copernicus.eu/imagery-](https://land.copernicus.eu/imagery-in-situ/eu-dem/eu-dem-v1.1)  
205 [in-situ/eu-dem/eu-dem-v1.1](https://land.copernicus.eu/imagery-in-situ/eu-dem/eu-dem-v1.1)). Land use/ land cover percentages of all the delineated sub-catchments were  
206 calculated from Corine Land Cover 2018 survey with a 25 ha spatial resolution (retrieved August 1, 2021,  
207 <https://land.copernicus.eu/pan-european/corine-land-cover/clc2018?tab=mapview>). For data analysis, we  
208 classified sub-catchments according to their dominant land cover (>50% of the total area) into forest (FOR),  
209 cropland (CRP), grassland (GRA), and wetland (WET), and further differentiated sub-catchments with the  
210 influence of settlement areas (S) and wastewater inflows (W). (Table 1). As drainage ditches (DD) in the Loisach  
211 catchment were added as an extra land use category, this classification resulted in 9 land use classes (for details,  
212 see Table 1).

## 213 2.3 Hydrological and water physico-chemical characteristics

214 In the Loisach and Schwingbach catchments, discharge was calculated (Gore, 2007) from stream depth  
215 and velocity measurements using an electromagnetic sensor (OTT-MF-Pro, Hydromet, Germany). For streams in  
216 the Neckar sub-catchments, velocity was measured using the electromagnetic sensor (OTT-MF-Pro, Hydromet,  
217 Germany), and depth and discharge was obtained directly from gauging stations maintained by the water  
218 authority of the state of Baden-Württemberg (<https://udo.lubw.baden-wuerttemberg.de/public/index.xhtml>). The  
219 slope of a ~5 m reach at each sampling point was measured using a laser rangefinder with a slope function  
220 (Nikon Model: 8381, Japan). The slopes and velocities were used to model the site-specific gas transfer  
221 velocities ( $k$  in  $\text{m d}^{-1}$ ) for the quantification of daily GHG fluxes per unit stream surface area ( $\text{mass m}^{-2} \text{d}^{-1}$ ) (see  
222 details in the flux calculation section).

223 Discharge measurements at each sampling location and every sampling event were complemented by *in*  
224 *situ* measurements of water temperature ( $^{\circ}\text{C}$ ), electrical conductivity ( $\mu\text{S cm}^{-1}$ ), dissolved oxygen (DO) ( $\text{mg L}^{-1}$ ),  
225 and pH using the Pro DSS multiprobe (YSI Inc., USA). Water samples for nutrient and organic carbon analyses  
226 were also collected and filtered on-site through polyethersulfone (PES) filters (0.45  $\mu\text{m}$  pore size, pre-leached  
227 with 60 ml of miliq water). The samples were stored in 30 ml acid-washed HDPE sample bottles in triplicates  
228 and transported within 24 h to the laboratories at Karlsruhe Institute of Technology, Campus Alpin, Justus  
229 Liebig University Giessen, or the University of Tübingen. On arrival, all samples were immediately frozen for  
230 later analysis.

231 After unfreezing the samples overnight in a  $4^{\circ}\text{C}$  refrigerator, the samples were directly analyzed for  
232 dissolved organic carbon (DOC), total dissolved nitrogen (TDN), nitrate ( $\text{NO}_3\text{-N}$ ), and ammonium ( $\text{NH}_4\text{-N}$ )  
233 concentrations. Dissolved organic nitrogen (DON) concentrations were estimated as the difference between the  
234 TDN and dissolved inorganic nitrogen DIN ( $\text{NO}_3\text{-N} + \text{NH}_4\text{-N}$ ) concentrations. DIN concentrations were  
235 determined using colorimetric methods, and the absorbance of the samples was measured using a microplate  
236 spectrophotometer (Model: Epoch, BioTek Inc., USA).  $\text{NO}_3\text{-N}$  concentrations were analyzed based on reactions  
237 with the Griess reagent (Patton & Kryskalla, 2011), and  $\text{NH}_4\text{-N}$  concentrations were analyzed using the  
238 indophenol method (Bolleter et al., 1961). The DOC concentrations were measured as non-purgeable organic



239 carbon (NPOC) using a TOC/ TN analyzer (Analytica-Jena; multi N/C 3100, Germany) after pre-treating the  
 240 sample with 25% HCl acid to remove the dissolved inorganic carbon (DIC). The TDN concentrations were  
 241 analyzed simultaneously with the same instrument (Analytica-Jena; multi N/C 3100, Germany).

## 242 2.4 Gas sampling, analysis, and calculations of annual areal fluxes

243 GHG stream, ditch, and wastewater samples were collected in triplicates simultaneously with the water  
 244 physico-chemical samples using the headspace equilibration technique (Raymond et al., 1997). In brief, 80 ml of  
 245 background water was equilibrated with 20 ml of atmospheric air in a syringe at *in situ* water temperatures. The  
 246 headspace gas sample was transferred into 10ml glass vials for GHG concentration analysis in the laboratory of  
 247 the Karlsruhe Institute of Technology, Campus Alpin (see full sampling details in Mwanake et al., 2022).  
 248 Atmospheric air samples were taken twice (morning and afternoon) on each sampling day to correct for  
 249 background atmospheric GHG concentrations. GHG concentrations from the headspace were analyzed using an  
 250 SRI gas chromatograph (GC) (8610C, Germany) with an electron capture detector (ECD) for N<sub>2</sub>O and a flame  
 251 ionization detector (FID) with an upstream methanizer for simultaneous measurements of CH<sub>4</sub> and CO<sub>2</sub>  
 252 concentrations. The standards used for the GC calibration were 450, 800, 1000, 1500, 2000, and 3000 ppm for  
 253 CO<sub>2</sub>, 1, 2, 3, 4, 5, and 6 ppm for CH<sub>4</sub> and 0.4, 0.8, 1, 1.5, 2, and 3 ppm for N<sub>2</sub>O. Dissolved GHG concentrations  
 254 in the stream water were calculated from post-equilibration gas concentrations in the headspace after correcting  
 255 for atmospheric (ambient) GHG concentrations (e.g., Aho et al., 2019; Mwanake et al., 2022).

256 Daily diffusive fluxes ( $F$ ) (moles m<sup>-2</sup> d<sup>-1</sup>) of the GHGs were estimated using Fick's Law of gas  
 257 diffusion, where the  $F$  is the product of the gas exchange velocity ( $k$ ) (m d<sup>-1</sup>) and the difference between the  
 258 stream water ( $C_{aq}$ ) (moles m<sup>-3</sup>) and the ambient atmospheric gas concentration in water assuming equilibrium  
 259 with the atmosphere ( $C_{sat}$ ) (moles m<sup>-3</sup>) (Equation 1). GHG concentrations and fluxes were expressed in mass  
 260 units by multiplying by the respective molar masses.

$$261 \quad F = k (C_{aq} - C_{sat}) \quad (1)$$

262 The temperature-specific gas transfer velocities ( $k$ ) for each of the gases were calculated from  
 263 normalized gas transfer velocities ( $k_{600}$ ) (m d<sup>-1</sup>) (corresponding to the  $k$  of CO<sub>2</sub> at 20° C with a Schmidt number  
 264 of 600) and temperature-dependent Schmidt numbers ( $Sc$ ) (unit-less) of the respective gases (Equation 2).

$$265 \quad k = k_{600} \times (600/Sc)^{0.5} \quad (2)$$

266 The  $k_{600}$  was modeled using Equation 3 (drawn from Equation 4 in Table 2 of Raymond et al. (2012)), which was  
 267 calibrated from headwater streams of similar characteristics as our study sites, where  $V$  is stream velocity (m s<sup>-1</sup>),  
 268 and  $S$  is the slope (m m<sup>-1</sup>).

$$269 \quad k_{600} = VS^{0.76} \times 951.5 \quad (3)$$

270 Before choosing the equation above for modeling the  $k_{600}$  values, we compared the  $k_{600}$  values  
 271 calculated from all seven empirical models by Raymond et al. (2012). The predicted  $k_{600}$  values from models 3,  
 272 4, 5, and 6 in Table 2 of Raymond et al. (2012), which all use velocity and slope as input parameters, were  
 273 mainly similar for the three discharge periods and across all stream orders 1–6 (ANOVA;  $p > 0.05$ ). In contrast,  
 274 the calculated  $k_{600}$  values from equations 1, 2, and 7, which use a stream depth parameter, were higher (ANOVA;

275  $p < 0.05$ ), particularly from the higher stream orders (5–6). This finding is inconsistent with the energy dissipation  
276 model of turbulent streams where  $k_{600}$  is predicted to decrease with stream order. We, therefore, interpreted this  
277 to indicate a breakdown of these models for higher stream orders. This also agrees with Raymond et al. (2012)  
278 recommendations, and we, therefore, choose not to use models 1, 2, and 7 for this study. Out of the remaining  
279 equations, 3, 4, 5, and 6, we used equation 4, which calculated  $k_{600}$  based on the slope and velocity parameters  
280 and was also in line with several previous studies spanning a wide range of stream orders similar to our study.  
281 (See, Aho et al., 2019; Borges et al., 2019; Mwanake et al., 2019; Hall & Ulseth, 2020; Aho et al., 2021;  
282 Mwanake et al., 2022). The uncertainties in the modeled gas transfer velocities were reduced in this study by  
283 parametrizing the velocities and slopes based on actual field measurements of both variables. Equation 3 also  
284 estimated the gas transfer velocities in the drainage ditches with a measurable flow velocity and slope.

285 Water-to-atmosphere fluxes for all three GHGs across all land use classes in each sub-catchment were  
286 calculated from the mean daily  $\text{CO}_2$ ,  $\text{CH}_4$ , and  $\text{N}_2\text{O}$  fluxes during different discharge conditions. Total GHG  
287 fluxes were expressed as  $\text{CO}_2$  equivalents emissions ( $\text{mg CO}_2\text{-eq m}^{-2} \text{d}^{-1}$ ) computed from global warming  
288 potentials ( $\text{GWP}_{100}$ ) using 28 for  $\text{CH}_4$  and 298 for  $\text{N}_2\text{O}$  (IPCC, 2014). We followed the procedure developed in  
289 Mwanake et al. (2022) to scale tri-weekly measurements to annual flux estimates. Briefly, we classified each  
290 sampling date of every location into low, medium, or high discharge conditions according to whether normalized  
291 discharge fell in the 0–33% percentile (low), 34–66% (medium), or 67–100% (high) days. Normalized discharge  
292 for each site was determined by dividing each absolute discharge measurement for every site visit during the  
293 year by the maximum measured discharge. The number of days in each discharge period was estimated as the  
294 ratio of observations in each discharge period to the total number of flux observations in individual land use  
295 classes in each catchment.  $\text{CO}_2$  equivalents fluxes were then calculated for the three different discharge periods  
296 in each land use class by multiplying the daily mean  $\text{CO}_2$  equivalents flux measured during each period and the  
297 number of days within each period. Annual fluxes were finally estimated by summing up the emissions of the  
298 low, medium, and high discharge periods for the individual land use classes in each catchment.

## 299 2.5 Statistical analysis

300 Linear mixed-effects models were used to investigate the effect of seasonality and land use on water  
 301 physico-chemical variables, GHG concentrations, and fluxes (“lme4” package in R version 4.1.1). Fixed effects  
 302 in the models consisted of land use classes in each catchment (Table 1) and seasons: summer June 1–August 31,  
 303 autumn September 1–November 30, winter December 1–February 28, and spring March 1–~~31<sup>st</sup>~~May 31~~May~~.  
 304 Random effects accounting for repeated measures were also included in the models. Model performance was  
 305 assessed based on the distribution of residuals (i.e., residuals should be normally distributed with a mean close to  
 306 zero) and conditional  $r^2$  values calculated from significant models (p-value <0.05) (“MuMIn” package in R). A  
 307 Tukey post-hoc test (p-value <0.05) of least-square means was used on the mixed models to identify individual  
 308 differences within each categorical fixed effect. GHG concentration and flux data and other water physico-  
 309 chemical variables were transformed using the natural logarithm to meet the assumption of normality. Because  
 310 we quantified occasional negative fluxes in some of our sites, constant flux values of  $50 \text{ mg m}^{-2} \text{ d}^{-1}$  for  $\text{CO}_2\text{-C}$ ,  
 311  $0.5 \text{ mg m}^{-2} \text{ d}^{-1}$  for  $\text{CH}_4\text{-C}$ , and  $10 \text{ } \mu\text{g m}^{-2} \text{ d}^{-1}$  for  $\text{N}_2\text{O-N}$  were added to the fluxes to enable the natural logarithm  
 312 transformations.

313 Path analysis from structural equation models (SEMs, “lavaan” package in R version 4.1.1) was used to  
 314 determine how environmental factors linked to seasonality and land use directly or indirectly influenced  
 315 *instream* GHG production and consumption processes as well as external GHG sources, i.e., dissolved GHG  
 316 inputs to the streams originating from either wastewater inflows or terrestrial landscapes which were not  
 317 produced *in situ*. In brief, these SEMs were constructed based on causal relationships between exogenous  
 318 variablesenvironmental variables (interpreted as ultimate drivers of GHG concentrations) and endogenous  
 319 substrate variables, which are affected by the environmental exogenous-variables and also act as immediate  
 320 drivers that affect GHG concentrations. Endogenous-Substrate variables in the models, which are known to  
 321 influence *in situ* biogeochemical GHG production and consumption processes directly, included dissolved  
 322 oxygen DO (% saturation), DOC ( $\text{mg L}^{-1}$ ),  $\text{NH}_4\text{-N}$  ( $\text{mg L}^{-1}$ ), and  $\text{NO}_3\text{-N}$  ( $\text{mg L}^{-1}$ ) concentrations (Battin et al.,  
 323 2008; Stanley et al., 2016; Quick et al., 2019). The exogenous environmental variables in the models, which  
 324 influence *in situ* GHG concentrations either directly by facilitating dissolved GHG inputs or indirectly by  
 325 controlling the substrate endogenous-variables, were water temperature ( $^{\circ}\text{C}$ ) (a proxy for different seasons),  
 326 stream velocity  $V$  ( $\text{m s}^{-1}$ ), % upstream agricultural area for each sampling point (AGR: grassland + cropland  
 327 area) and wastewater inflows (WW: Boolean numbers, i.e., 1 for the presence of wastewater inflow and 0 for  
 328 absence).

329 The hypothesized relationships between the substrate endogenous- and exogenous environmental drivers  
 330 of instream GHG concentrations were assessed in the overall theoretical SEM, which comprises several  
 331 multivariate regression equations shown in Equations 4-8. To get the best-fit SEM, the removal of parts of the  
 332 theoretical SEM was done manually until the model with the highest parsimony fit index (PNFI) and a root mean  
 333 squared error of approximation (RMSEA) of  $\leq 0.05$  was found (Schumacker and Lomax, 2016). Graphical  
 334 representations of the significant relationship pathways from the best-fit model, including standardized slope  
 335 parameter estimates, were done using the “semPlot” package in R software.

336  $\text{Log}_e \text{GHG concentration} = \text{DO} + \text{DOC} + \text{stream velocity} + \text{water temperature} + \text{Log}_e \text{NO}_3 +$   
337  $\text{Log}_e \text{NH}_4 + \text{wastewater inflow} + \text{agricultural area}$   
338 (4)

339  $\text{Log}_e \text{NO}_3 = \text{DO} + \text{Log}_e \text{NH}_4 + \text{DOC} + \text{wastewater inflow} + \text{agricultural area} +$   
340  $\text{stream velocity}$  (5)

341  $\text{Log}_e \text{NH}_4 = \text{DO} + \text{DOC} + \text{wastewater inflow} + \text{agricultural area} +$   
342  $\text{stream velocity}$  (6)

343  $\text{DOC} = \text{wastewater inflow} + \text{agricultural area} + \text{stream velocity}$  (7)

344  $\text{DO} = \text{DOC} + \text{wastewater inflow} + \text{agricultural area} + \text{stream velocity}$  (8)

Table 1: Summary descriptions of sampling sites located in the Schwingbach, Loisch, and Neckar sub-catchments (Goldersbach, Ammer and Steinlach) (Fig. 1). The land use (%) was calculated for the site-specific upstream sub-catchments based on the Corine Land Cover 2018 survey of Europe (See main text for details).

Main Catchment	Site	Stream order	Coordinates (decimal degrees)		Sub-catchment area (Ha)	Elevation at sampling point	Sub-catchment Landuse / landcover (%)			Wastewater inflow		Main sub-catchment landuse class	Main land use Abbreviations	
			Latitude	Longitude			Forest	Wetland	Grassland	Cropland	Urban			Yes
Loisch	Stream	1	47.5694	11.1554	4	651	40	60	0	0	0	No	Wetland	WET
Loisch	Stream	2	47.5689	11.1556	10	645	22	78	0	0	0	No	Wetland	WET
Loisch	Stream	1	47.5440	11.1193	11	660	0	0	100	0	0	No	Grassland	GRA
Loisch	Stream	1	47.5399	11.1105	13	663	19	0	81	0	0	No	Grassland	GRA
Loisch	Stream	1	47.4670	11.0537	40	750	86	0	14	0	0	No	Forest	FOR
Loisch	Stream	2	47.4691	11.0394	75	756	99	0	0	0	1	No	Forest	FOR
Loisch	Stream	2	47.5858	11.1429	102	719	100	0	0	0	0	No	Forest	FOR
Loisch	Drainage ditch		47.5963	11.1730	11	630	27	0	73	0	0	No	Drainage ditch	DD
Loisch	Drainage ditch		47.5953	11.1657	11	645	43	57	0	0	0	No	Drainage ditch	DD
Loisch	Drainage ditch		47.5696	11.1550	17	630	47	0	53	0	0	No	Drainage ditch	DD
Schwingbach	Stream	1	50.5051	8.6127	41	297	96	0	0	4	0	No	Forest	FOR
Schwingbach	Stream	1	50.4695	8.6179	60	187	0	0	0	100	0	No	Cropland	CRP
Schwingbach	Stream	2	50.4811	8.5407	62	241	98	0	2	0	0	No	Forest	FOR
Schwingbach	Stream	1	50.4756	8.5472	67	334	86	0	0	14	0	No	Forest	FOR
Schwingbach	Stream	2	50.4922	8.5971	220	260	47	0	0	53	0	No	Cropland	CRP
Schwingbach	Stream	2	50.5032	8.5553	220	272	65	0	0	35	0	No	Forest	FOR
Schwingbach	Stream	2	50.4887	8.5555	268	204	83	0	0	17	0	No	Forest	FOR
Schwingbach	Stream	1	50.4669	8.5792	355	207	14	0	0	84	2	No	Cropland	CRP
Schwingbach	Stream	3	50.5050	8.6148	2337	183	37	0	6	48	9	No	Cropland+settlement	CRP_S
Schwingbach	Stream	3	50.5166	8.5992	5345	189	44	0	4	45	7	No	Cropland+settlement	CRP_S
Goldersbach (Neckar)	Stream	5	48.5588	9.0591	11623	367	97	0	0	3	0	No	Forest	FOR
Ammer (Neckar)	Stream	5	48.5649	8.8986	26157	379	11	0	1	84	4	No	Cropland+settlement	CRP_S
Ammer (Neckar)	Stream	6	48.5640	8.8997	26361	377	11	0	1	83	5	Yes	Cropland+settlement+wastewater	CRP_S_W
Ammer (Neckar)	Stream	6	48.5271	8.9615	30441	348	14	0	2	77	8	No	Cropland+settlement	CRP_S
Steinlach/Neckar	Stream	6	48.4796	9.0634	51332	348	74	0	10	11	4	No	Forest+settlement	FOR_S
Steinlach/Neckar	Stream	6	48.4812	9.0639	51332	344	74	0	10	11	4	Yes	Forest+settlement+wastewater	FOR_S_W
Ammer/Neckar	Wastewater effluent		48.5644	8.8993									Wastewater	WWA
Steinlach/Neckar	Wastewater effluent		48.4805	9.0636									Wastewater	WWS

## 346 3 Results

### 347 3.1 Hydrological variables

348 Across all sampling points and seasons, tri-weekly sampled stream velocity measurements (annual  
349 mean  $\pm$  SE) were two-folds higher for streams ( $0.19 \pm 0.009 \text{ m s}^{-1}$ , range: 0.01- 1.17) than ditches ( $0.05 \pm 0.06 \text{ m}$   
350  $\text{s}^{-1}$ , range: 0.01–0.23) (Fig A1). Seasonality had an overall significant effect (p-value <0.05) on stream velocities  
351 across all sampling points, with higher stream velocities observed in spring ( $0.24 \pm 0.02 \text{ m s}^{-1}$ ) than in autumn  
352 ( $0.12 \pm 0.01 \text{ m s}^{-1}$ ) (Table 2; Table B2). Discharge in streams ( $3.9\text{--}18,500 \text{ L s}^{-1}$ ) and in ditches ( $0.1\text{--}37 \text{ L s}^{-1}$ ) was  
353 highly variable, reflecting differing stream sizes and seasonal variability (Fig. A1). The Neckar sub-catchments,  
354 dominated by streams (orders 5 - 6 ), had an order of magnitude higher mean annual discharge ( $874.7 \pm 178 \text{ L s}^{-1}$ )  
355 than the streams in the other catchments (Loisach:  $50.5 \pm 6 \text{ L s}^{-1}$  and Schwingbach:  $26.7 \pm 4 \text{ L s}^{-1}$ ). The  
356 average discharge at the stream and ditch sampling points in all our study catchments were 3 to 5-fold higher in  
357 spring and summer ( $384.1 \pm 96$  and  $526.4 \pm 171 \text{ L s}^{-1}$ , respectively) than in autumn and winter ( $86.25 \pm 13.07$   
358 and  $157.3 \pm 31.58$ , respectively; p-value <0.01; Table 2; Table B2).

359 Table 2: Results of multiple linear mixed-effects models predicting the effect of seasonality (summer, autumn,  
 360 winter, and spring) and sub-catchment land use (Table 1) on stream velocity, discharge, water physico-chemical  
 361 variables, GHG concentration, gas-transfer velocity, and GHG flux. The model performance was assessed based  
 362 on conditional  $r^2$  and the distribution of residuals, including the variances explained by fixed effects and repeated  
 363 measures' random effects.

Dependent variables	Conditional $r^2$	Type 2 ANOVA table	
		Season (df=3)	Land use (df=11)
		F-statistic/significance	F-statistic/significance
<b>Water physico-chemical and hydrological variables</b>			
Temperature ( $^{\circ}$ C)	0.87	66.3***	9.1***
pH	0.80	3.1*	97.8***
DO ( $\text{mg L}^{-1}$ )	0.83	20.1***	143.7***
Electrical Conductivity ( $\mu\text{s cm}^{-1}$ )	0.83	4.9**	86.1***
$\text{NO}_3\text{-N}$ ( $\text{mg L}^{-1}$ ) <sup>a</sup>	0.80	4.9**	141***
$\text{NH}_4\text{-N}$ ( $\text{mg L}^{-1}$ ) <sup>a</sup>	0.60	ns	32.3***
TDN ( $\text{mg L}^{-1}$ ) <sup>a</sup>	0.79	5.6**	93.8***
DON ( $\text{mg L}^{-1}$ ) <sup>a</sup>	0.55	ns	13.9***
DOC ( $\text{mg L}^{-1}$ ) <sup>a</sup>	0.59	ns	47.3***
DOC:DIN	0.84	3.2*	133.2***
DOC:DON	0.63	ns	15.1***
Velocity <sup>a</sup>	0.59	3.7*	34.5***
Discharge <sup>a</sup>	0.86	4.6**	96.9***
<b>k<sub>600</sub>, Gas concentration and flux</b>			
$\text{CO}_2\text{-C}$ concentration ( $\mu\text{g L}^{-1}$ ) <sup>a</sup>	0.86	25.6***	219.3***
$\text{CH}_4\text{-C}$ concentration ( $\mu\text{g L}^{-1}$ ) <sup>a</sup>	0.89	ns	273.1***
$\text{N}_2\text{O-N}$ concentration ( $\text{ng L}^{-1}$ ) <sup>a</sup>	0.75	3.3*	69***
$k_{600}$ ( $\text{m d}^{-1}$ ) <sup>a</sup>	0.57	ns	31.2***
$\text{CO}_2\text{-C}$ flux ( $\text{mg m}^{-2} \text{d}^{-1}$ ) <sup>a</sup>	0.57	ns	50.2***
$\text{CH}_4\text{-C}$ flux ( $\text{mg m}^{-2} \text{d}^{-1}$ ) <sup>a</sup>	0.79	ns	113***
$\text{N}_2\text{O-N}$ flux ( $\mu\text{g m}^{-2} \text{d}^{-1}$ ) <sup>a</sup>	0.70	3.9*	75.6***
Total fluxes $\text{CO}_2\text{-eq}$ ( $\text{g m}^{-2} \text{d}^{-1}$ ) <sup>a</sup>	0.67	ns	67***
Level of significance (p-value)	<sup>a</sup> Natural logarithm transformation		
* <0.05			
** <0.01			
*** <0.001	Conditional $r^2$ = Variance explained by fixed and random effects of sampling date		
ns >0.05	df= degrees of freedom		

364

365

## 366 3.2 Water physico-chemical variables

### 367 3.2.1 Seasonal variation

368 Water temperature, DO, and pH ranged from 0.9–24 $^{\circ}$  C, 1.1–15.7  $\text{mg O}_2 \text{L}^{-1}$  and 6.7–9.0, respectively.  
 369 Streams in the mountainous Loisach catchment had a mean annual ( $\pm$  SE) water temperature of  $9.0 \pm 0.2$   $^{\circ}$ C,  
 370 which was  $\sim 1$   $^{\circ}$ C colder than streams of the Schwingbach catchment ( $10.0 \pm 0.4$   $^{\circ}$ C) and 3 degrees colder than  
 371 streams in the Neckar sub-catchments ( $12.0 \pm 0.3$   $^{\circ}$ C). The annual ranges of  $\text{NH}_4\text{-N}$ ,  $\text{NO}_3\text{-N}$ , DON, TDN, and  
 372 DOC concentrations across all catchments were 0.05–1.0  $\text{mg L}^{-1}$ , 0.5–14.8  $\text{mg L}^{-1}$ , 0.05–10.9  $\text{mg L}^{-1}$ , 0.6–17.0

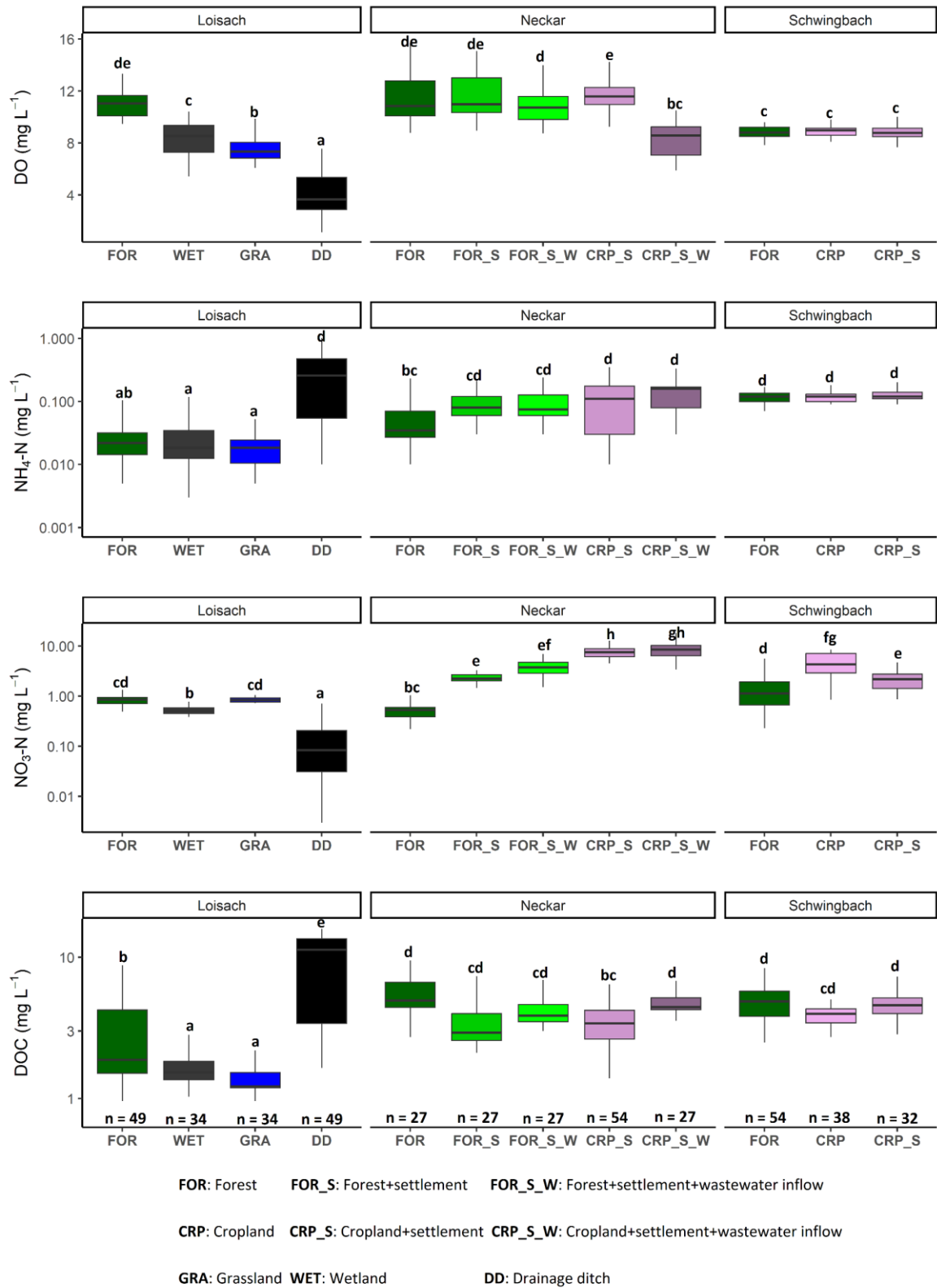
373 mg L<sup>-1</sup>, and 0.9–16.0 mg C L<sup>-1</sup>, respectively. DO, NO<sub>3</sub> and TDN concentrations showed significant seasonal  
374 variability (Table 2, Table B2). DO was higher in winter and spring than in summer and autumn (p-  
375 value<0.001). NO<sub>3</sub>-N and TDN concentrations were highest in winter and lowest in autumn and summer (p-  
376 value<0.01), while NH<sub>4</sub>-N, DOC, and DON showed no significant seasonal variation (p-value>0.05; Table 2;  
377 Table B2). We additionally calculated DOC: DIN and DOC: DON molar ratios, which had interquartile ranges  
378 from 0.9–4.9 and 4.1–29.0, respectively. DOC: DIN ratios showed significant seasonal variability, with higher  
379 values in summer and spring than in winter (p-value<0.05), while no seasonal variability was found for DOC:  
380 DON ratios (p-value>0.05; Table 2: Table B2).

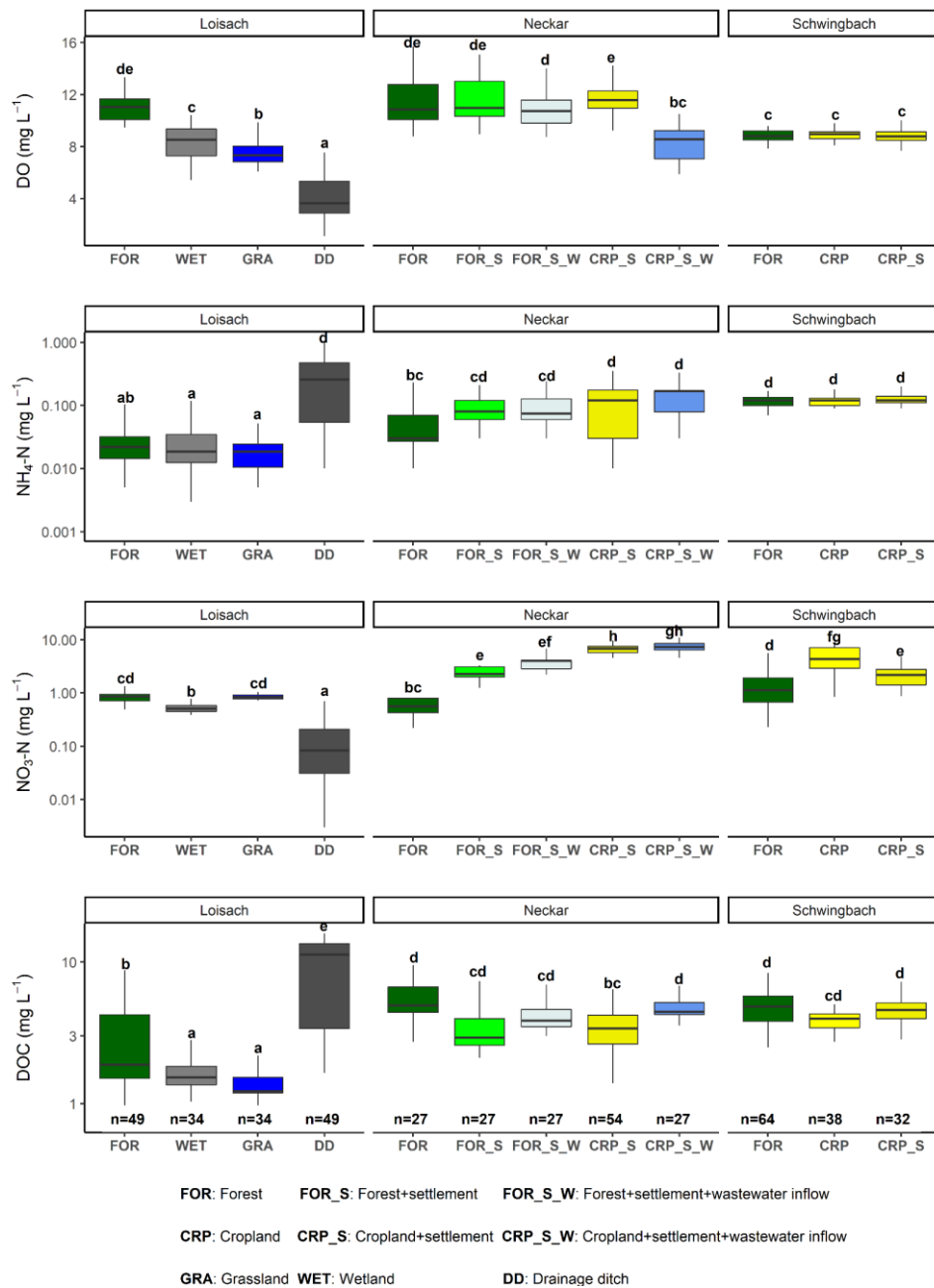
### 381 3.2.2 Land use variation

382 Catchment land use was more significant than seasonality in explaining the variability of most water  
383 physico-chemical variables (p-value<0.001; Table 2). In the Loisach catchment, ditches had up to 2.6 times  
384 lower DO and ~~up to~~ 8 times lower NO<sub>3</sub>-N concentrations than the streams across all land use types (Fig. 2; Table  
385 B3). In contrast, NH<sub>4</sub>-N and DOC concentrations, as well as the DOC: DIN ratio, were 6-10 times higher in the  
386 ditches than in the streams (Fig. 2; Table B3). In the Neckar sub-catchments, forested streams had 1-2 times  
387 higher DO and DOC concentrations than cropland, settlement, and wastewater-influenced streams. The opposite  
388 was true for NO<sub>3</sub>-N and DON concentrations, which were an order of magnitude higher in the cropland,  
389 settlement, and wastewater-influenced streams than in the forested streams (Fig. 2; Table B3). As a result, DOC:  
390 DIN and DOC: DON ratios in the Neckar sub-catchments were, therefore, higher in forested streams than in  
391 cropland, settlement, and wastewater-influenced streams (Table B3).

392 In addition, cropland streams directly receiving wastewater inflows also had significantly lower DO and  
393 higher DOC than cropland streams without wastewater inflows (Fig. 2; Table B3). While NO<sub>3</sub>-N and DON  
394 concentrations were not significantly different in cropland streams with or without wastewater inflows, the  
395 concentrations of both variables were slightly higher in cropland streams with wastewater inflows (Table B3). In  
396 streams of the Schwingbach catchment, surrounding croplands and settlement areas also influenced NO<sub>3</sub>-N  
397 concentrations, which were up to 3-fold higher than in the forested streams. Across all the three catchments, DO  
398 concentrations, DOC: DIN and DOC: DON ratios were higher in the forested streams and decreased in streams  
399 of sub-catchments with predominant agricultural land uses or settlement areas, while the opposite was found for  
400 NO<sub>3</sub>-N and DON concentrations (Table B3). Additionally, forested streams in the Loisach catchment had an  
401 order of magnitude higher DOC: DON ratios than forested streams in the Neckar and Schwingbach catchments  
402 (Table B3).







404

405 Fig. 2: Boxplots of DO, NH<sub>4</sub>-N, NO<sub>3</sub>-N, and DOC concentrations in stream and ditch waters in the three  
 406 catchments grouped by dominating land uses (see Table 1 methods). Letters on top of the boxplots represent  
 407 significant differences ( $p < 0.05$ ) among land use classes across the three catchments based on Tukey post-hoc  
 408 analyses from the linear mixed-effects model results (Table 2).

409

### 410 3.3 GHG concentrations and fluxes

#### 411 3.3.1 Seasonal variation

412 In all headwater streams, CH<sub>4</sub> and N<sub>2</sub>O concentrations varied greatly, spanning three orders of  
 413 magnitude, i.e., from 0.03– 58  $\mu\text{g-C L}^{-1}$  ( $p\text{CH}_4$  1.3–2,145  $\mu\text{atm}$ ) for CH<sub>4</sub> and from 20–18,717  $\text{ng-N L}^{-1}$  ( $p\text{N}_2\text{O}$ )

414 21– 15,813 natm) for N<sub>2</sub>O. In contrast, CO<sub>2</sub> concentrations varied less, spanning only one order of magnitude  
 415 from 219–4,868 µg-C L<sup>-1</sup> (*p*CO<sub>2</sub> 369–7,979 µatm). GHG concentrations in ditches also varied widely, with CH<sub>4</sub>,  
 416 N<sub>2</sub>O and CO<sub>2</sub> concentrations spanning 1-2 orders of magnitude ranging from 27–831 µg-C L<sup>-1</sup> (*p*CH<sub>4</sub> 1,469–  
 417 34,482 µatm), 56–1,540 ng-N L<sup>-1</sup> (*p*N<sub>2</sub>O 35–1,512 natm), and 1,722– 9,746 µg-C L<sup>-1</sup> (*p*CO<sub>2</sub> 2,888–13,400  
 418 µatm), respectively (Fig. A2, A3).

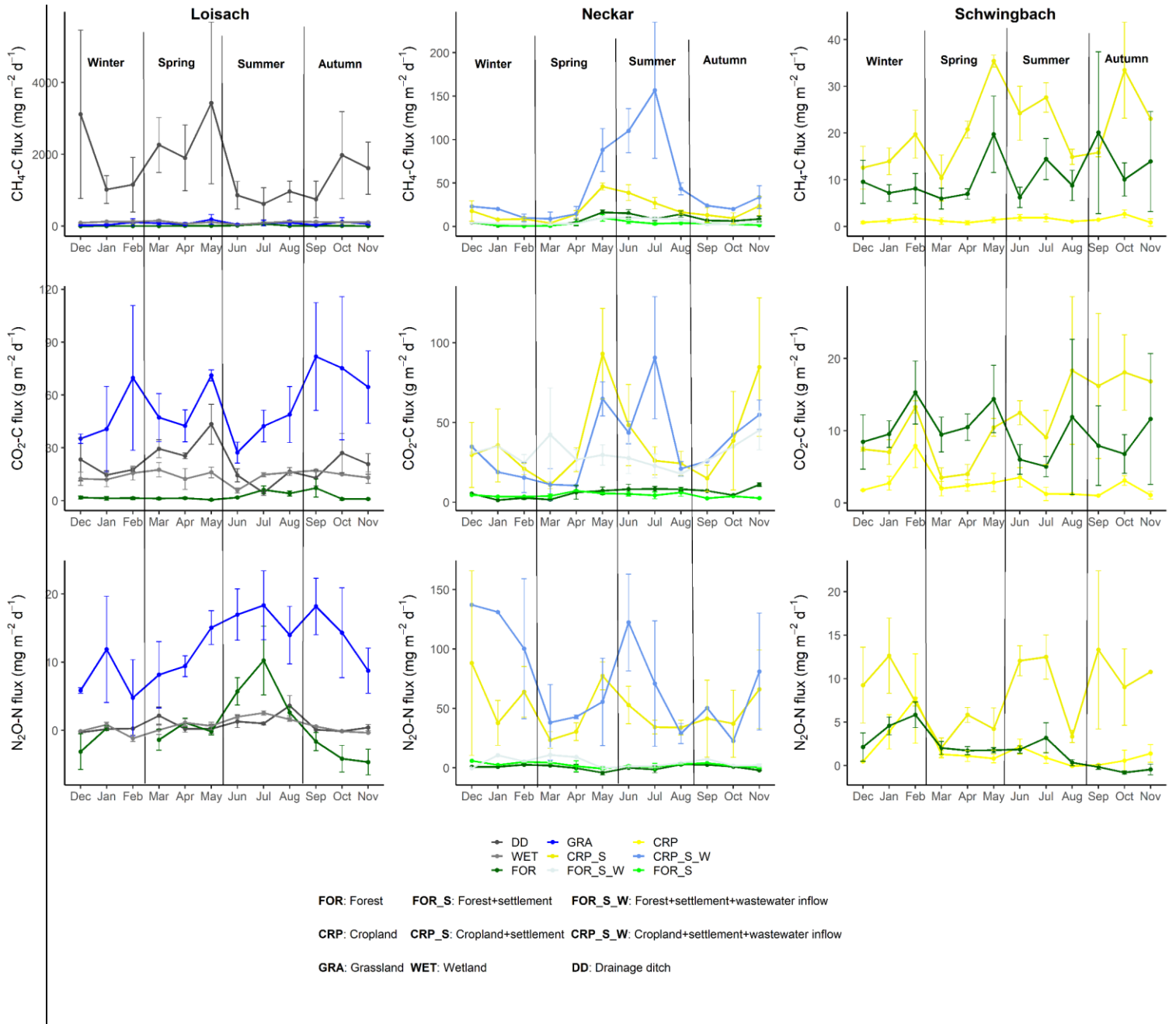
419 Streams and drainage ditches across all seasons were predominantly sources of atmospheric CH<sub>4</sub>, N<sub>2</sub>O,  
 420 and CO<sub>2</sub>, as indicated by concentrations mostly above the atmospheric background and the positive flux values  
 421 displayed in Figure 3. CO<sub>2</sub> fluxes from streams ranged from -0.05–179 g C m<sup>-2</sup> d<sup>-1</sup> (mean 19 g C m<sup>-2</sup> d<sup>-1</sup>), CH<sub>4</sub>  
 422 fluxes ranged from -0.40–325 mg C m<sup>-2</sup> d<sup>-1</sup> (mean 30 mg C m<sup>-2</sup> d<sup>-1</sup>), and N<sub>2</sub>O fluxes ranged from -9.2–199.5 mg  
 423 N m<sup>-2</sup> d<sup>-1</sup> (mean 12 mg N m<sup>-2</sup> d<sup>-1</sup>). CO<sub>2</sub> and CH<sub>4</sub> fluxes from the ditches varied between 2–63 g C m<sup>-2</sup> d<sup>-1</sup> (mean  
 424 13.7 g C m<sup>-2</sup> d<sup>-1</sup>) and from 117–7,933 mg C m<sup>-2</sup> d<sup>-1</sup> (mean 1,532 mg C m<sup>-2</sup> d<sup>-1</sup>), respectively, while N<sub>2</sub>O fluxes  
 425 ranged from -0.8–7.1 mg N m<sup>-2</sup> d<sup>-1</sup> (mean 1.2 mg N m<sup>-2</sup> d<sup>-1</sup>).

426 Seasonal variations in GHG concentrations and fluxes were GHG-dependent and varied across the land  
 427 uses within each catchment (Fig. 3; Fig. A2). In the Loisach catchment, there was a decline in *instream* CO<sub>2</sub>  
 428 concentrations in the summer, followed by a subsequent increase in autumn, particularly at non-forested  
 429 sampling points (Fig. A2). Similar *instream* CO<sub>2</sub> concentration trends, with lower values in the summer season  
 430 and increasing values in autumn, were also found for non-forested streams of the Neckar sub-catchments (Fig.  
 431 A2). However, non-forested streams of the Schwingbach catchments showed slightly different trends, with a  
 432 decline in CO<sub>2</sub> concentrations in spring and an increase in CO<sub>2</sub> concentrations in the late summer. (Fig. A2).  
 433 Considering all data over all catchments, seasonality had an overall significant effect on CO<sub>2</sub> (*p-value* <  
 434 0.05001), with summer concentrations being 1.6 times lower than in autumn, while CO<sub>2</sub> fluxes showed no  
 435 significant seasonal variability (*p-value*>0.05; Table 2; Table B2).

436 In contrast to CO<sub>2</sub>, N<sub>2</sub>O concentrations in the Loisach and Schwingbach catchments decreased from  
 437 summer to autumn but increased again towards the beginning of winter (Fig. A2). In autumn, N<sub>2</sub>O  
 438 concentrations at first and second-order forested streams in the Loisach and Schwingbach catchments were often  
 439 below atmospheric concentrations (Fig. A2), characterizing these sites as N<sub>2</sub>O sinks (Fig. 3). A similar autumn  
 440 decline in N<sub>2</sub>O concentrations was not observed in the streams of the Neckar sub-catchments, but rather, N<sub>2</sub>O  
 441 concentrations increased from autumn to winter (Fig. A2). Across all catchments and sampling points, N<sub>2</sub>O  
 442 concentrations were 2.4 times higher in winter than in the other seasons (*p-value*<0.05; Table B2).- N<sub>2</sub>O fluxes  
 443 were up to 1.6 times higher in summer and winter than in autumn and spring (*p-value*<0.05; Fig. 3; Table B2),  
 444 which represented periods of either high N<sub>2</sub>O concentrations and moderate gas transfer velocities (winter) or  
 445 moderate N<sub>2</sub>O concentrations and high gas transfer velocities (summer) (Table B2).

446 CH<sub>4</sub> concentrations showed a seasonal pattern only in the Schwingbach catchment (Fig. A4A2), which  
 447 showed a decline from summer through autumn and winter. This trend was not observed for the other  
 448 catchments (Fig. A2, A3) and resulted in a non-significant seasonal effect on both concentrations and fluxes  
 449 when all data from all catchments were considered together (*p-value*>0.05; Table 2; Table B2).- Overall, GHG  
 450 fluxes from streams within human-influenced land use classes (grasslands, croplands, and settlement areas) were  
 451 more temporally variable (annual coefficient of variation > 55 %) than those in strong seasonal trends of GHG

452 ~~fluxes throughout the year were mostly found in human-influenced land use classes such as streams and ditches~~  
453 ~~in grasslands, croplands, and settlement areas, but not at streams whose sub-catchments were~~ dominated by  
454 forests or wetlands (Fig. 3).



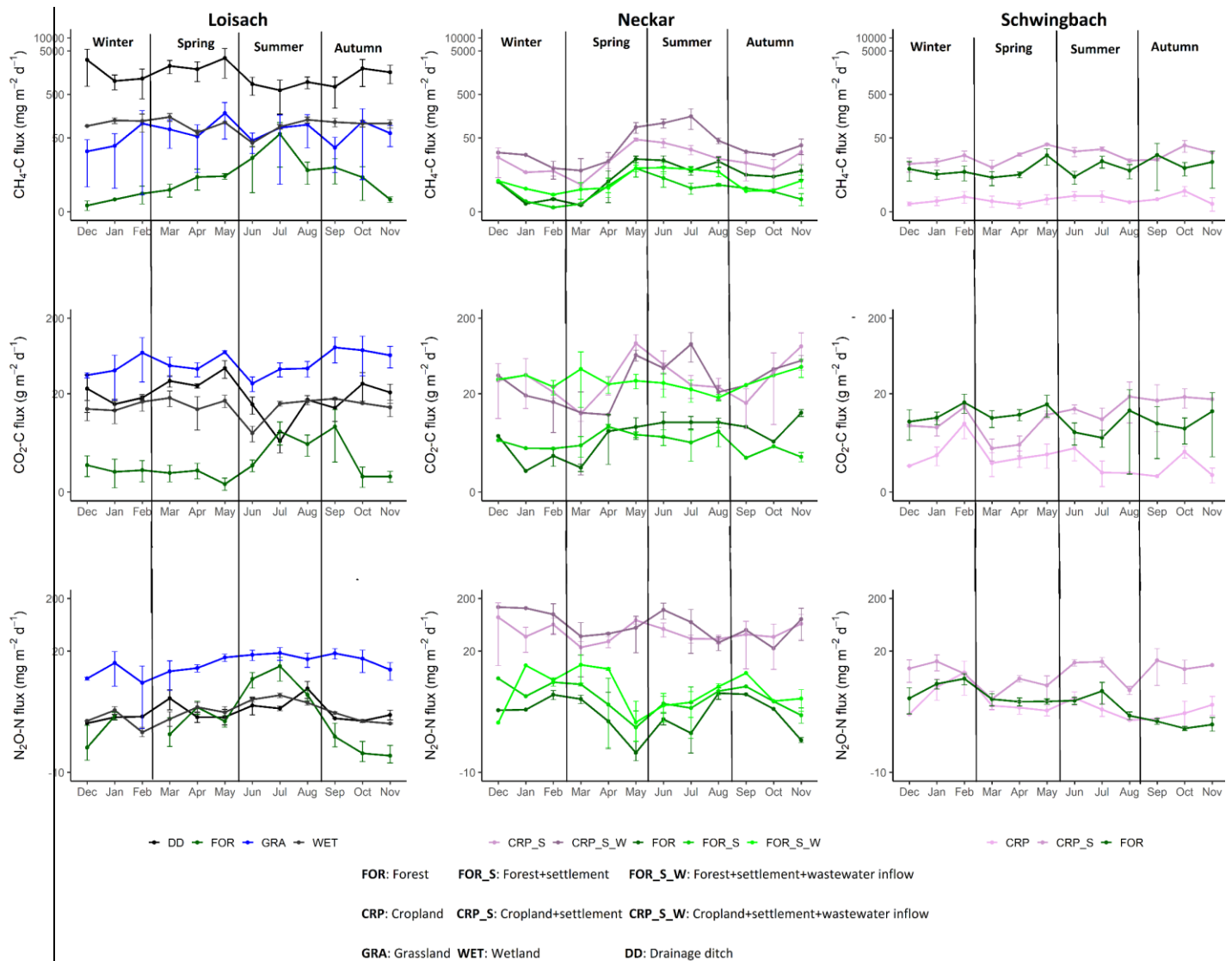


Fig. 3: Monthly mean  $\pm$  SE of  $\text{CO}_2$ ,  $\text{CH}_4$ , and  $\text{N}_2\text{O}$  fluxes across all 26 sampled streams and ditches in the Loiasach, Neckar, and Schwingbach catchments (see Table 1 methods). The colors of the lines and labels on the graph indicate the nine dominant land use classes.

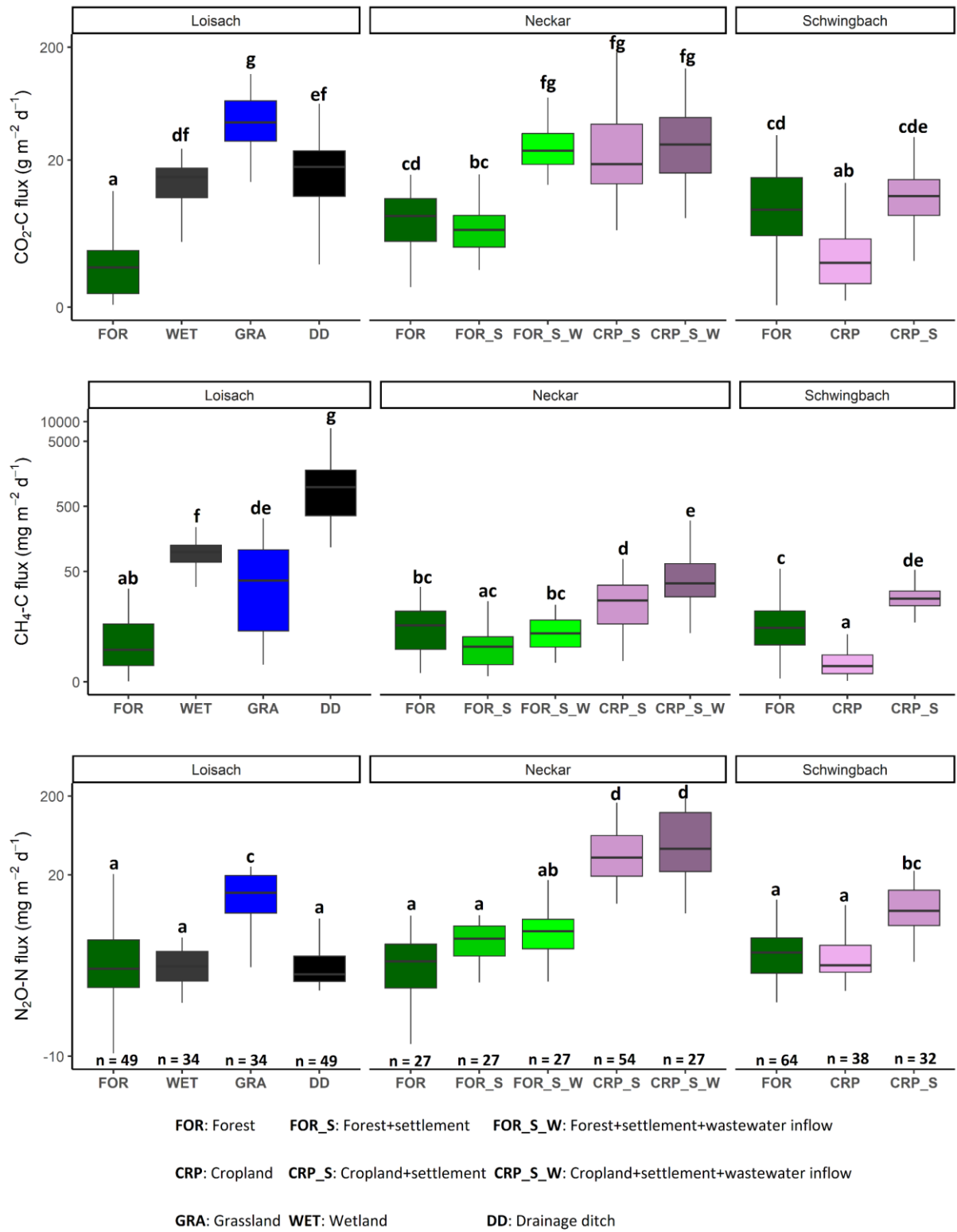
### 455 3.3.2 Land use variation

456 Like water physico-chemical variables, the variability in GHG concentrations and fluxes was more  
 457 strongly linked to catchment land use than seasonality ( $p\text{-value} < 0.001$ ; Table 2). In the Loiasach catchment,  $\text{CO}_2$   
 458 concentrations and fluxes were an order of magnitude higher for the ditch and stream sites dominated by  
 459 grassland land uses than forested-dominated sites (Fig. 3; Fig. 4; Table B3).  $\text{N}_2\text{O}$  concentrations and fluxes in  
 460 streams were also an order of magnitude higher in the grassland streams compared to the wetland and forested  
 461 ones, with the latter functioning as occasional sinks for atmospheric  $\text{N}_2\text{O}$  (Fig. 3; Fig. 4; Table B3). Wetland  
 462 streams had higher  $\text{CH}_4$  fluxes than the other streams (Fig. 3; Fig. 4; Table B3). Overall, ditches showed up to 14  
 463 times more elevated  $\text{CO}_2$  and up to 850 folds higher  $\text{CH}_4$  concentrations than the streams of the Loiasach  
 464 catchment (Fig. A3; Table B3). In contrast,  $\text{N}_2\text{O}$  concentrations in the ditches were highly variable, with higher  
 465 and lower than atmospheric concentrations over the sampling year (Fig. A2,A3).  $\text{CH}_4$  fluxes were two orders of  
 466 magnitude higher in ditches than in streams (Fig. 3; Fig. 4; Table B3). Interestingly, the ditches were even more

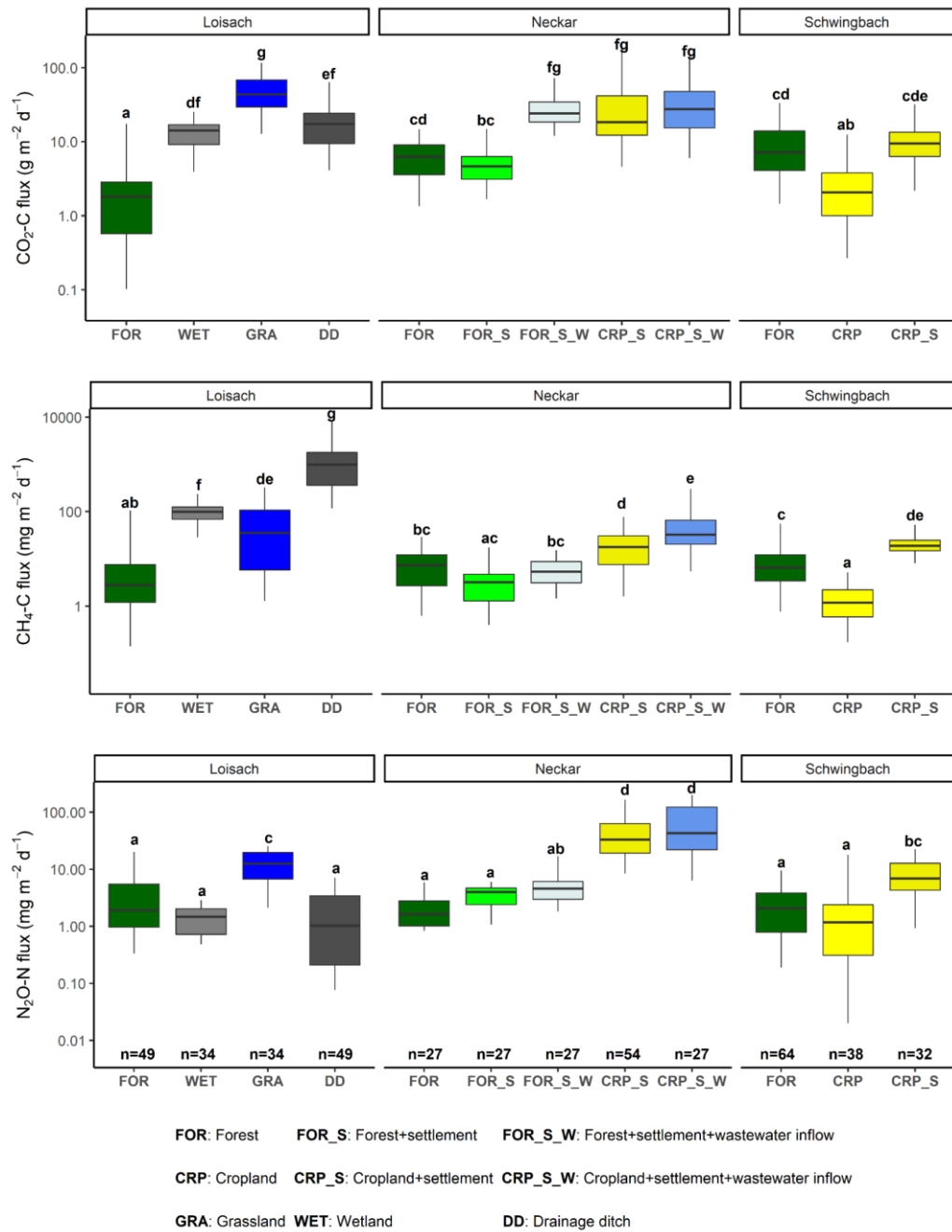
467 often N<sub>2</sub>O sinks than forests, which resulted in the overall lowest N<sub>2</sub>O fluxes, e.g., 10 times lower than the ones  
468 of grassland-dominated streams (Fig. 3; Table B3)

469 In the Neckar sub-catchments, CO<sub>2</sub>, CH<sub>4</sub>, and N<sub>2</sub>O concentrations and fluxes were 1-10 times higher in  
470 the streams located in cropland and settlement areas as compared to streams in forested areas (Fig. 3; Fig. 4; Fig.  
471 A3; Table B3). Generally, GHG concentrations and fluxes of streams in cropland and settlement areas further  
472 increased if wastewater inflows affected sampling points (Fig. 3; Fig. 4; Fig. A3; Table B3). For the latter, it is  
473 noteworthy that pronounced differences in wastewater characteristics existed in our study, even though the  
474 treatment procedures and the number of served households (80000) were comparable for the two wastewater  
475 treatment plants. Overall, the wastewater outflow in the Ammer catchment had higher TDN, DOC, CH<sub>4</sub>, and  
476 N<sub>2</sub>O concentrations than the Steinlach catchment's (Table B1). In contrast to the other two catchments, forested  
477 streams in the Schwingbach catchment had CO<sub>2</sub> and CH<sub>4</sub> concentrations and fluxes comparable to cropland and  
478 settlement-influenced streams within the catchment (Fig. 3; Fig. 4; Fig. A3; Table B3). However, N<sub>2</sub>O  
479 concentrations and fluxes were higher in streams with cropland and settlement influences than in forested  
480 streams (Fig. 3; Fig. 4; Fig. A3; Table B3).

481 In addition to land use effects, we also examined spatial variability in the GHG concentrations and  
482 fluxes linked to stream order differences. We found tendencies of higher CO<sub>2</sub>, CH<sub>4</sub>, and N<sub>2</sub>O concentrations and  
483 fluxes with increasing stream orders in the Schwingbach and Neckar catchments dominated by croplands and  
484 settlement areas. In contrast to the Neckar and Schwingbach catchments, GHG concentrations and fluxes in the  
485 more natural Loisach catchment decreased with stream order (Fig. A4). Comparing across catchments, higher  
486 stream orders (5&6) in the human-influenced Neckar catchment had higher or comparable GHG concentrations  
487 and fluxes than lower stream orders (1–3) in the Schwingbach and Loisach catchments (Fig. A4).







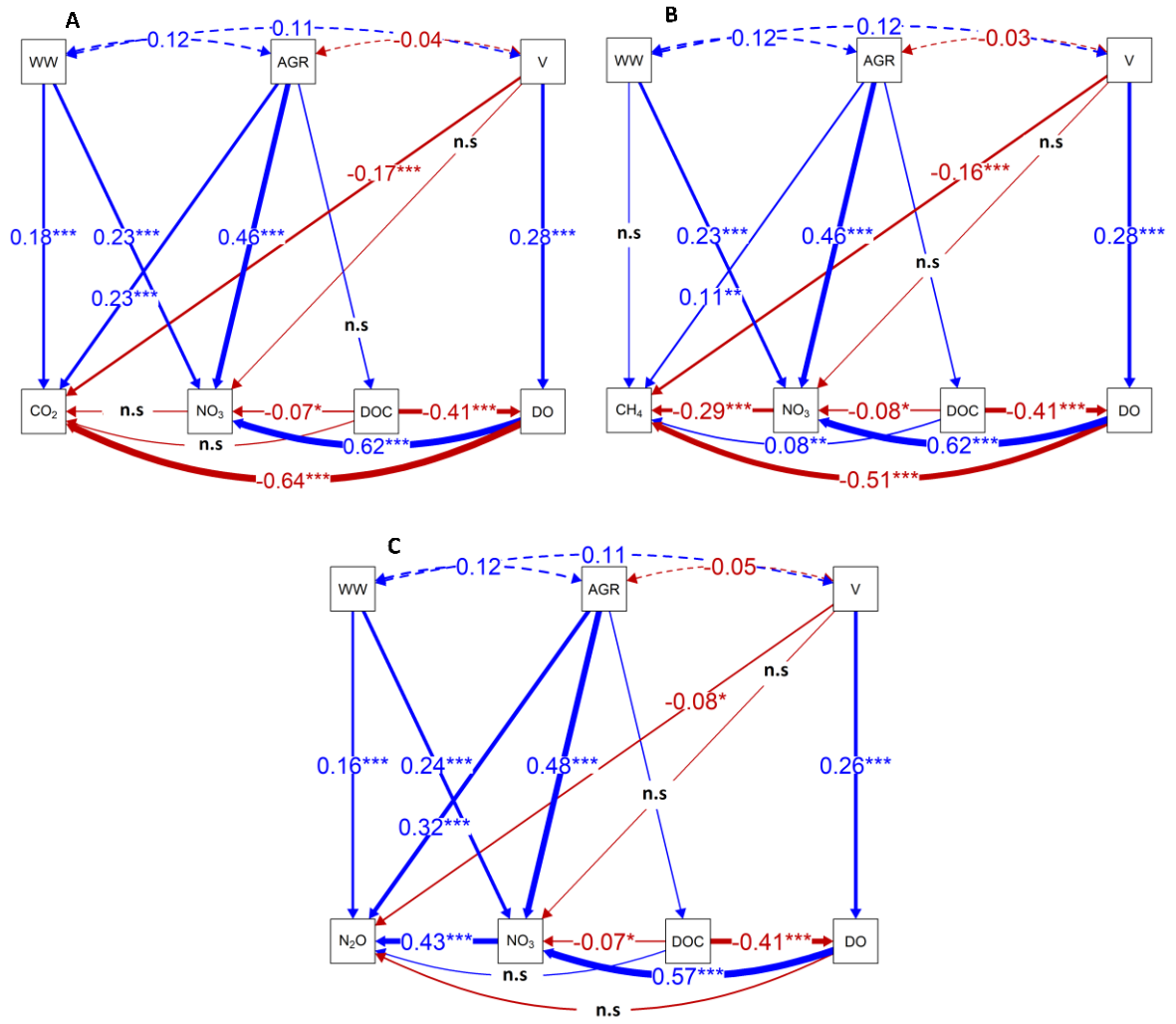
489

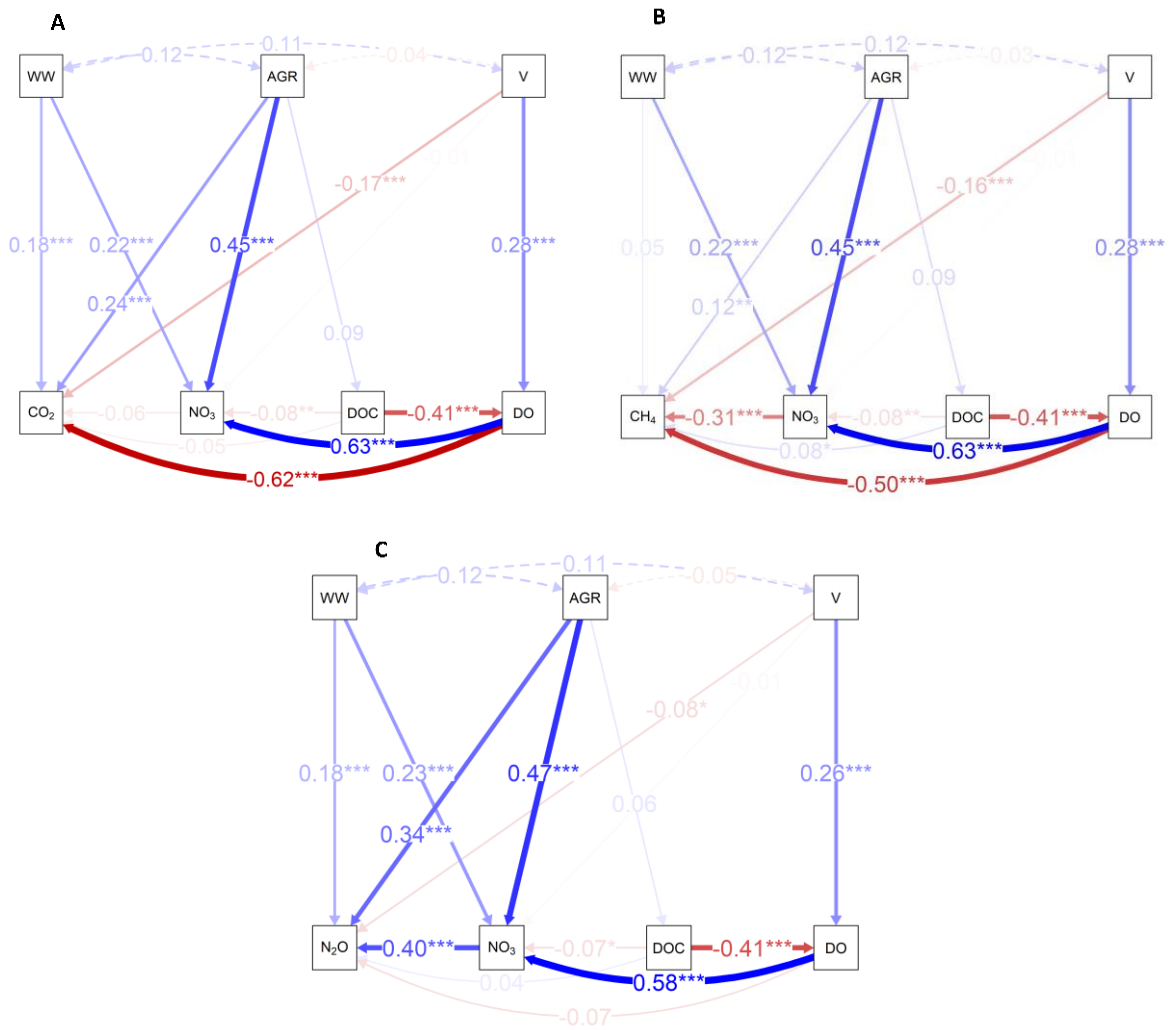
490 Fig. 4: Boxplots of CO<sub>2</sub>, CH<sub>4</sub>, and N<sub>2</sub>O fluxes in stream and ditch waters in the three catchments grouped by land  
 491 uses (see Table 1 methods). Letters on top of the boxplots represent significant differences (p < 0.05) amongst the  
 492 land use classes across the three catchments based on Tukey post-hoc analyses from the linear mixed-effects  
 493 models-models' results (Table 2).

### 494 3.4 Direct and indirect drivers of greenhouse gas concentrations

495 We used path analyses from best-fit SEMs based on all our datasets to explain how indirect  
496 environmental factors such as upstream agricultural area, wastewater inflow, and stream velocity controlled the  
497 spatial-temporal dynamics of GHG concentrations that drove the fluxes. The slopes parameter estimates from the  
498 SEMs revealed significant ( $p\text{-value}<0.05$ ) interactions between the environmental aforementioned indirect  
499 driversvariables and DO (% saturation), DOC mg L<sup>-1</sup> and NO<sub>3</sub>-N mg L<sup>-1</sup>, i.e., substrate drivers variables that  
500 directly control *in situ* GHG concentrations (Fig. 5, Table B4). In contrast to all other variables, water  
501 temperature and NH<sub>3</sub>-N mg L<sup>-1</sup> did not contribute significantly ( $p\text{-value}>0.05$ ) to the variance explained by the  
502 best-fit SEMs and were removed from the final path analyses (Table B4). That said, an increase in the  
503 upstream agricultural area resulted in a ~46% increase in *in situ* NO<sub>3</sub>-N concentrations. Wastewater inputs  
504 resulted in a ~23% increase in *in situ* NO<sub>3</sub> concentrations, while DOC concentrations were not significantly  
505 affected. DO decreased with increasing DOC concentrations, while NO<sub>3</sub>-N concentrations followed an opposite  
506 pattern and increased with increasing DO concentrations (Fig 5).

507 CO<sub>2</sub> and CH<sub>4</sub> concentrations had a negative relationship with DO (Fig 5A-B), but N<sub>2</sub>O concentrations  
508 were not significantly related to DO (Fig 5C). Besides DO, CO<sub>2</sub> concentrations decreased by 17% with stream  
509 velocity, increased by 18% with wastewater inflows, and increased by 23% with upstream agricultural area (Fig  
510 5A). CH<sub>4</sub> concentrations also decreased by 16% with increasing stream velocity. However, the effect of the  
511 increased share of agricultural areas (+11%) on CH<sub>4</sub> concentrations was lower than for CO<sub>2</sub>. Additionally, CH<sub>4</sub>  
512 concentrations also decreased by 29% with increasing NO<sub>3</sub>-N concentrations (Fig. 5B). In contrast to CO<sub>2</sub> and  
513 CH<sub>4</sub>, N<sub>2</sub>O concentrations increased by 43% with increasing NO<sub>3</sub>-N concentrations, while the effect of stream  
514 velocity was of minor importance (-8%). Compared to CH<sub>4</sub> and CO<sub>2</sub>, N<sub>2</sub>O concentrations in stream and river  
515 waters showed similar or stronger relationships to wastewater inflows (+16%) and upstream agricultural area  
516 (+32%) (Fig 5C). Overall, the best-fit SEMs explained 60, 66, and 46 % of the observed variances in CO<sub>2</sub>, CH<sub>4</sub>,  
517 and N<sub>2</sub>O concentrations, respectively (Table B4)





519

520

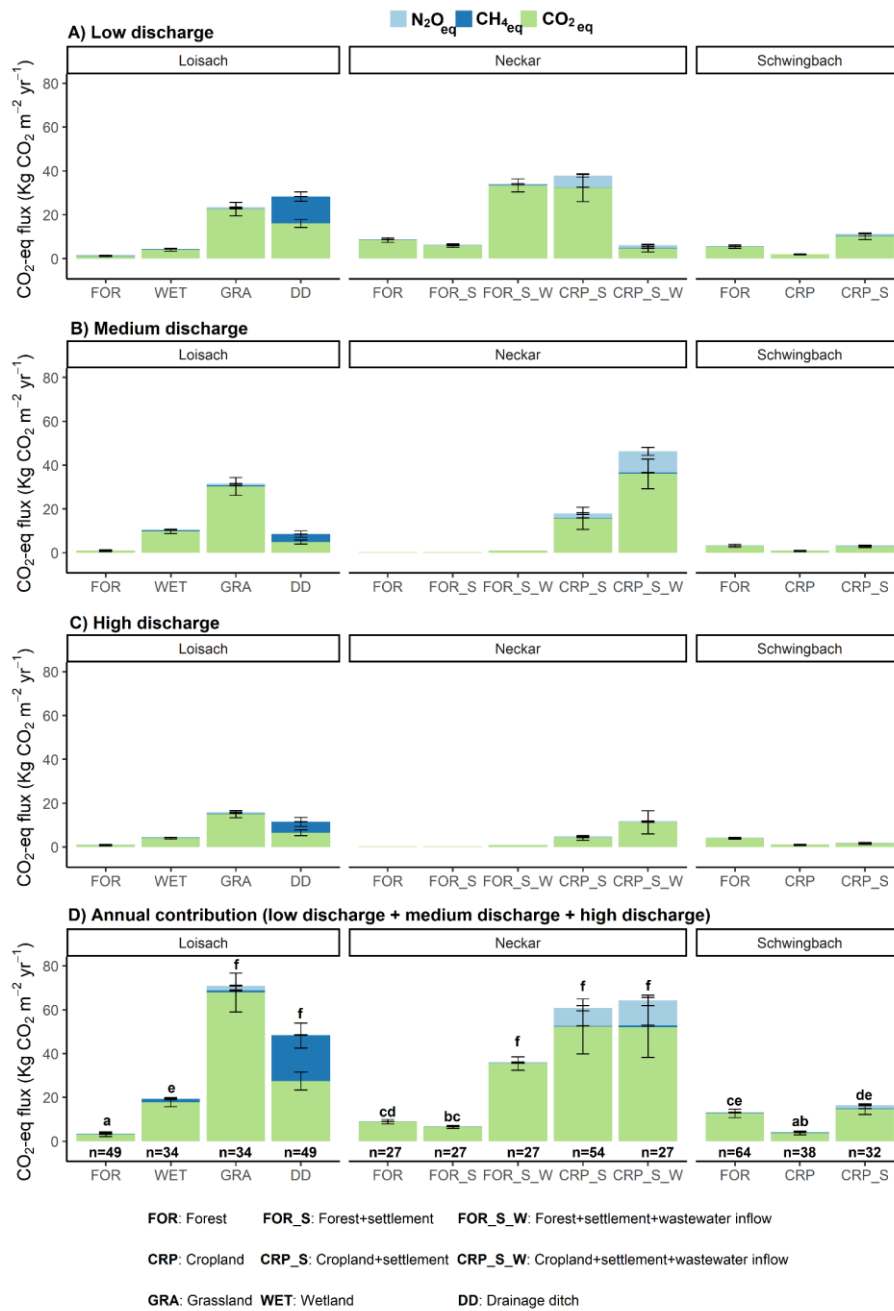
521 Fig. 5: Regression pathways predicting A)  $\text{Log}_e \text{CO}_2$  concentration  $\mu\text{g-C L}^{-1}$ , B)  $\text{Log}_e \text{CH}_4$  concentration  $\mu\text{g-C L}^{-1}$  and C)  $\text{Log}_e \text{N}_2\text{O}$  concentration  $\text{ng-N L}^{-1}$  across all sampling points and seasons from best-fit SEMs consisting  
 522 of endogenous-substrate (DO, DOC, and  $\text{NO}_3\text{-N}$ ) and exogenous-environmental variables (stream velocity (V),  
 523 percentage agricultural area (AGR; grassland+cropland areas), and wastewater inflows (WW)). The numbers on  
 524 the lines represent standardized slope parameters, with significant ( $p\text{-value} < 0.05$ ) relationships indicated by \*,  
 525 and non-significant ( $p\text{-value} > 0.05$ ) relationships indicated by *n.s.* Solid lines represent actual-fitted relationships,  
 526 while dashed lines represent co-variances in the exogenous-environmental variables. Blue lines represent positive  
 527 relationships, and red represents negative relationships, with width and color intensity representing the strength  
 528 of the relationships.

### 530 3.5 Annual areal fluxes

531 Based on global warming potential calculations,  $\text{CO}_2$  dominated the annual GHG emissions across all  
 532 headwater streams, with contributions ranging from 57 %–100%. The non- $\text{CO}_2$  gasses' contributions were much  
 533 lower and ranged from 0–43% for  $\text{CH}_4$  and 0–18% for  $\text{N}_2\text{O}$  (Fig. 6). The highest contribution of  $\text{CH}_4$  (43%) was

534 found at ditch sampling points in the Loisach, while the highest N<sub>2</sub>O contributions (up to 18%) were observed at  
535 the cropland-influenced streams fed by wastewater inflows in the Neckar sub-catchments (Fig. 6). Overall, the  
536 annual CO<sub>2</sub>-equivalent emissions from anthropogenic-influenced streams ( $\sim 71 \text{ kg CO}_2 \text{ m}^{-2} \text{ yr}^{-1}$ ) were up to 20  
537 times higher than from natural forested ~~and wetland~~ streams ( $\sim 71 \text{ kg CO}_2 \text{ m}^{-2} \text{ yr}^{-1}$  vs.  $\sim 3 \text{ kg CO}_2 \text{ m}^{-2} \text{ yr}^{-1}$   
538 ~~respectively~~; Fig. 6). It is also noteworthy that the total annual GHG emission from oligotrophic forested streams  
539 in the Loisach catchment was significantly lower than other forested catchments in the more human influenced  
540 Schwingbach and Neckar sub-catchments (Fig. 6).

541           Regarding different discharge periods, high and medium discharge periods contributed up to 91 % to  
542 total GHG emissions in anthropogenic-influenced streams but only 4% in forested streams (Fig. 6). Overall, the  
543 high and medium discharge periods contributed the most to the annual fluxes quantified in lower-order streams  
544 (Strahler 1-2) and ditch sampling points, which were prevalent in the Loisach and Schwingbach sub-catchments  
545 (Fig. 6B, C). The opposite was true for larger forested and cropland streams in the Neckar sub-catchment, where  
546 higher annual flux contributions occurred primarily in the low discharge period (Fig. 6A). However, this pattern  
547 did not hold for cropland streams with the wastewater inflows in the same catchment, with the sites showing an  
548 82% increase in annual emissions during the high and medium discharge periods (Fig. 6 B, C).



549

550 Fig. 6: Areal CO<sub>2</sub>-equivalent fluxes (mean ±SE) grouped by GHG type for each land use class during A) low, B)  
 551 medium, and C) high discharge periods. D) represents the total annual fluxes by summing up contributions from  
 552 the three discharge periods. Letters on the bar graphs represent significant differences (p<0.05) in the annual  
 553 areal emissions amongst the land use classes across the three catchments based on Tukey post-hoc analyses from  
 554 the linear mixed-effects models' results (Table 2)

## 4 Discussion

The GHG fluxes quantified from headwater streams and ditches in this study add to the growing evidence that both aquatic ecosystems are significant net emitters of GHGs to the atmosphere. In agreement with previous studies, CO<sub>2</sub> accounted for most (>81 %) of the annual fluvial GHG fluxes in CO<sub>2</sub> equivalents (e.g., Marescaux et al., 2018; Mwanake et al., 2022; Li et al., 2021). However, the presence of upstream agricultural and settlement areas seemed to alter these trends by reducing the contribution of CO<sub>2</sub> and increasing N<sub>2</sub>O and CH<sub>4</sub> contributions. The effects of the above anthropogenic activities on aquatic GHG dynamics were twofold. Drainage ditches were landscape hotspots for CH<sub>4</sub> emissions, while increasing upstream agricultural and settlement areas resulted in fluvial N<sub>2</sub>O hotspots. The emissions from human-influenced streams were further supplemented by wastewater inflows, which provided year-long nutrients, labile carbon, and GHGs supplies, resulting in much higher CO<sub>2</sub> and N<sub>2</sub>O annual emissions. Besides influencing GHG hotspots, the temporal dynamics observed seasonality of GHG fluxes from streams and ditches in our study were further impacted by anthropogenic influences land use across the three investigated catchments, with. While catchments dominated by wetlands or forested areas exhibited low seasonal variabilities due to limitations in conditions that favor peak emissions (increased gas transfer velocities and sufficient GHG supplies), opposite trends were found at catchments dominated by agricultural and settlement areas or affected by wastewater inflow. These sub-catchments dominated by wetlands or forested land uses exhibiting lower seasonal variabilities than sub-catchments dominated by agricultural land use or affected by wastewater inflow findings suggested that the occasional peak GHG emissions in the later catchments represented periods where external GHG sources from supersaturated terrestrial soils or wastewater inflows outweighed supply constraints during peak discharge periods with high gas transfer velocities. These findings suggest that future land use changes from natural forests to agricultural and settlement areas may increase the radiative forcing of aquatic GHG emissions by increasing the magnitudes of their annual fluxes, especially in a changing climate with more extreme discharge conditions. (Fig. 3).

### 3.64.1 Seasonal variability in GHG concentrations and fluxes

~~The GHG fluxes quantified from headwater streams and ditches in the three catchments in central and southern Germany add to the growing evidence that both aquatic ecosystems are significant net emitters of GHGs to the atmosphere. Seasonal trends in *in situ* GHG concentrations and fluxes were mainly linked to substrate availability (C and N), discharge, and temperature, similar to previous studies on other streams in temperate climates (Dismore et al., 2013; Herreid et al., 2021). However, the observed seasonality of GHG fluxes from streams and ditches in our study was further impacted by land use across the three investigated catchments, with sub-catchments dominated by wetlands or forested land uses exhibiting lower seasonal variabilities than sub-catchments dominated by agricultural land use or affected by wastewater inflow (Fig. 3).~~

The low *in situ* CO<sub>2</sub> concentrations (< 100% saturation) during summer (Table B2) suggested elevated photosynthetic uptake within the streams and ditches, which is in line with the results of a recent meta-analysis on lotic ecosystems (Gómez-Gener et al., 2021). The decline in CO<sub>2</sub> concentrations in summer was most obvious apparent at the non-forested stream sampling points, with higher canopy cover in the forested areas likely limiting *in situ* stream photosynthesis due to shading effects. We also found that stream ditch waters were

593 oversaturated with CO<sub>2</sub> in autumn and winter. These seasons are characterized on the one hand by low discharge  
594 and low stream velocity, conditions which likely reduce degassing rates, and on the other hand by elevated *in*  
595 *situ* C metabolism, as supported by low DO concentration in autumn, which indicates respiratory O<sub>2</sub>  
596 consumption (e.g., Borges et al., 2018). We attribute the lack of seasonality in CO<sub>2</sub> fluxes (Table B2) to the  
597 compensatory effects of seasonally varying stream velocities and CO<sub>2</sub> source strengths. For example, high CO<sub>2</sub>  
598 concentrations and low gas transfer velocities in autumn and vice versa in spring resulted in comparable CO<sub>2</sub>  
599 fluxes in the two seasons (Table B2).

600 N<sub>2</sub>O concentrations also varied significantly across seasons, but the pattern differed from that of CO<sub>2</sub>. In  
601 autumn, forested lower-order streams in the Loisach and Schwingbach catchments mainly showed N<sub>2</sub>O  
602 concentrations below atmospheric background concentrations and were temporary sinks of N<sub>2</sub>O (Fig. 3). This  
603 finding could be related to increased inputs of organic matter in these headwater catchments due to leaf fall,  
604 providing additional organic carbon for microbial metabolism in this period, which likely increased the demand  
605 for terminal electron acceptors such as O<sub>2</sub>, NO<sub>3</sub>, as well as N<sub>2</sub>O. This conclusion is also supported by the lowest  
606 DO and NO<sub>3</sub>-N concentrations during autumn, which could suggest the dominance of complete denitrification in  
607 the streams (Quick et al., 2019). With decreasing temperatures towards winter, lower productivity and N demand  
608 within the streams resulted in the accumulation of NO<sub>3</sub>-N, which seemed to favor internal N<sub>2</sub>O production, as  
609 seen by the positive relationship between the two variables (Fig. 5C). The high sensitivity of the N<sub>2</sub>O reductase  
610 to low temperatures might have further supported elevated N<sub>2</sub>O concentration and fluxes during winter (e.g.,  
611 Holtan-Hartwig et al., 2002). A similar finding of high winter N<sub>2</sub>O concentrations and fluxes was also found in  
612 other temperate streams, alluding to similar controls of temperature and nutrient availability (Herreid et al.,  
613 2021; Galantini et al., 2021). Thus, based on our results, winter periods can significantly contribute to annual  
614 N<sub>2</sub>O emission budgets. Yet, to the best of our knowledge, temperate studies covering the winter period are still  
615 scarce. In contrast to CO<sub>2</sub> and N<sub>2</sub>O, neither CH<sub>4</sub> concentrations nor fluxes showed any seasonal trends. Such a  
616 finding is similar to what was found in a global meta-analysis (Stanley et al., 2016), where multiple controls  
617 related to substrate availability, geomorphology, and hydrology were shown to result in a high spatial-temporal  
618 variance of CH<sub>4</sub>, thus masking any seasonal emission patterns.

### 619 **3.74.2 Effect of human impacts on GHG concentrations and fluxes**

620 Anthropogenic-influenced streams and ditches draining predominantly agricultural and settlement areas  
621 showed higher CO<sub>2</sub>-equivalent GHG emissions than forested streams (Fig. 6). Such a finding is similar to other  
622 studies in the temperate region (e.g., Borges et al., 2018; Galantini et al., 2021). The high GHG emissions of  
623 streams and ditches in agricultural and settlement areas are likely due to elevated hydrological inflow (e.g., via  
624 groundwater and interflow) of nitrogen and labile carbon (Lambert et al., 2017; Mwanake et al., 2019) or  
625 terrestrially originating dissolved GHGs linked to lower vegetation cover compared to forested catchments (e.g.,  
626 Mwanake et al., 2022). This interpretation could be supported by the significant positive relationships that we  
627 found between percentage agriculture and stream CO<sub>2</sub>, CH<sub>4</sub>, and N<sub>2</sub>O, as well as nitrate concentration and a  
628 positive trend for DOC (Figure 5).

629 Low DOC: DON ratios have been previously linked to more labile and less aromatic forms of dissolved  
630 organic matter (DOM) (Sebestyen et al., 2008; O'Donnell et al., 2010). We found significantly lower DOC:



631 DON ratios in streams and ditches in agricultural and settlement areas than in forested streams, suggesting that  
 632 the more bioavailable DOM in the human-influenced ecosystems favored elevated GHGs production through  
 633 heterotrophic processes (e.g., Bodmer et al., 2016). Such differences in DOC: DON ratios were also found  
 634 amongst forested streams, with a decreasing trend from Loisach, Neckar to Schwingbach catchments, which may  
 635 also explain the differences in their GHG emissions (Fig. 6). The differences in the DOM bioavailability of  
 636 forested streams in the three catchments may suggest differences in DOM flow paths during terrestrial-  
 637 groundwater-stream interactions. We contend that the moderately sloping streams of the Neckar and  
 638 Schwingbach catchments likely had lower DOC: DON ratios due to longer water residence time and higher  
 639 contributions of groundwater inflow (e.g., Sebestyen et al., 2008) than those in the steeper forested catchments of  
 640 the Loisach (Table B3). The distinct difference in water stable isotope signatures, i.e., the shift of precipitation  
 641 vs. stream water seasonality across the three catchments (data not shown), further supported the difference in  
 642 water residence times and their relationships with stream slope (e.g., Zhou et al., 2021).

643 In addition to land use influences, wastewater inflows into streams in agricultural and settlement areas  
 644 further increased GHG concentrations and fluxes. The two sampled wastewater effluents, which drained into the  
 645 Steinlach and Ammer streams of the Neckar sub-catchments, showed higher GHG concentrations than the  
 646 stream water upstream of the inflows (Fig. A5, Table B1), which mainly led to increased GHG concentration and  
 647 fluxes also downstream of the wastewater inflows. This finding is similar to what was found in other temperate  
 648 studies comparing stream GHG concentration upstream and downstream of wastewater inflows (e.g., Marescaux  
 649 et al., 2018; Aho et al., 2022). However, due to higher background GHG fluxes in the cropland than in the  
 650 forested sub-catchments (Fig. 4), differences in the total GHG emissions before and after wastewater inflow  
 651 were more pronounced in the forested sub-catchments (Fig. 6). In addition to the pronounced differences in the  
 652 quality of the wastewater effluent (Table B1), this finding also shows the importance of background GHG fluxes  
 653 as influenced by catchment land use in assessing how wastewater inflows affect riverine GHG emissions.

654 Apart from land use influences, GHG fluxes from streams have been previously shown to decrease  
 655 with stream order, as dissolved GHG inputs from groundwater and terrestrial sources also reduce (e.g., Hotchkiss  
 656 et al., 2015; Turner et al., 2015; Mwanake et al., 2022). While our study design was not meant to explicitly  
 657 assess stream order influences due to limited replication across a wide range of stream orders, we did find an  
 658 opposite trend with stream order, similar to other studies in anthropogenic-influenced catchments (e.g., Borges et  
 659 al., 2018; -Marescaux et al., 2018). For example, higher-order streams (stream orders > 5) in the Neckar sub-  
 660 catchments dominated by croplands and with wastewater influences had mostly-either higher or comparable  
 661 GHG fluxes than lower-order streams (stream orders < 3) in the Loisach and Schwingbach catchments. We  
 662 therefore, therefore, show a potential breakdown of stream order-GHG relationships in highly human-impacted  
 663 lotic ecosystems, with disproportionately higher GHG emissions than in more natural ecosystems. We also show  
 664 that significant nutrient and labile carbon supplies to higher-order streams, which create ideal conditions for  
 665 GHG production and emission, may outweigh the physical disadvantages (e.g., lower surface area to volume  
 666 ratio) of higher-order streams relative to lower-order streams.

667 Drainage ditches, characterized by low flow velocities and high DOC: DIN ratios, functioned as strong  
 668 sources of CO<sub>2</sub> and CH<sub>4</sub> fluxes compared to streams. In addition to draining CO<sub>2</sub> and CH<sub>4</sub>-rich wetland and  
 669 grassland soils, wWe assume that the low DO, high DOC, and low NO<sub>3</sub>-N concentrations, along with high water  
 670 retention times, supported high *in situ* CH<sub>4</sub> production rates in the ditch sediments, resulting in their overall

671 highest contribution of CH<sub>4</sub> fluxes to total annual GHG emission budgets than streams (Figure 6). This  
672 interpretation is further supported by a significant negative relationship between CH<sub>4</sub> and DO, as well as NO<sub>3</sub>-N  
673 concentrations, and a positive relationship with DOC concentrations, associations which have also been  
674 previously linked to *in situ* methane production in fluvial ecosystems (e.g., Baulch et al., 2011b; Schade et al.,  
675 2016). High CH<sub>4</sub> fluxes from drainage ditches were also found in other studies from both forested and wetland  
676 areas (e.g., Schrier-Uijl et al., 2011; Peacock et al., 2021b). Contrastingly, ditches were only weak sources or  
677 even sinks for atmospheric N<sub>2</sub>O. This finding suggests N<sub>2</sub>O reduction to N<sub>2</sub> via complete denitrification, an  
678 interpretation already made in previous studies on lotic ecosystems (e.g., Baulch et al., 2011; Mwanake et al.,  
679 2019).

### 680 **3.84.3 Comparison of GHG flux magnitudes with regional and global ~~other regional~~ studies**

681 This study's daily CH<sub>4</sub> and N<sub>2</sub>O diffusive flux ranges from both streams and ditches are mostly within  
682 the same order of magnitude as those previously reported in global synthesis studies (Table 3: Hu et al., 2016;  
683 Stanley et al., 2016). In contrast, ~~This~~ this study reported among the highest fluvial CO<sub>2</sub> emissions compared to  
684 other ~~regional studies and global studies~~, with significant mean fluxes of up to 51 g-C m<sup>-2</sup> d<sup>-1</sup> (Table 43). We  
685 attribute this finding to moderate-steep slopes such as those quantified in the mountainous streams of the Loisach  
686 catchment or diffuse and point terrestrial dissolved CO<sub>2</sub> GHG inputs from the more human-influenced  
687 Schwingbach and Neckar catchments, translating to higher fluvial CO<sub>2</sub> GHG fluxes (Fig. 6). However, our high  
688 CO<sub>2</sub> fluxes are comparable with those quantified from other temperate streams in Canada and Switzerland with  
689 similar moderate-steep slopes and considerable dissolved CO<sub>2</sub> inputs from terrestrial landscapes (e.g., Mcdowell  
690 & Johnson. 2018; Horgby et al., 2019). The CH<sub>4</sub> fluxes from streams in this study are comparable with those  
691 previously found in temperate sub-catchments with similar land uses and altitudes, but are lower than those  
692 reported from permafrost streams in China (Table 3; Zhang et al., 2020). Our N<sub>2</sub>O fluxes from cropland,  
693 settlement, and wastewater-influenced streams are higher than those previously reported in a mixed land use  
694 catchment (Schade et al., 2016). Still, our forest N<sub>2</sub>O fluxes are in the same range as those of other temperate  
695 forested streams (Aho et al., 2022). That said, these comparisons may be hampered, particularly for fluvial N<sub>2</sub>O  
696 fluxes, by the limited number of available studies (Table 3).

697 The average ditch CH<sub>4</sub> fluxes in this study are higher than those reported for forest and wetland draining  
698 ditches in boreal and temperate regions (Table 3: Schrier-Uijl et al., 2011, Peacock et al., 2021a) and the global  
699 mean provided by Peacock et al., (2021), which includes estimates from large canals. In contrast, N<sub>2</sub>O fluxes

700 from ditches in this study are lower than those quantified from NO<sub>3</sub>-N-rich agricultural ditches in temperate  
701 regions (Table 3: Reay et al., 2003).

Table 43: Compilation of GHG emissions from temperate streams and ditches with comparable land use, climate, and altitude ranges.

Land use/ land cover	Climate	Country	Geographical coordinates	Altitude (m)	Number of study reaches	Number of observations	CO <sub>2</sub> -C flux (g m <sup>-2</sup> d <sup>-1</sup> )			CH <sub>4</sub> -C flux (mg m <sup>-2</sup> d <sup>-1</sup> )			N <sub>2</sub> O-N flux (mg m <sup>-2</sup> d <sup>-1</sup> )			Reference		
							Range	Mean	Duration of study	Range	Mean	Duration of study	Range	Mean	Duration of study		Range	Mean
Forest/Loisach streams	Temperate	Germany	Table 1	616–2963	3	51	-0.05–17.4	2.4	Annual, 2022	-0.4–164	10.5	-9.2–20.3	1.1	This study				
Forest/Schwingbach streams	Temperate	Germany	Table 1	176–480	5	27	0.08–33.4	9.5	Annual, 2022	-0.02–54.6	9.9	-1.6–9.6	2.1	This study				
Forest/Neckar rivers	Temperate	Germany	Table 1	319–610	1	80	0.6–14.7	6.6	Annual, 2022	0.6–28.9	9.1	-6.9–5.9	0.3	This study				
Forest+settlement/Neckar rivers	Temperate	Germany	Table 1	319–610	1	27	0.6–14.9	4.9	Annual, 2022	0.4–17.3	3.9	-7.7–6.0	2.2	This study				
Forest+settlement+wastewater/Neckar rivers	Temperate	Germany	Table 1	319–610	1	27	12–71.7	28.3	Annual, 2022	1.4–15.2	6.5	-2.8–17.1	3.9	This study				
Wetland/Loisach streams	Temperate	Germany	Table 1	616–2963	2	34	2.8–25.2	13.3	Annual, 2022	17.2–237.5	101.7	-1.6–2.9	0.8	This study				
Grassland/Loisach streams	Temperate	Germany	Table 1	616–2963	2	34	6.1–115.9	50.7	Annual, 2022	1.3–324.5	73.2	-0.8–25.5	12.4	This study				
Cropland/Schwingbach streams	Temperate	Germany	Table 1	176–480	3	48	0.3–9.0	2.1	Annual, 2022	0.07–5.6	0.9	-0.8–18	1.9	This study				
Cropland+settlement/Schwingbach streams	Temperate	Germany	Table 1	176–480	2	32	0.6–32.0	8.6	Annual, 2022	0.6–52.6	14.9	-0.8–22.4	6.5	This study				
Cropland+settlement/Neckar rivers	Temperate	Germany	Table 1	319–610	2	54	4.5–181.3	39.1	Annual, 2022	1.6–77.5	21	8.4–165.7	46.9	This study				
Cropland+settlement+wastewater/Neckar rivers	Temperate	Germany	Table 1	319–610	1	27	1.1–129.9	38.8	Annual, 2022	0.8–301.9	58.2	6.3–198.2	67.6	This study				
Forest streams	Temperate	USA	43.0760° N, 107.2903° W	1211–3311	1	253	1.5–6.79	1.3	June–October, 2014	14.4–576	28.8			Kuhn et al., 2017				
Forest streams	Temperate	USA	40.2140° N, 105.4332° W	2780–3505	2	11	0.2–1.6	0.49	June–July, 2013	0.3–7.8	2.1			Crawford et al., 2015				
Forest streams	Temperate	USA	41.6032° N, 73.0877° W	270–810	7	608			4 years, 2016–2019			-0.4–29		Abo et al., 2022				
Forest streams	Temperate	USA	41.6032° N, 73.0877° W	270–810	7	608	-1.2–152	3.4	4 years, 2016–2019	0.3–2870	28.7			Abo et al., 2021				
Forest streams	Temperate	Canada	49.270° N, 122.560° W	1200–3050	1		8.7–1980	55.9	Annual, 2017					McDowell and Johnson, 2018				
Mixed streams	Temperate	USA	43.123° N, 71.1219° W	165–348	3	37		0.4–1.1	Annual, 2012	6–43.8				Schade et al., 2016				
Mixed streams	Temperate	Switzerland	46.1512° N, 7.0634° E	1190–3051	1	300	13.3–494.5	31	Annual, 2016					Forgy et al., 2019				
Mixed streams	Temperate	Europe			34	107	-0.8–5.8		Annual, 2017					Attermeier et al., 2021				
Grassland drainage ditches	Temperate	Netherlands	Table 1	616–2963	3	50	2–63.3	13.7	Annual, 2022	116.6–7933	1532	-0.8–7.1	1.2	This study				
Wetland drainage ditches	Temperate	Scotland	52.2200° N, 4.5300° E	1–10	7	14		0.8	June–July, 2009		606.6			Schrier-Ujji et al., 2011				
Agricultural drainage ditches	Temperate	Scotland	65.5000° N, 3.2400° W	58–68	10	22			June–November, 2001			1.5–15.3	2.5	Reay et al., 2003				

Land use/ land cover	Climate	Country	Geographical coordinates	Altitude (m)	Number of study reaches	Number of observations	Duration of study	CO <sub>2</sub> -C flux (g m <sup>-2</sup> d <sup>-1</sup> )			CH <sub>4</sub> -C flux (mg m <sup>-2</sup> d <sup>-1</sup> )			N <sub>2</sub> O-N flux (mg m <sup>-2</sup> d <sup>-1</sup> )			Reference
								Range	Mean	Standard deviation	Range	Mean	Standard deviation	Range	Mean	Standard deviation	
Forest/Loisach streams	Temperate	Germany	Table 1	616–2963	3	51	Annual, 2022	-0.05–17.4	2.4	-0.4–164	10.5	-9.2–20.3	1.1	This study			
Forest/Schwabach streams	Temperate	Germany	Table 1	176–480	5	27	Annual, 2022	0.08–33.4	9.5	-0.02–54.6	9.9	-1.6–9.6	2.1	This study			
Forest/Neckar rivers	Temperate	Germany	Table 1	319–610	1	80	Annual, 2022	0.6–14.7	6.6	0.6–28.9	9.1	-6.9–5.9	0.3	This study			
Forest-settlement/Neckar rivers	Temperate	Germany	Table 1	319–610	1	27	Annual, 2022	0.6–14.9	4.9	0.4–17.3	3.9	-7.7–6.0	2.2	This study			
Wetland/Loisach streams	Temperate	Germany	Table 1	616–2963	2	34	Annual, 2022	12–71.7	28.3	1.4–15.2	6.5	-2.8–17.1	3.9	This study			
Grassland/Loisach streams	Temperate	Germany	Table 1	616–2963	2	34	Annual, 2022	2.8–25.2	13.3	17.2–237.5	101.7	-1.6–2.9	0.8	This study			
Cropland/Schwabach streams	Temperate	Germany	Table 1	176–480	3	48	Annual, 2022	6.1–115.9	50.7	1.3–324.5	73.2	-0.8–25.5	12.4	This study			
Cropland-settlement/Schwabach streams	Temperate	Germany	Table 1	176–480	2	32	Annual, 2022	0.3–9.0	2.1	0.07–5.6	0.9	-0.8–18	1.9	This study			
Cropland-settlement/Neckar rivers	Temperate	Germany	Table 1	319–610	2	54	Annual, 2022	0.6–32.0	8.6	0.6–52.6	14.9	-0.8–22.4	6.5	This study			
Cropland-settlement/wastewater/Neckar rivers	Temperate	Germany	Table 1	319–610	1	27	Annual, 2022	4.5–181.3	39.1	1.6–77.5	21	8.4–165.7	46.9	This study			
Forest streams	Temperate	USA	43.0760° N, 107.2903° W	1211–3311	1	253	June–October, 2014	1.1–129.9	38.8	0.8–301.9	58.2	6.3–198.2	67.6	This study			
Forest streams	Temperate	USA	40.2140° N, 105.4332° W	2780–3505	2	11	June–July, 2013	1.5–6.79	1.3	14.4–576	28.8	-0.4–29		Kuhn et al., 2017			
Forest streams	Temperate	USA	41.6032° N, 73.0877° W	270–810	7	608	4 years, 2016–2019	0.2–1.6	0.49	0.3–7.8	2.1			Crawford et al., 2015			
Forest streams	Temperate	USA	41.6032° N, 73.0877° W	270–810	7	608	4 years, 2016–2019	-1.2–152	3.4	0.3–2870	28.7			Alto et al., 2022			
Forest streams	Temperate	Canada	49.270° N, 122.560° W	1200–3050	1	37	Annual, 2017	8.7–1980	55.9					Alto et al., 2021			
Mixed streams	Temperate	USA	43.123° N, 71.1219° W	165–348	3	300	Annual, 2012	0.4–1.1						Meadwell and Johnson, 2018			
Mixed streams	Temperate	Switzerland	46.1512° N, 7.0634° E	1190–3051	1	107	Annual, 2016	13.3–494.5	31	6–43.8				Schude et al., 2016			
Mixed streams	Temperate	Europe			34	107	Annual, 2017	-0.8–5.8		0.5–8820				Horghy et al., 2019			
Wetland streams	Subtropical	China	33.0000° N, 88.0000° E	1659–4600	4	17	3 years, 2016–2018		2.9		100.8			Zhang et al., 2020			
	Global													Li et al., 2021			
	Global													Hu et al., 2016			
	Global													Stanley et al., 2016			
Drainage ditches	Global				64												
Grassland drainage ditches	Temperate		Table 1	616–2963	3	50	Annual, 2022	2–63.3	13.7	0.2–793	130	-0.8–7.1	1.2	Peacock et al., 2021			
Forest drainage ditches	Hemiboreal	Sweden	59.5129° N, 17.3844° E	21–65	109	109	June–August, 2020	0.2–3.3		116.6–7933	1532			This study			
Wetland drainage ditches	Temperate	Netherlands	52.2200° N, 4.5300° E	1–10	7	14	June–July, 2009	0.2–53		0.2–53				Peacock et al., 2021a			
Agricultural drainage ditches	Temperate	Scotland	65.5000° N, 3.2400° W	58–68	10	22	June–November, 2001		0.8	606.6		1.5–15.3	2.5	Schrier-Ujji et al., 2011			

## 705 Conclusions

706 ~~Compared to forests and wetlands, streams and ditches in agricultural and settlement areas were~~  
707 ~~characterized by significantly higher GHG fluxes with greater intra-annual variability. Streams and ditches in~~  
708 ~~agricultural and settlement areas were characterized by significantly higher GHG fluxes with more significant~~  
709 ~~intra-annual variabilities than forests and wetlands. A combination of wastewater inflows and agricultural land~~  
710 ~~use resulted in the highest fluvial CO<sub>2</sub>, CH<sub>4</sub>, and N<sub>2</sub>O fluxes, particularly during high discharge periods with~~  
711 ~~substantial external dissolved GHGs. In general, anthropogenic activities resulted in a potential breakdown of the~~  
712 ~~expected decrease of the GHG source strengths with increasing stream order, as higher-order streams in the~~  
713 ~~Neckar sub-catchments with cropland and settlement influences had either higher or comparable concentrations~~  
714 ~~and fluxes than small streams in the Loisach and Schwingbach catchments. As most studies use stream order to~~  
715 ~~upscale local and regional riverine fluxes, we show from our results that caution must be taken in applying the~~  
716 ~~methodology, particularly across catchments differing in land use intensity.~~

717 ~~Our findings indicate that future work should focus more on human-influenced headwater stream~~  
718 ~~ecosystems, as they contribute disproportionately large annual fluxes and are more temporally variable than~~  
719 ~~natural ones. Our study also found higher winter N<sub>2</sub>O fluxes, emphasizing the need for continuous sampling~~  
720 ~~regimes covering full years to reduce uncertainty in annual GHG emission estimates. Combining continuous~~  
721 ~~sampling regimes of all three biogenic GHGs (CO<sub>2</sub>, N<sub>2</sub>O, and CH<sub>4</sub>) across catchments with contrasting land uses~~  
722 ~~will further constrict riverine emissions and aid in developing targeted emission reduction mitigation strategies.~~  
723 ~~A combination of wastewater inflows and agricultural land use resulted in the highest riverine CO<sub>2</sub> and N<sub>2</sub>O~~  
724 ~~fluxes, particularly during high discharge periods with substantial contributions of external dissolved GHGs. In~~  
725 ~~general, anthropogenic activities resulted in a potential breakdown of the expected decrease of the GHG source~~  
726 ~~strengths with increasing stream order, as higher order streams in the Neckar sub-catchments with cropland and~~  
727 ~~settlement influences had higher concentrations and areal fluxes than small streams in the Loisach and~~  
728 ~~Schwingbach catchments. As most studies use stream order to upscale local and regional riverine fluxes, we~~  
729 ~~show from our results that caution must be taken in applying the methodology, particularly across catchments~~  
730 ~~differing in land use intensity.~~

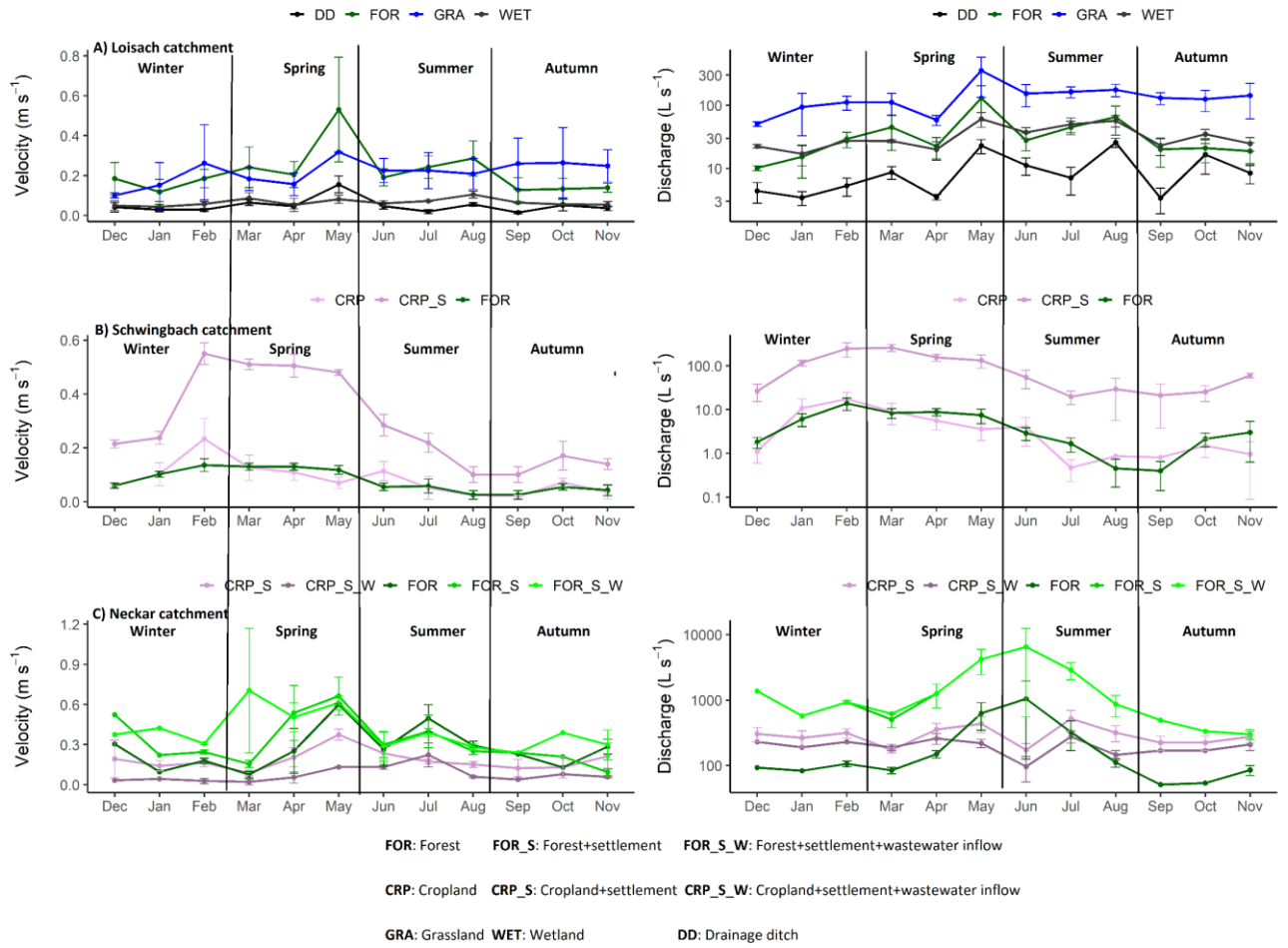
731 ~~In general, our findings indicate that future work should focus more on human-influenced headwater~~  
732 ~~stream ecosystems, as they contribute disproportionately large annual fluxes and are more temporally variable~~  
733 ~~than natural ones. Our study also found higher winter N<sub>2</sub>O fluxes, emphasizing the need for continuous sampling~~  
734 ~~regimes covering full years in order to reduce uncertainty in annual GHG emission estimates. Combining~~  
735 ~~continuous sampling regimes of all three biogenic GHGs (CO<sub>2</sub>, N<sub>2</sub>O, and CH<sub>4</sub>) across catchments with~~  
736 ~~contrasting land uses will further constrict riverine emissions and aid in developing targeted emission reduction~~  
737 ~~mitigation strategies.~~

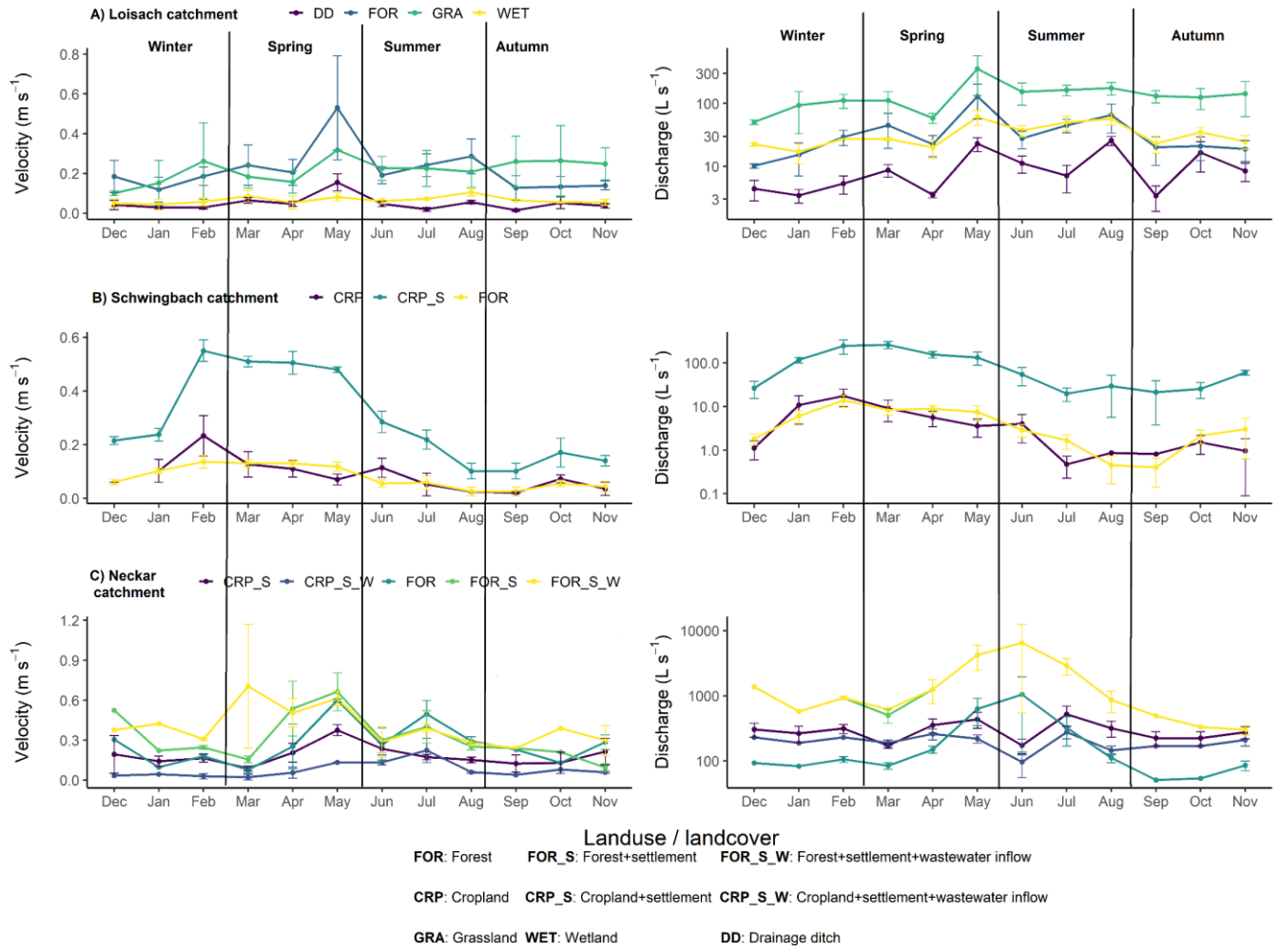


738      **Appendices**

739      **Appendix A: Figures**



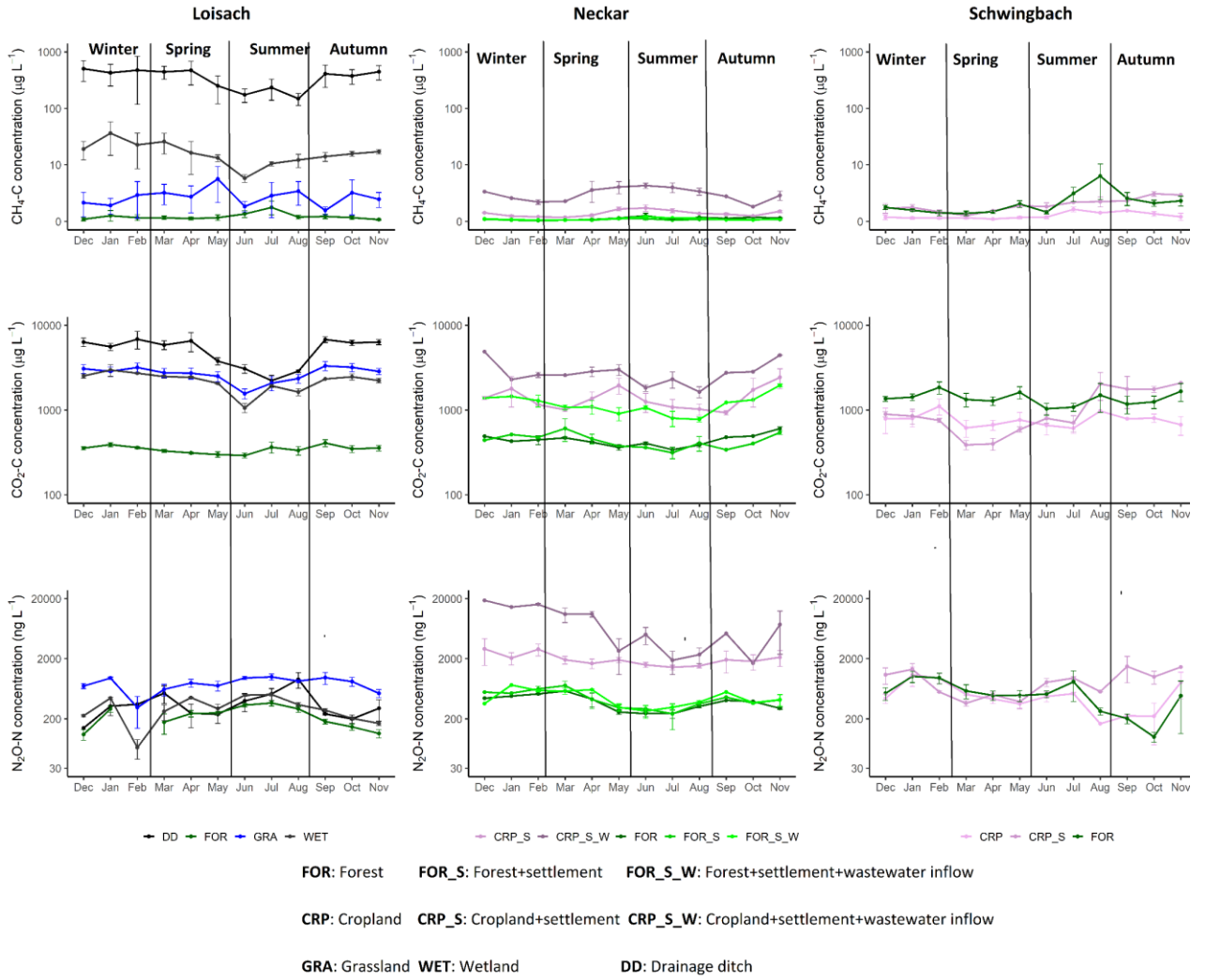


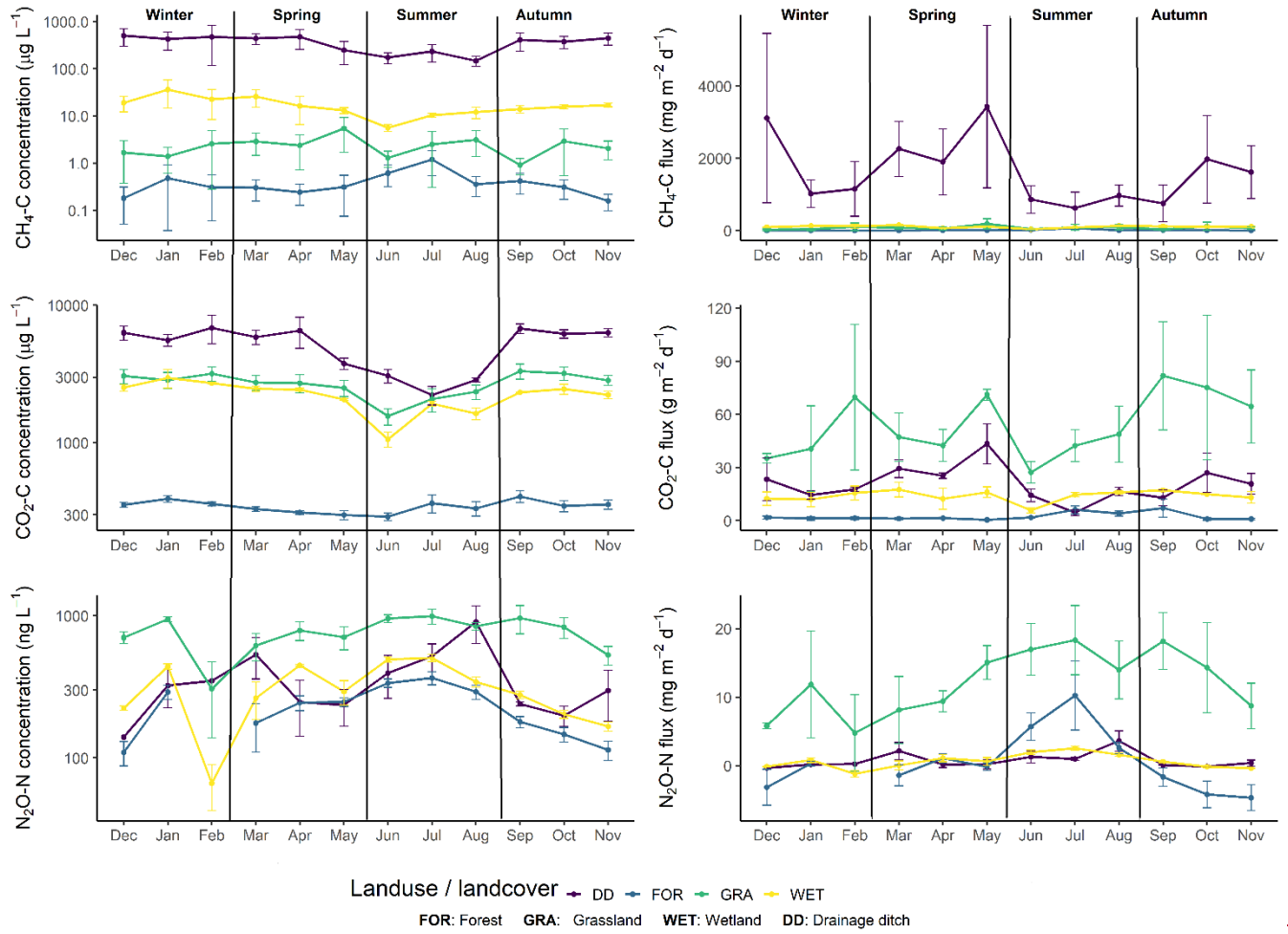


741

742 Fig. A1: Monthly mean  $\pm$  SE velocity and discharge grouped by landuse / landcover classes in the A) Loisach,

743 B) Schwingbach and C) Neckar catchments.

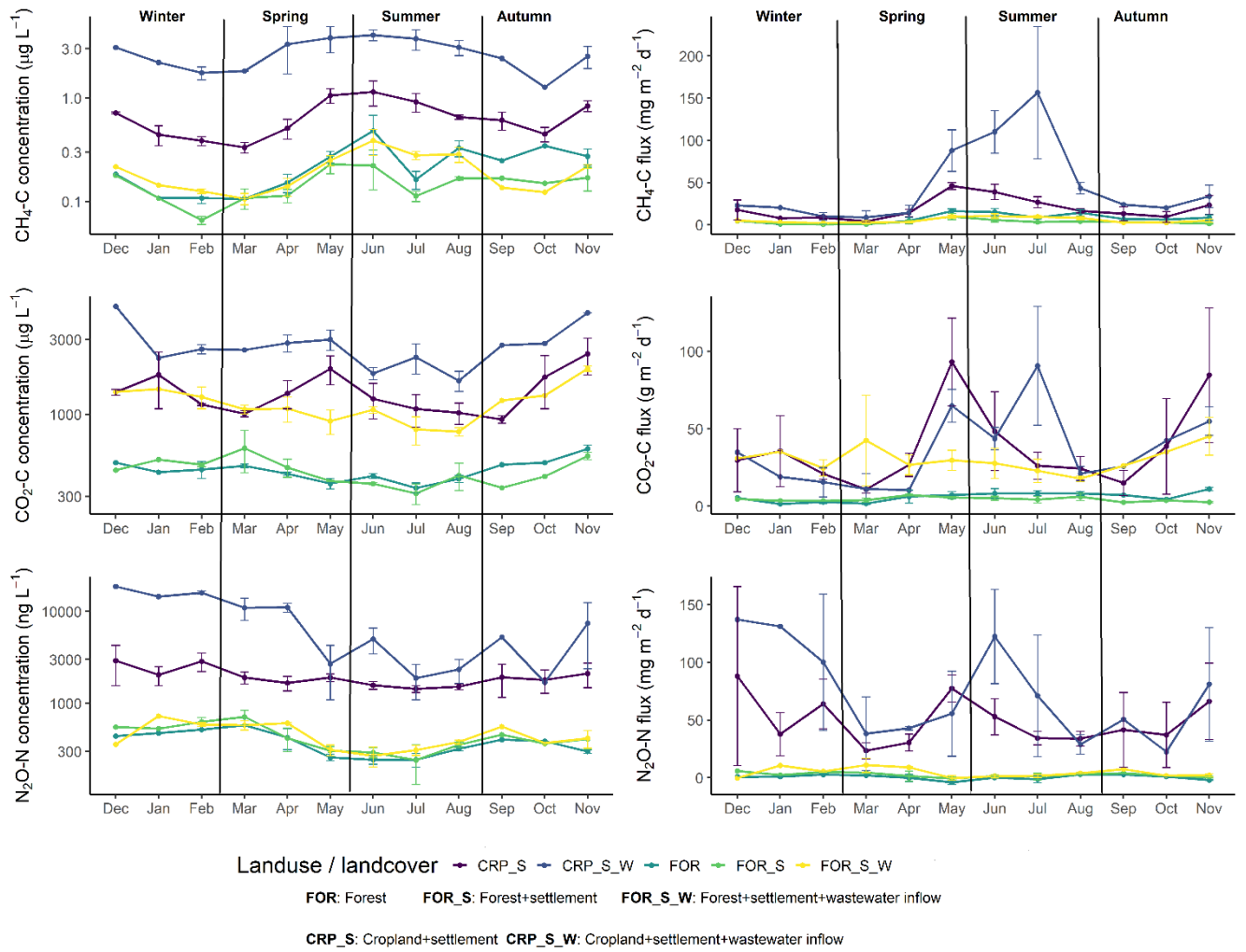




745

746

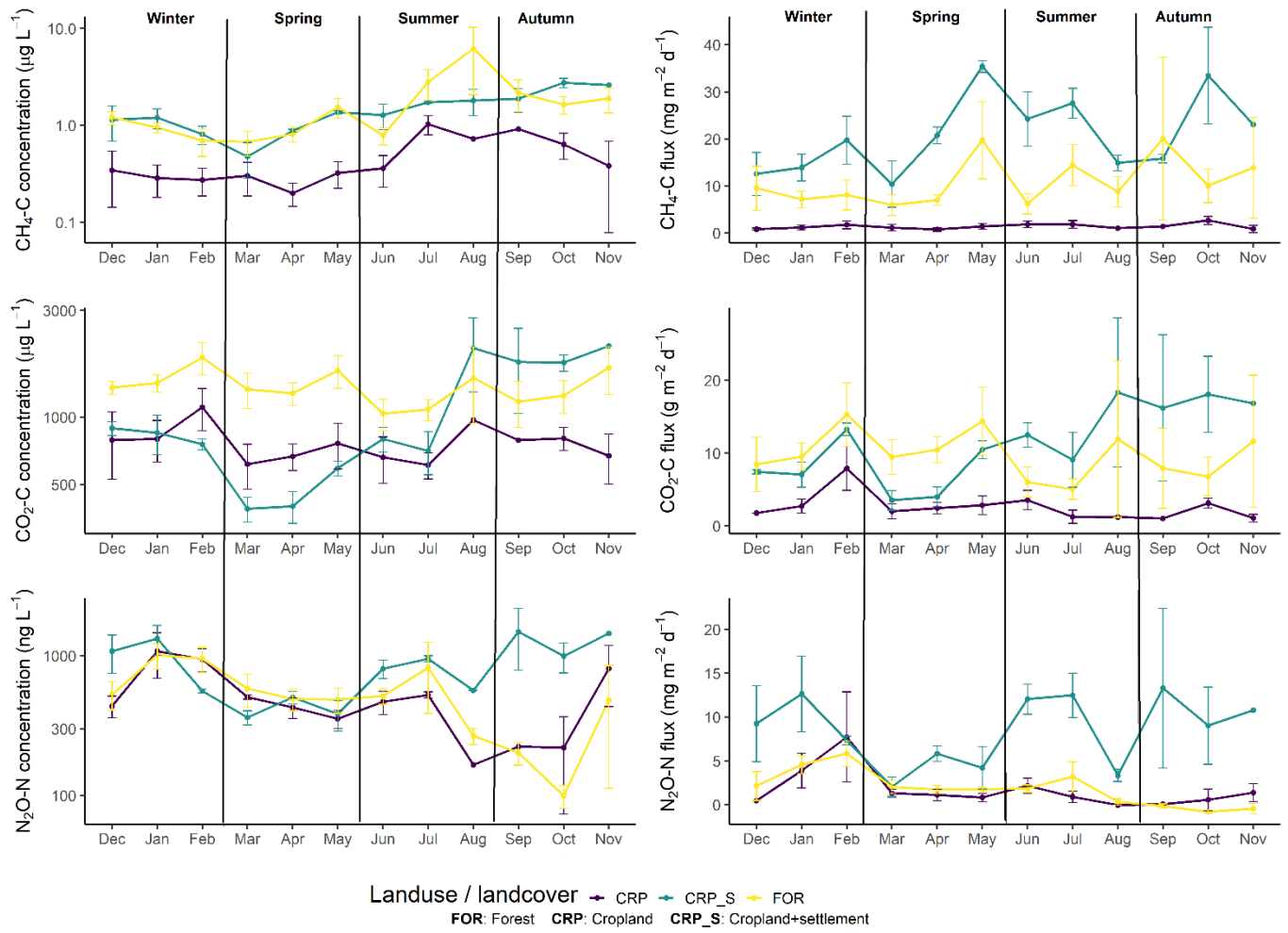
747 Fig. A2: Monthly mean  $\pm$  SE CO<sub>2</sub>, CH<sub>4</sub> and N<sub>2</sub>O concentrations and fluxes at forested (FOR), wetland (WET),  
 748 grassland (GRA) and ditch (DD) sites at sites within the in-the-Loisach, Neckar and Schwingbach catchments.  
 749 (see Table 1 methods).



750

751

752 **Fig. A3: Monthly mean  $\pm$  SE CO<sub>2</sub>, CH<sub>4</sub> and N<sub>2</sub>O concentrations and fluxes at forested (FOR), forested + urban**  
 753 **(FOR\_S), forested + urban + wastewater (FOR\_S\_W), cropland + urban (CRP\_S) and cropland + urban +**  
 754 **wastewater (CRP\_S\_W) sites in the Neckar catchment (see Table 1 methods).**

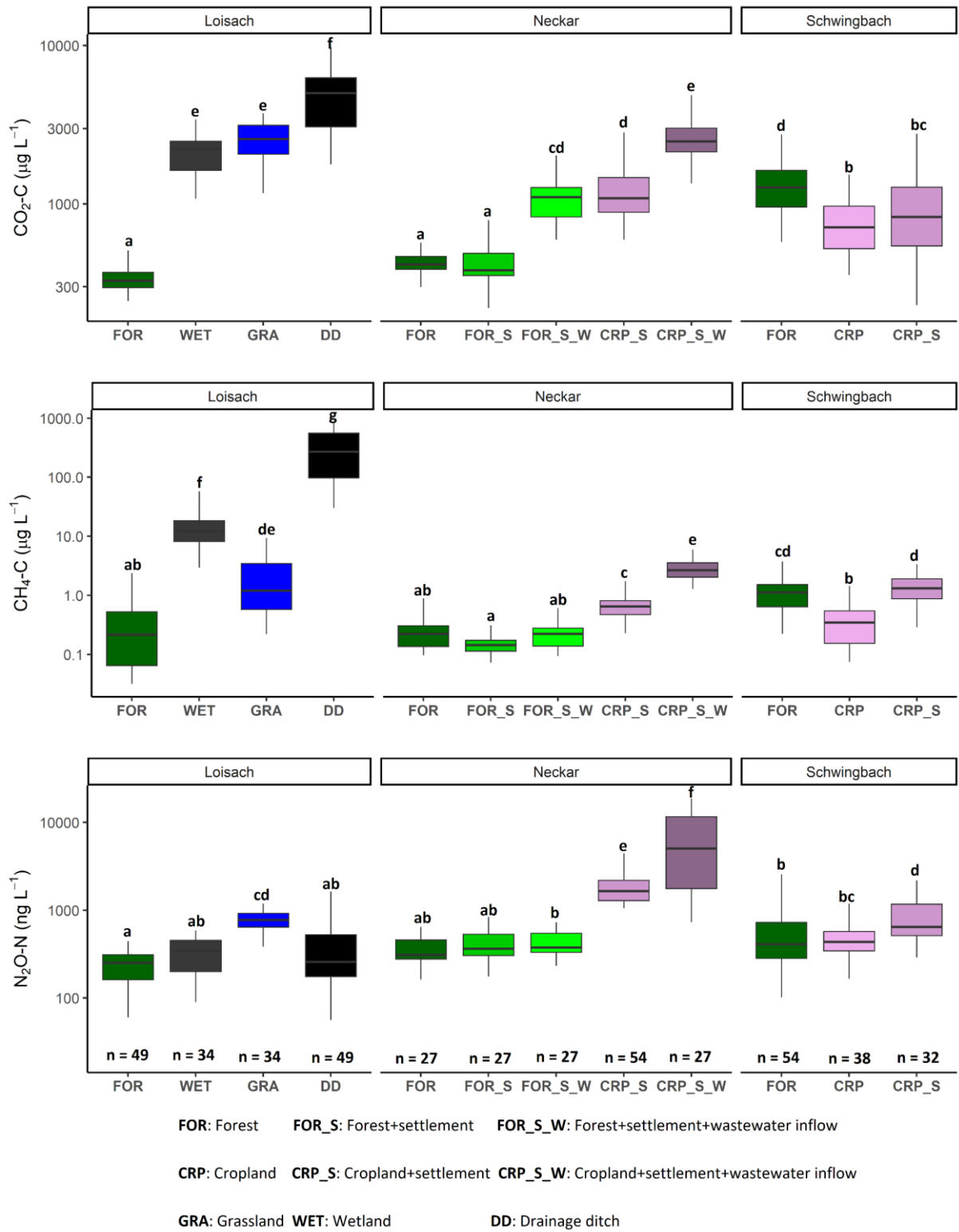


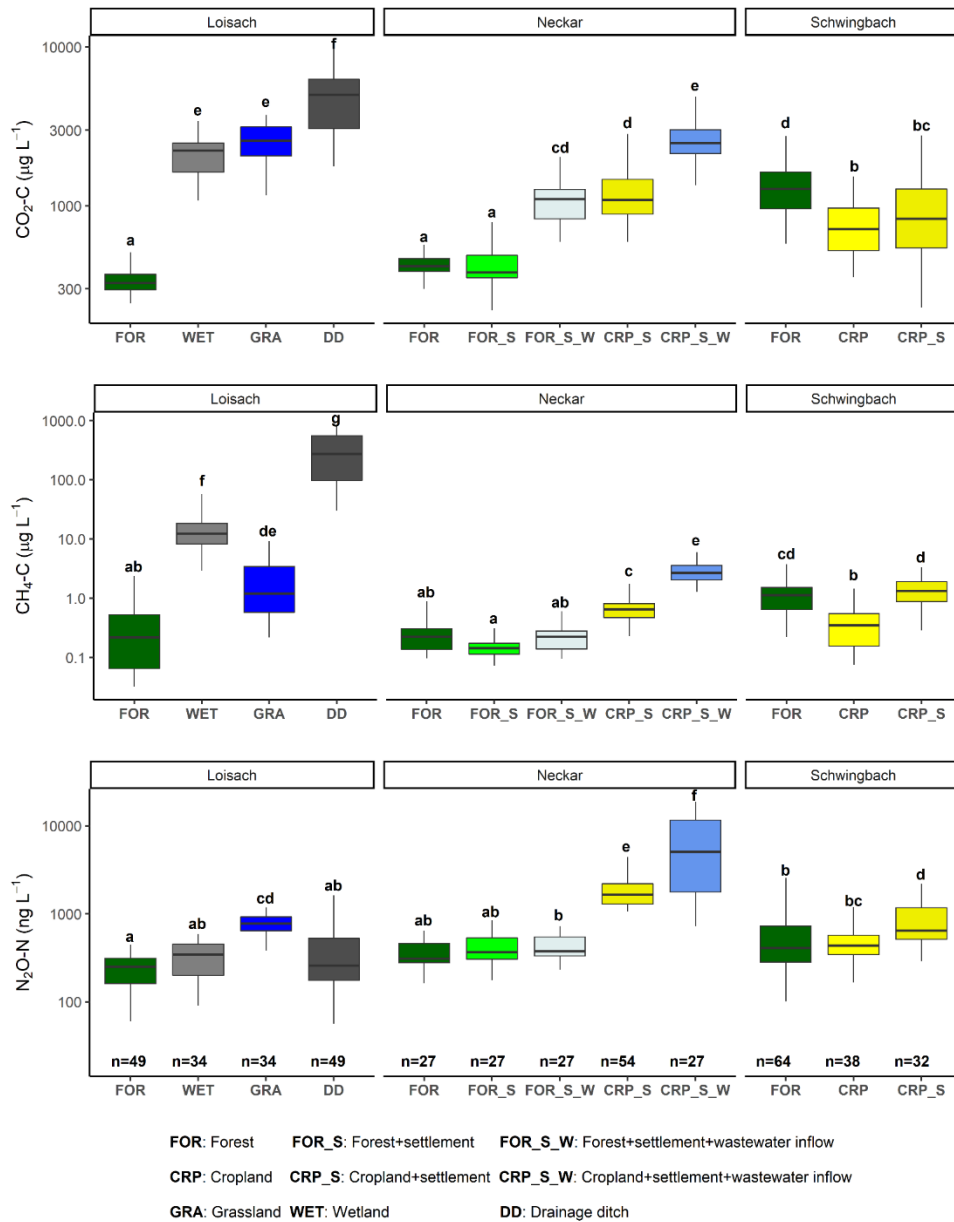
755

756

757 **Fig. A4: Monthly mean ± SE CO<sub>2</sub>, CH<sub>4</sub> and N<sub>2</sub>O concentrations and fluxes at forested (FOR), cropland (CRP)**

758 **and cropland + urban (CRP\_S) sites in the Schwingbach catchment (see Table 1 methods).**



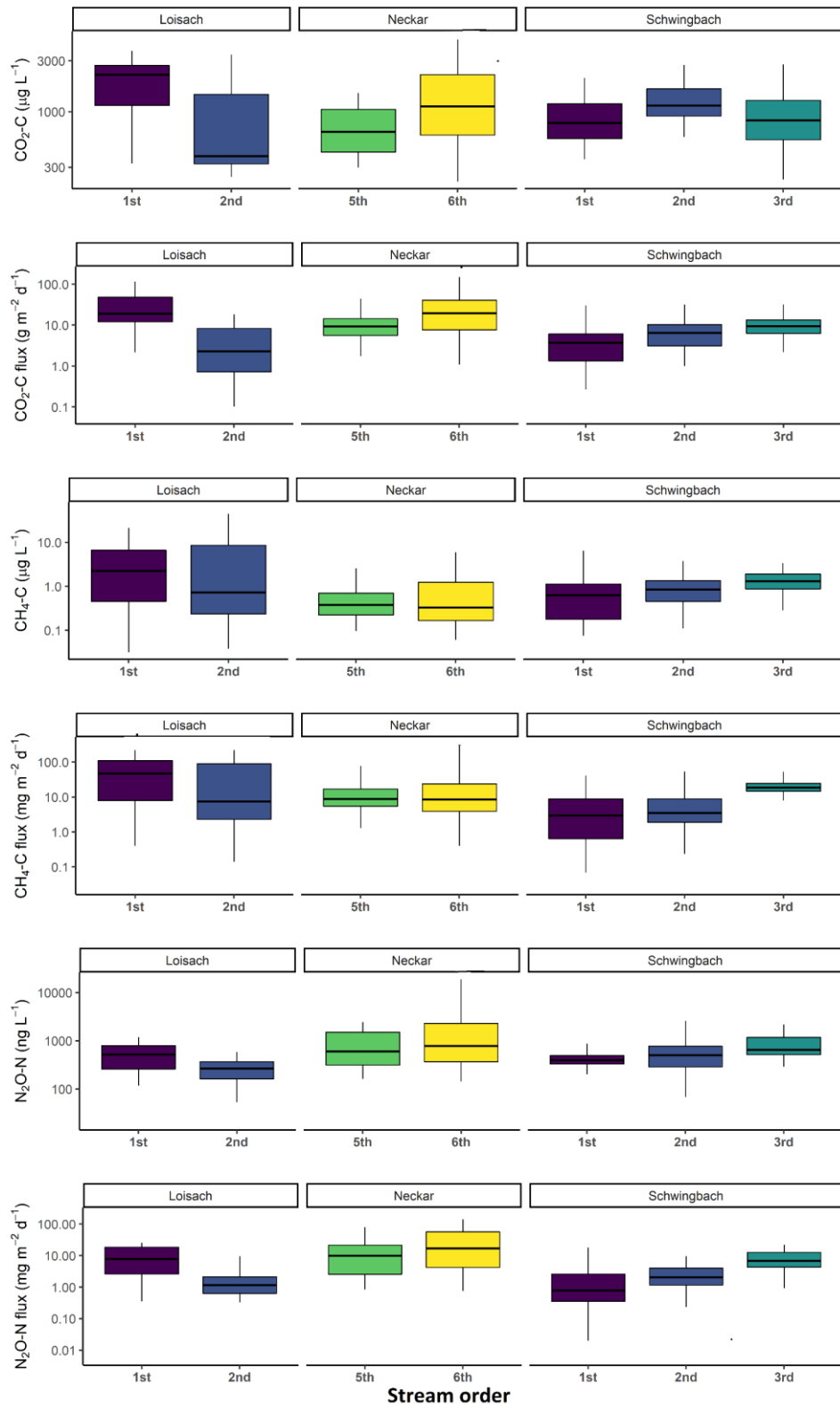


760

761 Fig. A35: Boxplots of CO<sub>2</sub>, CH<sub>4</sub>, and N<sub>2</sub>O concentrations in stream and ditch waters in the three catchments  
 762 grouped by dominating land uses (see Table 1 methods). Letters on top of the boxplots represent significant  
 763 differences (p<0.05) amongst the land use classes across the three catchments based on Tukey post-hoc analyses  
 764 from the linear mixed-effects models-models' results (Table 32).

765





766

767

768

Fig. A4: Boxplots of stream CO<sub>2</sub>, CH<sub>4</sub>, and N<sub>2</sub>O concentrations and fluxes in the three catchments grouped by stream order (see Table 1 methods).

S

769 **Appendix B: Tables**

770 Table B1: Annual means (+SE) of water chemistry variables and gas concentration measured in the effluents of  
 771 the Ammer (WWA) and Steinlach (WWS) wastewater treatment plants.

Water quality variables and discharge	Wastewater effluent quality from inflow zones (Annual Mean $\pm$ SE)	
	Ammer WWA	Steinlach WWS
Temperature ( $^{\circ}$ C)	13.85 $\pm$ 0.61	13.72 $\pm$ 0.65
pH	7.58 $\pm$ 0.07	7.37 $\pm$ 0.09
DO (mg L <sup>-1</sup> )	6.01 $\pm$ 0.32	5.99 $\pm$ 0.34
Specific Conductivity	1017.96 $\pm$ 63.08	776.68 $\pm$ 63.48
NO <sub>3</sub> -N (mg L <sup>-1</sup> )	7.57 $\pm$ 0.6	6.33 $\pm$ 0.47
NH <sub>4</sub> -N (mg L <sup>-1</sup> )	0.14 $\pm$ 0.02	0.09 $\pm$ 0.03
DOC (mg L <sup>-1</sup> )	6.8 $\pm$ 0.33	5.66 $\pm$ 0.58
TDN (mg L <sup>-1</sup> )	8.43 $\pm$ 0.88	7.58 $\pm$ 0.88
CO <sub>2</sub> -C concentration ( $\mu$ g L <sup>-1</sup> )	4020.08 $\pm$ 192.75	4529.3 $\pm$ 224.37
CH <sub>4</sub> -C concentration ( $\mu$ g L <sup>-1</sup> )	2.13 $\pm$ 0.3	0.73 $\pm$ 0.09
N <sub>2</sub> O-N concentration (ng L <sup>-1</sup> )	9255.11 $\pm$ 1563.23	483.23 $\pm$ 61.35

772

773 Table B2: Seasonal means (+SE) of water physico-chemical variables, gas concentration and flux measured in  
 774 the Loisach, Neckar and Schwingbach catchments. Letters beside the means represent significant differences  
 775 ( $p < 0.05$ ) amongst the seasons across the three catchments based on Tukey post-hoc analyses from the linear  
 776 mixed-effects models' results (Table 2).

	<b>Summer</b>	<b>Autumn</b>	<b>Winter</b>	<b>Spring</b>
Temperature ( $^{\circ}$ C)	14.04 $\pm$ 0.2 <b>d</b>	9.83 $\pm$ 0.32 <b>c</b>	5.55 $\pm$ 0.21 <b>a</b>	8.38 $\pm$ 0.22 <b>b</b>
pH	7.85 $\pm$ 0.03 <b>a</b>	7.88 $\pm$ 0.04 <b>ab</b>	7.98 $\pm$ 0.04 <b>b</b>	7.96 $\pm$ 0.04 <b>ab</b>
DO ( $\text{mg L}^{-1}$ )	8.71 $\pm$ 0.18 <b>a</b>	8.55 $\pm$ 0.29 <b>a</b>	9.63 $\pm$ 0.27 <b>b</b>	9.85 $\pm$ 0.22 <b>b</b>
Specific Conductivity	612.03 $\pm$ 21.8 <b>a</b>	606.91 $\pm$ 28.44 <b>b</b>	600.86 $\pm$ 32.62 <b>ab</b>	555.63 $\pm$ 24.03 <b>a</b>
NO <sub>3</sub> -N ( $\text{mg L}^{-1}$ )	2.54 $\pm$ 0.22 <b>a</b>	2.14 $\pm$ 0.29 <b>a</b>	2.86 $\pm$ 0.28 <b>b</b>	2.6 $\pm$ 0.22 <b>ab</b>
NH <sub>4</sub> -N ( $\text{mg L}^{-1}$ )	0.11 $\pm$ 0.01 <b>a</b>	0.14 $\pm$ 0.02 <b>a</b>	0.13 $\pm$ 0.02 <b>a</b>	0.1 $\pm$ 0.01 <b>a</b>
TN ( $\text{mg L}^{-1}$ )	2.9 $\pm$ 0.22 <b>a</b>	2.49 $\pm$ 0.3 <b>a</b>	3.01 $\pm$ 0.36 <b>b</b>	3 $\pm$ 0.29 <b>ab</b>
DON ( $\text{mg L}^{-1}$ )	0.5 $\pm$ 0.07 <b>a</b>	0.75 $\pm$ 0.15 <b>a</b>	1.56 $\pm$ 0.26 <b>a</b>	1.3 $\pm$ 0.24 <b>a</b>
DOC ( $\text{mg L}^{-1}$ )	4.37 $\pm$ 0.24 <b>a</b>	4.26 $\pm$ 0.36 <b>a</b>	4.1 $\pm$ 0.31 <b>a</b>	4.66 $\pm$ 0.26 <b>a</b>
DOC:DIN	11.45 $\pm$ 2.9 <b>b</b>	7.21 $\pm$ 1.37 <b>ab</b>	4.14 $\pm$ 0.75 <b>a</b>	7.21 $\pm$ 1.81 <b>b</b>
DOC:DON	103.91 $\pm$ 56.91 <b>a</b>	183.33 $\pm$ 140.18 <b>a</b>	13.19 $\pm$ 2.37 <b>a</b>	28.33 $\pm$ 7.31 <b>a</b>
Stream velocity ( $\text{m s}^{-1}$ )	0.18 $\pm$ 0.01 <b>ab</b>	0.12 $\pm$ 0.01 <b>a</b>	0.16 $\pm$ 0.01 <b>ab</b>	0.24 $\pm$ 0.02 <b>b</b>
Discharge $\text{L s}^{-1}$	526.41 $\pm$ 171.4 <b>ab</b>	86.25 $\pm$ 13.07 <b>a</b>	157.3 $\pm$ 31.58 <b>ab</b>	384.08 $\pm$ 96.29 <b>b</b>
CO <sub>2</sub> concentration ( $\mu\text{g-C L}^{-1}$ )	1198.93 $\pm$ 71.66 <b>a</b>	2222.22 $\pm$ 208.63 <b>c</b>	1869.06 $\pm$ 185.95 <b>c</b>	1666.03 $\pm$ 148.04 <b>b</b>
CH <sub>4</sub> concentration ( $\mu\text{g-C L}^{-1}$ )	20.94 $\pm$ 5.36 <b>a</b>	58.08 $\pm$ 17.8 <b>a</b>	46.98 $\pm$ 18 <b>a</b>	40.94 $\pm$ 13.03 <b>a</b>
N <sub>2</sub> O concentration ( $\text{ng-N L}^{-1}$ )	816.06 $\pm$ 75.58 <b>ab</b>	796.45 $\pm$ 169.08 <b>a</b>	1691.19 $\pm$ 400.62 <b>b</b>	1021.38 $\pm$ 185.45 <b>ab</b>
$k_{600} \text{ md}^{-1}$	32.31 $\pm$ 3.09 <b>ab</b>	22.71 $\pm$ 2.8 <b>a</b>	24.54 $\pm$ 3.36 <b>ab</b>	33.92 $\pm$ 3.42 <b>b</b>
CO <sub>2</sub> flux ( $\text{mg-C m}^{-2} \text{ d}^{-1}$ )	17008.98 $\pm$ 1876.63 <b>a</b>	22710.21 $\pm$ 3422.95 <b>a</b>	14836.51 $\pm$ 1835.54 <b>a</b>	20592.21 $\pm$ 2563.97 <b>a</b>
CH <sub>4</sub> flux ( $\text{mg-C m}^{-2} \text{ d}^{-1}$ )	121.65 $\pm$ 30.93 <b>a</b>	233.99 $\pm$ 84.4 <b>a</b>	157.33 $\pm$ 73.04 <b>a</b>	262.87 $\pm$ 89.31 <b>a</b>
N <sub>2</sub> O flux ( $\text{mg-N m}^{-2} \text{ d}^{-1}$ )	13.69 $\pm$ 2.22 <b>b</b>	9.63 $\pm$ 2.86 <b>a</b>	16.12 $\pm$ 4.05 <b>b</b>	10.64 $\pm$ 2.11 <b>ab</b>

777

Table B3: Annual mean  $\pm$  standard errors of measured water physico-chemical variables, GHG concentration, and flux for land use classes in the Loissach (FOR: forest, WET: wetland, GRA: grassland, and DD: drainage ditches), the Neckar (FOR, FOR\_S: forest+settlement, FOR\_S\_W: forest+settlement+wastewater inflow, CRP\_S: cropland+settlement, and CRP\_S\_W: cropland+settlement+wastewater inflow, and the Schwingbach catchment (FOR, CRP: cropland and CRP\_S). The number of observations in each land use class is represented by "n" in brackets. Letters beside the means represent significant differences ( $p < 0.05$ ) amongst the land use classes across the three catchments based on Tukey post-hoc analyses from the linear mixed-effects models' results (Table 2).

	Loissach					Neckar					Schwingbach				
	FOR (n=49)	WET (n=34)	GRA (n=34)	DD (n=49)	FOR (n=27)	FOR_S (n=27)	FOR_S_W (n=27)	CRP_S_W (n=27)	FOR (n=64)	CRP (n=38)	CRP_S (n=32)	FOR (n=64)	CRP (n=38)	CRP_S (n=32)	
Temperature ( $^{\circ}$ C)	8 $\pm$ 0.5 a	8.6 $\pm$ 0.4 ab	9.5 $\pm$ 0.2 bd	9 $\pm$ 0.5 bc	10.44 $\pm$ 1.01 bd	11.6 $\pm$ 1.01 de	12.14 $\pm$ 0.85 ef	13.06 $\pm$ 0.63 f	9.7 $\pm$ 0.5 bc	9.9 $\pm$ 0.7 cdef	9.8 $\pm$ 0.8 bc	9.7 $\pm$ 0.5 bc	9.9 $\pm$ 0.7 cdef	9.8 $\pm$ 0.8 bc	
pH	8.3 $\pm$ 0.01 de	7.7 $\pm$ 0.01 b	7.6 $\pm$ 0.01 b	7.3 $\pm$ 0.01 a	8.45 $\pm$ 0.05 e	8.44 $\pm$ 0.05 e	8.07 $\pm$ 0.05 cd	7.72 $\pm$ 0.08 b	7.7 $\pm$ 0.01 b	8 $\pm$ 0.01 c	8 $\pm$ 0.1 c	7.7 $\pm$ 0.01 b	8 $\pm$ 0.01 c	8 $\pm$ 0.1 c	
DO ( $\text{mg L}^{-1}$ )	11 $\pm$ 0.1 de	8.3 $\pm$ 0.2 c	7.4 $\pm$ 0.2 b	4.2 $\pm$ 0.3 a	11.49 $\pm$ 0.39 de	11.57 $\pm$ 0.33 de	10.62 $\pm$ 0.31 d	8.3 $\pm$ 0.29 bc	8.8 $\pm$ 0.1 c	8.9 $\pm$ 0.1 c	9 $\pm$ 0.1 c	8.8 $\pm$ 0.1 c	8.9 $\pm$ 0.1 c	9 $\pm$ 0.1 c	
Specific Conductivity	365.1 $\pm$ 8.1 a	436.9 $\pm$ 9.4 ab	447.7 $\pm$ 2.3 bc	484.9 $\pm$ 16.2 bcd	738.51 $\pm$ 51.37 g	582.07 $\pm$ 13.96 de	700.87 $\pm$ 31.16 fg	971.46 $\pm$ 41.76 h	389.7 $\pm$ 18.8 ab	597.2 $\pm$ 13 ef	566.4 $\pm$ 20.2 ce	389.7 $\pm$ 18.8 ab	597.2 $\pm$ 13 ef	566.4 $\pm$ 20.2 ce	
NO <sub>3</sub> -N ( $\text{mg L}^{-1}$ )	0.8 $\pm$ 0.01 cd	0.5 $\pm$ 0.01 b	0.8 $\pm$ 0.01 cd	0.1 $\pm$ 0.01 a	0.57 $\pm$ 0.04 bc	2.39 $\pm$ 0.13 e	3.73 $\pm$ 0.29 ef	7.18 $\pm$ 0.38 gh	1.5 $\pm$ 0.1 d	4.9 $\pm$ 0.4 fg	2.3 $\pm$ 0.2 e	1.5 $\pm$ 0.1 d	4.9 $\pm$ 0.4 fg	2.3 $\pm$ 0.2 e	
NH <sub>4</sub> -N ( $\text{mg L}^{-1}$ )	0.01 $\pm$ 0.001 ab	0.01 $\pm$ 0.001 a	0.01 $\pm$ 0.001 a	0.3 $\pm$ 0.001 d	0.07 $\pm$ 0.02 bc	0.1 $\pm$ 0.01 cd	0.11 $\pm$ 0.02 cd	0.14 $\pm$ 0.02 d	0.1 $\pm$ 0.01 d	0.1 $\pm$ 0.01 d	0.1 $\pm$ 0.01 d	0.1 $\pm$ 0.01 d	0.1 $\pm$ 0.01 d	0.1 $\pm$ 0.01 d	
TN ( $\text{mg L}^{-1}$ )	0.7 $\pm$ 0.01 b	0.4 $\pm$ 0.01 a	0.7 $\pm$ 0.01 b	0.9 $\pm$ 0.1 b	0.73 $\pm$ 0.06 b	2.3 $\pm$ 0.11 cd	3.92 $\pm$ 0.3 ef	7.24 $\pm$ 0.53 h	2.2 $\pm$ 0.2 c	6.1 $\pm$ 0.5 fg	3 $\pm$ 0.3 de	2.2 $\pm$ 0.2 c	6.1 $\pm$ 0.5 fg	3 $\pm$ 0.3 de	
DON ( $\text{mg L}^{-1}$ )	0.08 $\pm$ 0.02 ab	0.03 $\pm$ 0.02 a	0.06 $\pm$ 0.03 acd	0.45 $\pm$ 0.04 cd	0.35 $\pm$ 0.05 d	0.26 $\pm$ 0.08 bd	1.02 $\pm$ 0.33 de	3.6 $\pm$ 1.03 e	0.65 $\pm$ 0.11 d	1.45 $\pm$ 0.24 ce	0.75 $\pm$ 0.1 de	0.65 $\pm$ 0.11 d	1.45 $\pm$ 0.24 ce	0.75 $\pm$ 0.1 de	
DOC ( $\text{mg L}^{-1}$ )	2.9 $\pm$ 0.3 b	1.8 $\pm$ 0.1 a	1.5 $\pm$ 0.1 a	9.5 $\pm$ 0.7 g	5.9 $\pm$ 0.67 fg	4.22 $\pm$ 0.35 bc	4.12 $\pm$ 0.39 cdf	4.67 $\pm$ 0.23 ef	4.8 $\pm$ 0.2 ef	3.8 $\pm$ 0.1 cde	4.7 $\pm$ 0.2 ef	4.8 $\pm$ 0.2 ef	3.8 $\pm$ 0.1 cde	4.7 $\pm$ 0.2 ef	
DOC:DIN	4.23 $\pm$ 0.46 ef	4.48 $\pm$ 0.73 ef	2.06 $\pm$ 0.22 d	45.14 $\pm$ 8.27 h	13.19 $\pm$ 2.32 g	1.84 $\pm$ 0.24 cd	1.64 $\pm$ 0.23 cd	0.85 $\pm$ 0.09 ab	5.89 $\pm$ 1.1 f	1.25 $\pm$ 0.17 bc	2.82 $\pm$ 0.3 de	5.89 $\pm$ 1.1 f	1.25 $\pm$ 0.17 bc	2.82 $\pm$ 0.3 de	
DOC:DON	694.26 $\pm$ 615.24 g	861.15 $\pm$ 610.89 h	93.39 $\pm$ 57.03 cdf	37.84 $\pm$ 3.02 fg	60.73 $\pm$ 30.87 efg	46.02 $\pm$ 16.38 dfg	18.06 $\pm$ 10.65 acd	5.68 $\pm$ 1.9 a	37.19 $\pm$ 15.88 df	9.02 $\pm$ 2.67 ac	13.13 $\pm$ 2.9 bcde	37.19 $\pm$ 15.88 df	9.02 $\pm$ 2.67 ac	13.13 $\pm$ 2.9 bcde	
Stream velocity ( $\text{m s}^{-1}$ )	0.22 $\pm$ 0.03 cd	0.07 $\pm$ 0.01 b	0.22 $\pm$ 0.02 cd	0.05 $\pm$ 0.01 a	0.3 $\pm$ 0.04 de	0.34 $\pm$ 0.04 ce	0.4 $\pm$ 0.04 e	0.19 $\pm$ 0.02 d	0.09 $\pm$ 0.01 ab	0.1 $\pm$ 0.01 ab	0.29 $\pm$ 0.03 de	0.09 $\pm$ 0.01 ab	0.1 $\pm$ 0.01 ab	0.29 $\pm$ 0.03 de	
Discharge $\text{L s}^{-1}$	37.7 $\pm$ 7.3 c	34.5 $\pm$ 3.2 cd	142.1 $\pm$ 20.6 ef	11.1 $\pm$ 1.4 b	290.56 $\pm$ 109.66 efg	2053.15 $\pm$ 705.38 g	2117.15 $\pm$ 730.03 g	318.55 $\pm$ 32.65 f	5.4 $\pm$ 0.7 a	5.4 $\pm$ 1.3 a	94 $\pm$ 15.5 de	5.4 $\pm$ 0.7 a	5.4 $\pm$ 1.3 a	94 $\pm$ 15.5 de	
CO <sub>2</sub> -C concentration ( $\mu\text{g L}^{-1}$ )	337.9 $\pm$ 9.1 a	2075.3 $\pm$ 107.8 e	2559.5 $\pm$ 123.8 e	4913.5 $\pm$ 285.4 f	423.85 $\pm$ 14.6 a	426.67 $\pm$ 24.18 a	1093.04 $\pm$ 71.11 cd	1372.92 $\pm$ 104.52 d	1350 $\pm$ 65.3 d	748.9 $\pm$ 45.1 b	1018.1 $\pm$ 117.6 bc	1350 $\pm$ 65.3 d	748.9 $\pm$ 45.1 b	1018.1 $\pm$ 117.6 bc	
CH <sub>4</sub> -C concentration ( $\mu\text{g L}^{-1}$ )	0.4 $\pm$ 0.1 ab	16.2 $\pm$ 2.2 f	2.4 $\pm$ 0.4 de	338 $\pm$ 37 g	0.25 $\pm$ 0.03 ab	0.15 $\pm$ 0.01 a	0.23 $\pm$ 0.02 ab	3.01 $\pm$ 0.25 e	1.5 $\pm$ 0.2 cd	0.4 $\pm$ 0.1 b	1.5 $\pm$ 0.1 d	1.5 $\pm$ 0.2 cd	0.4 $\pm$ 0.1 b	1.5 $\pm$ 0.1 d	
N <sub>2</sub> O-N concentration ( $\text{ng L}^{-1}$ )	240.9 $\pm$ 16.3 a	323 $\pm$ 25.1 ab	771.1 $\pm$ 42.2 cd	431.3 $\pm$ 64.9 ab	355.91 $\pm$ 24.26 ab	405.94 $\pm$ 32.61 ab	421.75 $\pm$ 28.5 b	6600.11 $\pm$ 1121.92 f	569 $\pm$ 59.6 b	540 $\pm$ 64.5 bc	864.5 $\pm$ 89.4 d	569 $\pm$ 59.6 b	540 $\pm$ 64.5 bc	864.5 $\pm$ 89.4 d	
k <sub>600</sub> $\text{md}^{-1}$	80.9 $\pm$ 10.6 f	10.5 $\pm$ 0.7 bc	31.5 $\pm$ 3.1 df	6.5 $\pm$ 0.6 a	52.58 $\pm$ 5.1 f	37.66 $\pm$ 3.56 ef	43.41 $\pm$ 3.2 ef	19.95 $\pm$ 2.62 cd	11.7 $\pm$ 1.1 ac	7.1 $\pm$ 0.9 ab	22.9 $\pm$ 1.8 de	11.7 $\pm$ 1.1 ac	7.1 $\pm$ 0.9 ab	22.9 $\pm$ 1.8 de	
CO <sub>2</sub> -C flux ( $\text{g m}^{-2} \text{d}^{-1}$ )	2.39 $\pm$ 0.4 a	13.33 $\pm$ 0.9 df	50.71 $\pm$ 5.3 g	20.52 $\pm$ 1.9 ef	6.66 $\pm$ 0.8 cd	4.89 $\pm$ 0.55 bc	28.26 $\pm$ 2.8 fg	38.81 $\pm$ 6.5 fg	9.54 $\pm$ 0.9 cd	2.8 $\pm$ 0.4 ab	10.96 $\pm$ 1.3 cde	9.54 $\pm$ 0.9 cd	2.8 $\pm$ 0.4 ab	10.96 $\pm$ 1.3 cde	
CH <sub>4</sub> -C flux ( $\text{mg m}^{-2} \text{d}^{-1}$ )	10.5 $\pm$ 4.3 ab	101.7 $\pm$ 8.3 f	73.2 $\pm$ 15.7 de	1532.9 $\pm$ 244.8 g	9.09 $\pm$ 1.5 bc	3.88 $\pm$ 0.7 ac	6.54 $\pm$ 0.81 bc	58.23 $\pm$ 13.33 e	9.9 $\pm$ 1.3 c	1.5 $\pm$ 0.2 a	21.5 $\pm$ 2 de	9.9 $\pm$ 1.3 c	1.5 $\pm$ 0.2 a	21.5 $\pm$ 2 de	
N <sub>2</sub> O-N flux ( $\text{mg m}^{-2} \text{d}^{-1}$ )	1.1 $\pm$ 0.9 a	0.8 $\pm$ 0.2 a	12.4 $\pm$ 1.4 c	1.2 $\pm$ 0.4 a	0.32 $\pm$ 0.63 a	2.2 $\pm$ 0.64 a	3.96 $\pm$ 0.85 ab	67.59 $\pm$ 11.34 d	2.1 $\pm$ 0.3 a	1.9 $\pm$ 0.6 a	8.8 $\pm$ 1.1 bc	2.1 $\pm$ 0.3 a	1.9 $\pm$ 0.6 a	8.8 $\pm$ 1.1 bc	

Table B4: Indices highlighting the performance of the best-fit SEMs, which indicate significant interaction pathways of both direct and indirect drivers of in-situ GHG concentrations in temperate streams, rivers, and drainage ditches. The goodness of fit index (GFI), comparative fit index (CFI), Tucker Lewis index, standardized root mean square residual (SRMR), and root means squared error of approximation (RMSEA) are measures of model goodness of fit, while the parsimony fit index (PNFI) compares the best-fit model to the theoretical-model.

Greenhouse gas (GHG)	Performance indices for the best-fit SEMs						Model comparison PNFI	
	GFI	CFI	TLI	SRMR	RMSEA	r <sup>2</sup>	Theoretical SEM	Best-fit SEM
CO <sub>2</sub> concentration (µg-C L <sup>-1</sup> )	1.00	1.00	1.00	0.02	<0.01	0.60	0.13	0.22
CH <sub>4</sub> concentration (µg-C L <sup>-1</sup> )	1.00	1.00	1.00	0.02	<0.01	0.66	0.13	0.22
N <sub>2</sub> O concentration (ng-N L <sup>-1</sup> )	0.99	1.00	0.98	0.03	0.04	0.47	0.13	0.22

**Best-fit SEM structure:-**

1. Log GHG = DO + DOC + Log NO<sub>3</sub> + agricultural area + wastewater inflow + stream velocity
2. Log NO<sub>3</sub> = DO + DOC + agricultural area + wastewater inflow + stream velocity
3. DOC = agricultural area
4. DO = DOC + stream velocity

**Goodness of fit assesment:-** GFI, CFI and TLI: 0.90 - 0.95; Good fit and >0.95 Excellent fit  
SRMR and RMSEA: 0.05 - 0.08; Good fit and <0.05 Excellent fit

### **Data availability**

\_\_\_\_\_The appendixes contain monthly, seasonal and land use specific water physico-chemical and GHG data used in this research. All raw data (xlsx format) will be made available upon request to the corresponding author via email.

### **Author contribution**

RM, RK, GG, CG, and KB designed the field experiments. RK, KB, TH, and LB provided the infrastructural funding and RM and EW did the field and laboratory work. RM did the statistical analysis, consulting with RK and GG. RM prepared the first draft manuscript, consulting with RK. All co-authors contributed to the final version.

### **Acknowledgments**

This research was funded by the German academic exchange service (DAAD) as part of RM's doctoral studies. Infrastructure for the research was provided by the TERENO Bavarian Alps/ Pre-Alps Observatory, funded by the Helmholtz Association and the Federal Ministry of Education and Research (BMBF). The authors would like to thank the entire laboratory staff at Karlsruhe Institute of Technology, Campus Alpin, Justus Liebig University Giessen, and the University of Tübingen for providing logistical support and supporting the gas and nutrient analyses. We also acknowledge the contributions of Alisson Kolar, Paul Levin Degott, Franz Weyerer, and Raphael Boehm during the field campaigns.

### **Declaration of competing interest**

The authors declare that they have no conflict of interest.

## References

- Aho, K. S., & Raymond, P. A.: Differential response of greenhouse gas evasion to storms in forested and wetland streams. *Journal of Geophysical Research: Biogeosciences* **124**, 649–662. <https://doi.org/10.1029/2018JG004750>, 2019.
- Aho, K. S., Fair, J. H., Hosen, J. D., Kyzivat, E. D., Logozzo, L. A., Rocher-Ros, G., Weber, L. C., Yoon, B., & Raymond, P. A.: Distinct concentration-discharge dynamics in temperate streams and rivers: CO<sub>2</sub> exhibits chemostasis while CH<sub>4</sub> exhibits source limitation due to temperature control. *Limnology and Oceanography*, **66**, 3656-3662. <https://doi.org/10.1002/lno.11906>, 2021.
- Aho, K. S., Fair, J. H., Hosen, J. D., Kyzivat, E. D., Logozzo, L. A., Weber, L. C., Yoon, B., Zarnetske, J. P., & Raymond, P. A.: An intense precipitation event causes a temperate forested drainage network to shift from N<sub>2</sub>O source to sink. *Limnology and Oceanography*, **67**, S242-S257. <https://doi.org/10.1002/lno.12006>, 2022.
- Attermeyer, K., Casas-Ruiz, J.P., Fuss, T., Pastor, A., Cauvy-Fraunié, S., Sheath, D., Nydahl, A.C., Doretto, A., Portela, A.P., Doyle, B.C. and Simov, N.: Carbon dioxide fluxes increase from day to night across European streams. *Communications Earth & Environment*, 2(1), 118. <https://doi.org/10.1038/s43247-021-00192-w>, 2021
- Allen, G. H., Pavelsky, T. M., Barefoot, E. A., Lamb, M. P., Butman, D., Tashie, A., & Gleason, C. J.: Similarity of stream width distributions across headwater systems. *Nature Communications* **9**, 610. <https://doi.org/10.1038/A41467-018-02991-w>, 2018.
- Audet, J., Bastviken, D., Bundschuh, M., Buffam, I., Feckler, A., Klemedtsson, L., Laudon, H., Löfgren, S., Natchimuthu, S., Öquist, M., Peacock, M., & Wallin, M. B.: Forest streams are important sources for nitrous oxide emissions. *Global Change Biology* **26**, 629–641. <https://doi.org/10.1111/gcb.14812>, 2019.
- Battin, T. J., Kaplan, L. A., Findlay, S., Hopkinson, C. S., Marti, E., Packman, A. I., Newbold, J. D., & Sabater, F.: Biophysical controls on organic carbon fluxes in fluvial networks. *Nature Geoscience* **1**, 95–100. <https://doi.org/10.1038/ngeo101>, 2008.
- [Battin, Tom J., Ronny Lauerwald, Emily S. Bernhardt, Enrico Bertuzzo, Lluís Gómez Gener, Robert O. Hall Jr, Erin R. Hotchkiss et al.:River ecosystem metabolism and carbon biogeochemistry in a changing world. \*Nature\* 613, 449-459, <https://doi.org/10.1038/s41586-022-05500-8>, 2021.](#)
- Baulch, H. M., Schiff, S. L., Maranger, R., & Dillon, P. J.: Nitrogen enrichment and the emission of nitrous oxide from streams. *Global Biogeochemical Cycles* **25**. <https://doi.org/10.1029/2011GB004047>, 2011.
- Baulch, H. M., Dillon, P. J., Maranger, R., & Schiff, S. L.: Diffusive and ebullitive transport of methane and

- nitrous oxide from streams: Are bubble-mediated fluxes important? *Journal of Geophysical Research: Biogeosciences* **116**, <https://doi.org/10.1029/2011JG001656>, 2011a.
- Beaulieu, J. J., Arango, C. P., & Tank, J. L.: The effects of season and agriculture on nitrous oxide production in headwater streams. *Journal of Environment Quality* **38**, 637, <https://doi.org/10.2134/jeq2008.0003>, 2009.
- Begum, M.S., Bogard, M.J., Butman, D.E., Chea, E., Kumar, S., Lu, X., Nayna, O.K., Ran, L., Richey, J.E., Tareq, S.M. and Xuan, D.T.: Localized pollution impacts on greenhouse gas dynamics in three anthropogenically modified Asian river systems. *Journal of Geophysical Research: Biogeosciences*, 126(5), 2020JG006124, <https://doi.org/10.1029/2020JG006124>, 2021.
- Bodmer, P., Heinz, M., Pusch, M., Singer, G., & Premke, K.: Carbon dynamics and their link to dissolved organic matter quality across contrasting stream ecosystems. *Science of the Total Environment* **553**, 574–586, <https://doi.org/10.1016/j.scitotenv.2016.02.095>, 2016.
- Bolleter, W. T., Bushman, C. J., & Tidwell, P. W.: Spectrophotometric determination of ammonia as indophenol. *Analytical Chemistry* **33**, 592–594, <https://doi.org/10.1021/ac60172a034>, 1961.
- Borges, A.V., Darchambeau, F., Teodoru, C.R., Marwick, T.R., Tamooh, F., Geeraert, N., Omengo, F.O., Guérin, F., Lambert, T., Morana, C. and Okuku, E.: Globally significant greenhouse-gas emissions from African inland waters. *Nature Geoscience*, 8(8), 637-642, <https://doi.org/10.1038/ngeo2486>, 2015.
- Borges, A.V., Darchambeau, F., Lambert, T., Bouillon, S., Morana, C., Brouyère, S., Hakoun, V., Jurado, A., Tseng, H.C., Descy, J.P., & Roland, F.A.: Effects of agricultural land use on fluvial carbon dioxide, methane and nitrous oxide concentrations in a large European river, the Meuse (Belgium). *Science of the Total Environment* **610–611**, 342–355, <https://doi.org/10.1016/j.scitotenv.2017.08.047>, 2018.
- Borges, A.V., Darchambeau, F., Lambert, T., Morana, C., Allen, G.H., Tambwe, E., Toengaho Sembaito, A., Mambo, T., Nlandu Wabakhangazi, J., Descy, J.P., & Teodoru, C.R.: Variations in dissolved greenhouse gases (CO<sub>2</sub>, CH<sub>4</sub>, N<sub>2</sub>O) in the Congo river network overwhelmingly driven by fluvial-wetland connectivity. *Biogeosciences* **16**, 3801–3834, <https://doi.org/10.5194/bg-16-3801-2019>, 2019.
- Crawford, J. T., Dornblaser, M. M., Stanley, E. H., Clow, D. W., & Striegl, R. G.: Source limitation of carbon gas emissions in high-elevation mountain streams and lakes. *Journal of Geophysical Research: Biogeosciences*, **120**, 952-964, <https://doi.org/10.1002/2014JG002861>, 2015.
- Dinsmore, K. J., Wallin, M. B., Johnson, M. S., Billett, M. F., Bishop, K., Pumpanen, J., & Ojala, A.: Contrasting CO<sub>2</sub> concentration discharge dynamics in headwater streams: A multi-catchment comparison. *Journal of Geophysical Research: Biogeosciences*, **118**, 445-461, <https://doi.org/10.1002/jgrg.20047>, 2013.
- Drake, T. W., Raymond, P. A., & Spencer, R. G.: Terrestrial carbon inputs to inland waters: A current synthesis of estimates and uncertainty. *Limnology and Oceanography Letters*, 3(3), 132-142, <https://doi.org/10.1002/lol2.10055>, 2018.
- Galantini, L., Lapiere, J. F., & Maranger, R.: How are greenhouse gases coupled across seasons in a large temperate river with differential land use?. *Ecosystems*, **24**, 2007-2027, <https://doi.org/10.1007/A10021->



021-00629-5, 2021.

Gomez-Gener, L., Rocher-Ros, G., Battin, T., Cohen, M.J., Dalmagro, H.J., Dinsmore, K.J., Drake, T.W., Duvert, C., Enrich-Prast, A., Horgby, Å., & Johnson, M.S.: Global carbon dioxide efflux from rivers enhanced by high nocturnal emissions. *Nature Geoscience*, **14**, 289-294. <https://doi.org/10.1038/A41561-021-00722-3>, 2021.

Glaser, C., Schwientek, M., Junginger, T., Gilfedder, B.S., Frei, S., Werneburg, M., Zwiener, C., & Zarfl, C.: Comparison of environmental tracers including organic micropollutants as groundwater exfiltration indicators into a small river of a karstic catchment. *Hydrological Processes*, **34**, 4712-4726. <https://doi.org/10.1002/hyp.13909>, 2020.

Gore, J. A.: Discharge measurements and streamflow analysis. In F. R. Hauer & G. A. Lamberti (Eds.), *Methods in stream ecology*. (2<sup>nd</sup> ed., chap. 3, pp. 51–77). Cambridge, MA: Academic Press. <https://doi.org/10.1016/B978-012332908-0.50005-X>, 2007.

Intergovernmental Panel on Climate Change.: Climate change 2013—the physical science basis: Working group I contribution to the fifth assessment report of the Intergovernmental Panel on Climate Change. Cambridge: Cambridge University Press. doi:10.1017/CBO9781107415324, 2014.

Hall Jr, R. O., & Ulseth, A. J.: Gas exchange in streams and rivers. *Wiley Interdisciplinary Reviews: Water*, 7(1), e1391. <https://doi.org/10.1002/wat2.1391>, 2020.

Herreid, A. M., Wymore, A. S., Varner, R. K., Potter, J. D., & McDowell, W. H.: Divergent controls on stream greenhouse gas concentrations across a land-use gradient. *Ecosystems*, **24**, 1299-1316. <https://doi.org/10.1007/A10021-020-00584-7>, 2021.

Holtan-Hartwig, L., Dörsch, P., & Bakken, L. R.: Low temperature control of soil denitrifying communities: kinetics of N<sub>2</sub>O production and reduction. *Soil Biology and Biochemistry*, **34**, 1797-1806. [https://doi.org/10.1016/S0038-0717\(02\)00169-4](https://doi.org/10.1016/S0038-0717(02)00169-4), 2002.

Horgby, Å., Boix Canadell, M., Ulseth, A. J., Vennemann, T. W., & Battin, T. J.: High-resolution spatial sampling identifies groundwater as driver of CO<sub>2</sub> dynamics in an Alpine stream network. *Journal of Geophysical Research: Biogeosciences*, **124**, 1961-1976. <https://doi.org/10.1029/2019JG005047>, 2019.

Hotchkiss, E. R., Hall Jr, R. O., Sponseller, R. A., Butman, D., Klaminder, J., Laudon, H., Rosvall, M., & Karlsson, J.: Sources of and processes controlling CO<sub>2</sub> emissions change with the size of streams and rivers. *Nature Geoscience* **8**, 696–699. <https://doi.org/10.1038/ngeo2507>, 2015.

[Hu, M., Chen, D. and Dahlgren, R.A.: Modeling nitrous oxide emission from rivers: a global assessment. \*Global change biology\*, 22\(11\), 3566-3582. <https://doi.org/10.1111/gcb.13351>, 2016.](https://doi.org/10.1111/gcb.13351)

Kuhn, C., Bettigole, C., Glick, H. B., Seegmiller, L., Oliver, C. D., & Raymond, P.: Patterns in stream greenhouse gas dynamics from mountains to plains in northcentral Wyoming. *Journal of Geophysical Research: Biogeosciences*, **122**, 2173-2190. <https://doi.org/10.1002/2017JG003906>, 2017.

Lambert, T., Bouillon, S., Darchambeau, F., Morana, C., Roland, F. A. E., Descy, J., & Borges, A. V.: Effects of human land use on the terrestrial and aquatic sources of fluvial organic matter in a temperate river basin

- (The Meuse River, Belgium). *Biogeochemistry* **136**, 191–211. <https://doi.org/10.1007/A10533-017-0387-9>, 2017.
- Li, M., Peng, C., Zhang, K., Xu, L., Wang, J., Yang, Y., Li, P., Liu, Z., & He, N.: Headwater stream ecosystem: an important source of greenhouse gases to the atmosphere. *Water Research*, **190**, 116738. <https://doi.org/10.1016/j.watres.2020.116738>, 2021.
- Marescaux, A., Thieu, V., & Garnier, J.: Carbon dioxide, methane and nitrous oxide emissions from the human-impacted Seine watershed in France. *Science of the Total Environment*, **643**, 247-259. <https://doi.org/10.1016/j.scitotenv.2018.06.151>, 2018.
- McDowell, M. J., & Johnson, M. S.: Gas transfer velocities evaluated using carbon dioxide as a tracer show high streamflow to be a major driver of total CO<sub>2</sub> evasion flux for a headwater stream. *Journal of Geophysical Research: Biogeosciences*, **123**, 2183-2197. <https://doi.org/10.1029/2018JG004388>, 2018.
- Mwanake, R. M., Gettel, G. M., Aho, K. S., Namwaya, D. W., Masese, F. O., Butterbach-Bahl, K., & Raymond, P. A.: Land use, not stream order, controls N<sub>2</sub>O concentration and flux in the upper Mara River basin, Kenya. *Journal of Geophysical Research: Biogeosciences* **124**, 3491–3506. <https://doi.org/10.1029/2019jg005063>, 2019.
- Mwanake, R. M., Gettel, G. M., Ishimwe, C., Wangari, E. G., Butterbach-Bahl, K., & Kiese, R.: Basin-scale estimates of greenhouse gas emissions from the Mara River, Kenya: Importance of discharge, stream size, and land use/land cover. *Limnology and Oceanography*, **67**, 1776-1793. <https://doi.org/10.1002/lno.12166>, 2022.
- O'Donnell, J. A., Aiken, G. R., Kane, E. S., & Jones, J. B.: Source water controls on the character and origin of dissolved organic matter in streams of the Yukon River basin, Alaska. *Journal of Geophysical Research: Biogeosciences*, **115**. <https://doi.org/10.1029/2009JG001153>, 2010.
- [Park, J.H., Nayna, O.K., Begum, M.S., Chea, E., Hartmann, J., Keil, R.G., Kumar, S., Lu, X., Ran, L., Richey, J.E. and Sarma, V.V.: Reviews and syntheses: Anthropogenic perturbations to carbon fluxes in Asian river systems—concepts, emerging trends, and research challenges. \*Biogeosciences\*, \*\*15\*\*\(9\), 3049-3069. <https://doi.org/10.5194/bg-15-3049-2018>, 2018.](https://doi.org/10.5194/bg-15-3049-2018)
- Patton, C. J., & Kryskalla, J. R.: Colorimetric determination of nitrate plus nitrite in water by enzymatic reduction, automated discrete analyzer methods. *US Geological Survey Techniques and Methods, Book 5* **34**. <https://doi.org/10.3133/tm5B8>, 2011.
- Peacock, M., Audet, J., Bastviken, D., Futter, M.N., Gauci, V., Grinham, A., Harrison, J.A., Kent, M.S., Kosten, S., Lovelock, C.E., & Veraart, A.J.: Global importance of methane emissions from drainage ditches and canals. *Environmental Research Letters*, **16**, 044010. <https://doi.org/10.1088/1748-9326/abeb36>, 2021.
- Peacock, M., Granath, G., Wallin, M. B., Högbom, L., & Futter, M. N.: Significant Emissions From Forest Drainage Ditches—An Unaccounted Term in Anthropogenic Greenhouse Gas Inventories?. *Journal of Geophysical Research: Biogeosciences*, **126**. <https://doi.org/10.1029/2021JG006478>, 2021a.
- Quick, A. M., Reeder, W. J., Farrell, T. B., Tonina, D., Feris, K. P., & Benner, S. G.: Nitrous oxide from streams

- and rivers: A review of primary biogeochemical pathways and environmental variables. *Earth-science reviews*, **191**, 224–262. <https://doi.org/10.1016/j.earscirev.2019.02.021>, 2019.
- Raymond, P.A., Zappa, C.J., Butman, D., Bott, T.L., Potter, J., Mulholland, P., Laursen, A.E., McDowell, W.H. & Newbold, D.: Scaling the gas transfer velocity and hydraulic geometry in streams and small rivers. *Limnology and Oceanography* **2**, 41–53. <https://doi.org/10.1215/21573689-1597669>, 2012.
- Reay, D. S., Smith, K. A., & Edwards, A. C.: Nitrous oxide emission from agricultural drainage waters. *Global Change Biology*, **9**, 195–203. <https://doi.org/10.1046/j.1365-2486.2003.00584.x>, 2003.
- Rocher-Ros, G., Sponseller, R. A., Lidberg, W., Mörth, C. M., & Giesler, R.: Landscape process domains drive patterns of CO<sub>2</sub> evasion from river networks. *Limnology and Oceanography Letters*, **4**, 87–95. <https://doi.org/10.1002/lol2.10108>, 2019.
- Schade, J. D., Bailio, J., & McDowell, W. H.: Greenhouse gas flux from headwater streams in New Hampshire, USA: Patterns and drivers. *Limnology and Oceanography* **61**, 165–174. <https://doi.org/10.1002/lno.10337>, 2016.
- Schrier-Uijl, A. P., Veraart, A. J., Leffelaar, P. A., Berendse, F., & Veenendaal, E. M.: Release of CO<sub>2</sub> and CH<sub>4</sub> from lakes and drainage ditches in temperate wetlands. *Biogeochemistry*, **102**, 265–279. <https://doi.org/10.1007/A10533-010-9440-7>, 2011.
- Schumacker, R. E., & Lomax, R. G.: A Beginner's-Beginner's Guide to Structural Equation Modeling (4th Ed.). New York: Routledge. 2016.
- Sebestyen, S. D., Boyer, E. W., Shanley, J. B., Kendall, C., Doctor, D. H., Aiken, G. R., & Ohte, N.: Sources, transformations, and hydrological processes that control stream nitrate and dissolved organic matter concentrations during snowmelt in an upland forest. *Water Resources Research*, **44**. <https://doi.org/10.1029/2008WR006983>, 2008.
- Shelley, F., Grey, J., & Trimmer, M.: Widespread methanotrophic primary production in lowland chalk rivers. *Proceedings of the Royal Society B: Biological Sciences*, **281** (1783). <https://doi.org/10.1098/rspb.2013.2854mWAN>, 2014.
- Stanley, E. H, Casson, N. J., Christel, S. T., Crawford, J. T., Loken, L. C., & Oliver, S. K.: The ecology of methane in streams and rivers: patterns, controls, and global significance. *Ecological Monographs* **86**, 146–171. <https://doi.org/10.1890/15-1027>, 2016.
- Strahler, A. N.: Hypsometric (area-altitude) analysis of erosional topography. *GSA Bulletin* **63**, 1117–1142. [https://doi.org/10.1130/0016-7606\(1952\)63\[1117:HAAOET\]2.0.CO;2](https://doi.org/10.1130/0016-7606(1952)63[1117:HAAOET]2.0.CO;2), 1952.
- Turner, P. A., Griffis, T. J., Lee, X., Baker, J. M., Venterea, R. T., & Wood, J. D.: Indirect nitrous oxide emissions from streams within the US Corn Belt scale with stream order. *Proceedings of the National Academy of Sciences* **112**, 9839–9843. <https://doi.org/10.1073/pnas.1503598112>, 2015.
- Wallin, M. B., Audet, J., Peacock, M., Sahlée, E., & Winterdahl, M.: Carbon dioxide dynamics in an agricultural headwater stream driven by hydrology and primary production. *Biogeosciences* **17**, 2487–2498. <https://doi.org/10.5194/bg-17-2487-2020>, 2020.

- Wallin, M.B., Campeau, A., Audet, J., Bastviken, D., Bishop, K., Kokic, J., Laudon, H., Lundin, E., Löfgren, S., Natchimuthu, S. and Sobek, S.: Carbon dioxide and methane emissions of Swedish low-order streams—A national estimate and lessons learnt from more than a decade of observations. *Limnology and Oceanography* **3**, 156–167. <https://doi.org/10.1002/lol2.10061>, 2018.
- Wang, D.; Ye, W., Wu, G., Li, R., Guan, Y., Zhang, W., Wang, J., Shan, Y., Hubacek, K.: Greenhouse gas emissions from municipal wastewater treatment facilities in China from 2006 to 2019. *Sci Data* **9**, 317. <https://doi.org/10.1038/s41597-022-01439-7>, 2022.
- Wangari, E.G., Mwanake, R.M., Kraus, D., Werner, C., Gettel, G.M., Kiese, R., Breuer, L., Butterbach-Bahl, K. and Houska, T.: Number of chamber measurement locations for accurate quantification of landscape-scale greenhouse gas fluxes: Importance of land use, seasonality, and greenhouse gas type. *Journal of Geophysical Research: Biogeosciences*, **127**. <https://doi.org/10.1029/2022JG006901>, 2022.
- Winkler, K., Fuchs, R., Rounsevell, M., & Herold, M.: Global land use changes are four times greater than previously estimated. *Nature communications*, **12**, 1-10. <https://doi.org/10.1038/A41467-021-22702-2>, 2021.
- Zhang, L., Xia, X., Liu, S., Zhang, S., Li, S., Wang, J., Wang, G., Gao, H., Zhang, Z., Wang, Q. and Wen, W.: Significant methane ebullition from alpine permafrost rivers on the East Qinghai–Tibet Plateau. *Nature Geoscience*, **13**, 349-354. <https://doi.org/10.1038/A41561-020-0571-8>, 2020.
- Zhang, W., Li, H., Xiao, Q., & Li, X.: Urban rivers are hotspots of riverine greenhouse gas (N<sub>2</sub>O, CH<sub>4</sub>, CO<sub>2</sub>) emissions in the mixed-landscape chaohu lake basin. *Water Research*, **189**, 116624. <https://doi.org/10.1016/j.watres.2020.116624>, 2021.
- Zhou, J., Liu, G., Meng, Y., Xia, C., Chen, K., & Chen, Y.: Using stable isotopes as tracer to investigate hydrological condition and estimate water residence time in a plain region, Chengdu, China. *Scientific reports*, **11**, 1-12. <https://doi.org/10.1038/s41598-021-82349-3>, 2021.